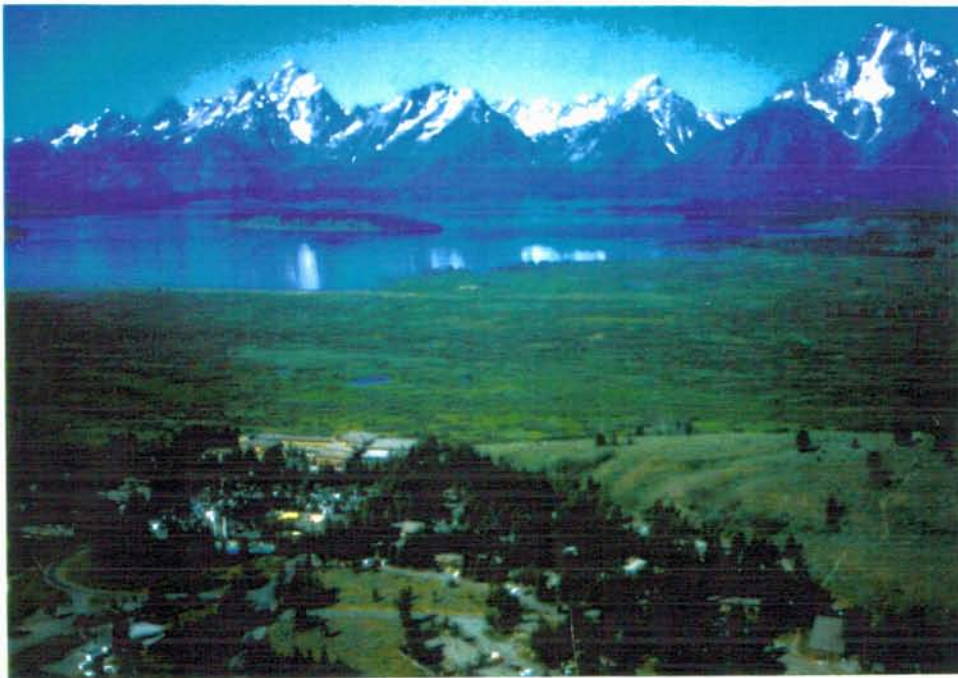


**Proceedings of the
Third International Symposium on
Vibrations of Continuous Systems**

**Jackson Lake Lodge
Grand Teton National Park, Wyoming, USA
July 23-27, 2001**



View of the Grand Tetons with Jackson Lake and the Lodge in the foreground

Contents

Preface	1
The Influence of Discretization on the Nonlinear Vibrations of Shallow Shells K. A. Alhazza and A. H. Nayfeh	2
Axial Vibration of Compound Bars and Helical Springs C. W. Bert	5
Non-Linear Dynamics of Aeroelastic Systems E. H. Dowell	8
Vibration Frequencies of Variable Thickness Rectangular Plates M. Eisenberger	11
A Nonlinear Analysis of A Nonideal Beam-Motor System A. Fenili, J. M. Balthazar, and D. T. Mook	13
Free Vibrations Analysis of Bridge Decks Resting on Combinations of Elastic and Inelastic Supports D. J. Gorman	16
A Mathematical Model for Vibrating Piezoelectric Shells P. Hagedorn and M. Berg	19
Identification of Elastic Parameters for Laminated Circular Cylindrical Shells K. Hosokawa and K. Matsumoto	22
Shear Coefficients for Thin-Walled Timoshenko Beams J. R. Hutchinson	25
Vibration Instability in Circular Saws S. G. Hutton	28
The Rayleigh-Riz Method without Admissibility Requirements S. Ilanko	31
Approximate Methods for the Vibration of Gyroscopic Continua R. K. Jha and R. G. Parker	33
Equivalences between Transcendental and Linear Eigenvalue Problems of Free Structural Vibration D. Kennedy , F. W. Williams, M. S. Djoudi, and S. Yuan	36

Reduced-Order Model for Nonlinear Vibration Analysis Using the Finite-Element Method Y. Kobayashi , G. Yamada, and A. Harada	39
Responses of Nonlinear Asymmetric Forced Vibrations of Circular Plate M. H. Yeo and W. K. Lee	42
Exact Solutions for the Free Vibrations of Rectangular Plates with Linearly Varying in-Plane Loading A. W. Leissa	45
Development of Fourier-p Shape Functions for Vibration of Plates C. W. Lim and A. Y. T. Leung	47
Chaotic Oscillations of a Cylindrical Shell-Panel with Concentrated Mass under Gravity and Cyclic Load K. Nagai and T. Yamaguchi	49
Applicability of the Donnell-type Theory to Open Cylindrical Shells Composed of Composite Materials Y. Narita	52
Continuum Representations for the Vibration of Vehicle Tracks N. C. Perkins and C. Scholar	55
Vibrations of Ballooning Strings C. D. Rahn	57
Vibrations of a Flexible Rod Induced by Friction Y. Sato	60
Forced Linear and Non-Linear Vibration of a Piezoceramic Transformer W. Seemann and R. Gausmann	62
Vibration Characteristics of Thin FGM Cylindrical Shells C. B. Sharma and M. N. Naeem	64
Free Vibration Analysis of Thick Shells of Revolution A. V. Singh	67
Vibration Studies of Composite Laminated Structural Components K. P. Soldatos and A. Messina	70

Vibration Analysis of A rotating Vessel Composed of Circular plates and a Circular Cylindrical Shell, 1 st Stage: In-Plane Vibrations of a Rotating Circular Plate	73
K. Suzuki, T. Hijiki, and K. Suzuki	
Useful Analogies with Finding Natural Frequencies of Structures From Dynamic Stiffness Matrix Formulations	76
F. W. Williams, W. X. Zhong, W. P. Howson, and A. Watson	
Biosketches of Authors	79

PREFACE

The International Symposium on Vibrations of Continuous Systems is a forum for leading researchers from across the globe to meet with their colleagues and present both old and new ideas on the field. Each participant has been encouraged to either present results of recent, significant research or to reflect on some aspect of the vibration of continuous systems which is particularly interesting, unexpected, or unusual. This latter type of presentation – of which there are several in the program – was proposed to encourage participants to draw on understanding obtained through – in many cases – decades of research.

The location of the Third ISVCS is in one of the most beautiful places in North America - Grand Teton National Park in northwestern Wyoming, just south of Yellowstone National Park. The rugged Grand Teton mountain group rises there dramatically to several peaks over 12,000 ft (3700 m) from a large, relatively flat basin (known as Jackson Hole) at about 6800 ft (2100 m). There are no foothills between the mountains and the basin, and therefore visitors have spectacular views of the mountains. The highest peak, named the Grand Teton (13,770 ft, 4197 m), thrusts its way far above the basin.

This Proceeding contains short summaries of the presentations to be made at the Symposium and short biographical sketches submitted by many of the participants.

Editor

Ali H. Nayfeh

Reviewing Editors

Charles W. Bert

Stuart M. Dickinson

Peter Hagedorn

General Chairman

Arthur W. Leissa

THE INFLUENCE OF DISCRETIZATION ON THE NONLINEAR VIBRATIONS OF SHALLOW SHELLS

K. A. Alhazza and A. H. Nayfeh

Department of Engineering Science and Mechanics, MC 0219
Virginia Polytechnic Institute and State University
Blacksburg, VA 24061 USA

INTRODUCTION

There has been an increasing interest in the nonlinear vibrations of laminated composite shells during the past three decades. Due to the complexity of the nonlinear partial-differential equations governing their motions, relatively a limited number of papers has been presented on the nonlinear vibrations of doubly-curved shells. A common approach for analyzing nonlinear vibrations of distributed-parameter systems, in general, and shells, in particular, is to discretize the governing partial-differential equations and associated boundary conditions to obtain a system of infinite number of nonlinearly coupled second-order ordinary-differential equations. This system is usually truncated to a finite number of equations, which are then treated either analytically or numerically. In most studies, only one mode is retained in the truncation, especially if the shell is excited near the linear natural frequency of that specific mode. Such an approach is referred to as a single-mode discretization. Using several examples of distributed-parameter systems and an experiment, Nayfeh and coworkers^{1,2} showed that such truncations might lead to quantitatively, and in some cases qualitatively, erroneous results. Kobayashi et al.³ used single-mode and two-mode approximations to analyze the nonlinear responses of doubly-curved shells to primary-resonance excitations. For the first mode of the transverse displacement, both the one-mode and two-mode analyses led to the same results. While for the second mode, the two-mode approximation led to a qualitative and quantitative difference in the response. In this paper, we investigate the influence of the number of retained modes in the discretization on the predicted response of a doubly-curved cross-ply laminated shallow shell with simply supported boundary conditions to a primary resonant excitation of its fundamental mode (i.e., $\Omega \approx \omega_{11}$). The nonlinear partial-differential equations governing the motion of the shell are based on the von Karman-type geometric nonlinear theory and the first-order shear-deformation theory. We use these equations and their associated boundary conditions to determine the linear natural frequencies and their associated mode shapes. Then, we use these results and the Galerkin method to reduce the problem into an infinite system of nonlinearly coupled second-order ordinary-differential equations. An approximate solution of this system of equations is obtained by using the method of multiple scales.^{5,6} This solution consists of the spatial and temporal variations of the shell response, with the time variation being governed by two nonlinear first-order ordinary-differential equations. The latter depend on a so-called effective nonlinearity coefficient, which depends on the modes retained in the discretization. The closed-form expression for the effective nonlinearity is independent of the symmetric modes for the case of primary resonance of the fundamental mode.

Numerical results for single-layered shells are obtained. The influence of the number of modes retained in the discretization on the shell response and the effective nonlinearity is investigated. The results show that single-mode and two-mode approximations can lead to quantitatively, and in some cases qualitatively, erroneous results. A multi-mode approximation that includes as many modes as needed for convergence is used to characterize the shell response.

ANALYSIS

The equations of motion for doubly-curved cross-ply shallow shells are⁴

$$\begin{aligned} D_{11} \frac{\partial^4 w}{\partial x^4} + 2(D_{12} + 2D_{66}) \frac{\partial^4 w}{\partial y^2 \partial x^2} + D_{22} \frac{\partial^4 w}{\partial y^4} + k_x \frac{\partial^2 \Phi}{\partial y^2} + k_y \frac{\partial^2 \Phi}{\partial x^2} + C \frac{\partial w}{\partial t} + \rho h \frac{\partial^2 w}{\partial t^2} \\ = \frac{\partial^2 \Phi}{\partial y^2} \frac{\partial^2 w}{\partial x^2} + \frac{\partial^2 \Phi}{\partial x^2} \frac{\partial^2 w}{\partial y^2} - 2 \frac{\partial^2 \Phi}{\partial y \partial x} \frac{\partial^2 w}{\partial y \partial x} + F \cos(\Omega t) \end{aligned} \quad (1)$$

where ρ is the mass density, C is the linear viscous damping coefficient, k_y and k_x are the curvatures, N_x, N_{xy}, N_y are the in-plane force resultants, and M_x, M_{xy}, M_y are the moment resultants. A second equation is obtained from the compatibility conditions for cross-ply shells as⁴

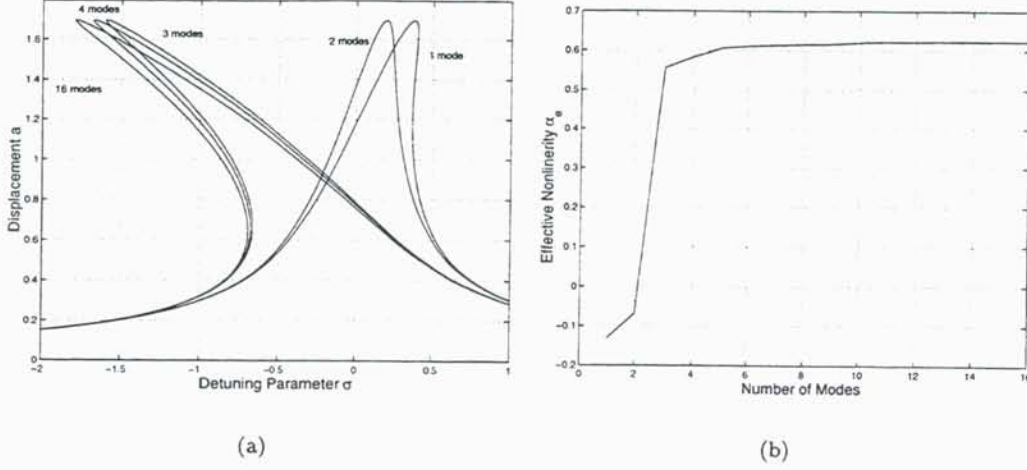


Figure 1: (a) Frequency-response curves of a single-layered shell when $k_x = 0$, $k_y = 0.0935$, and $\mu_{11} = 0.25$. (b) Effective nonlinearity for a single-layered shell when $k_x = 0$ and $k_y = 0.0935$.

$$-K_{11} \frac{\partial^4 \Phi}{\partial x^4} - (2K_{12} + K_{66}) \frac{\partial^4 \Phi}{\partial y^2 \partial x^2} - K_{22} \frac{\partial^4 \Phi}{\partial y^4} + k_x \frac{\partial^2 w}{\partial y^2} + k_y \frac{\partial^2 w}{\partial x^2} = - \left(\frac{\partial^2 w}{\partial y \partial x} \right)^2 + \frac{\partial^2 w}{\partial x^2} \frac{\partial^2 w}{\partial y^2} \quad (2)$$

Using the Galerkin procedure, we reduce Eqs. (1) and (2) into the following system of nonlinear ordinary-differential equations:

$$\begin{aligned} \ddot{W}_{\eta\nu} + 2\mu_{\eta\nu} \dot{W}_{\eta\nu} + \omega_{\eta\nu}^2 W_{\eta\nu} + \sum_{n,m=1}^{\infty} \sum_{l,j=1}^{\infty} P_{\eta\nu nmlj} W_{nm} W_{lj} \\ + \sum_{n,m=1}^{\infty} \sum_{l,j=1}^{\infty} \sum_{p,q=1}^{\infty} \sum_{r,s=1}^{\infty} S_{\eta\nu nmljpqrs} W_{nm} W_{rs} W_{pq} = F_{\eta\nu} \cos(\Omega t) \end{aligned} \quad (3)$$

where the $P_{\eta\nu nmlj}$ and $S_{\eta\nu nmljpqrs}$ are given in quadrature in terms of the mode shapes.

An approximate solution for the system of equations (3) is obtained by using the method of multiple scales^{5,6} to obtain the modulation equations

$$2\omega_{11}a' + \mu_{11}\omega_{11}a - f \sin(\gamma) = 0 \quad , \quad -2\omega_{11}a\beta' - f \cos(\gamma) - 2\omega_{11}\alpha_e a^3 = 0 \quad (4)$$

where α_e the effective nonlinearity coefficient is given by

$$\alpha_e = \sum_{i,j}^{N,M} (P_{11ij11} + P_{1111ij}) \left(\frac{P_{ij1111}}{8\omega_{11}(\omega_{ij}^2 - 4\omega_{11}^2)} + \frac{P_{ij1111}}{4\omega_{11}\omega_{ij}^2} \right) - \sum_{i,j}^{N,M} \frac{3S_{1111ij11}}{8\omega_{11}} \quad (5)$$

It follows from Eq. (5) that $\alpha_e \rightarrow \infty$ if any $\omega_{ij} \rightarrow 2\omega_{11}$, which corresponds to a two-to-one internal resonance.

Next, we use Eqs. (4) and (5) to investigate the influence of the number of terms retained in the Galerkin approximation on the accuracy of the calculated response. We consider a cylindrical single-layered graphite/epoxy shell with the following parameters:

$$\nu_{12} = 0.3, \quad l_x = 1, \quad l_y = 1, \quad f = 30, \quad \frac{E_1}{E_2} = 15.4, \quad \frac{G_{12}}{E_2} = 0.79, \quad \frac{G_{23}}{E_2} = 0.5 \quad (6)$$

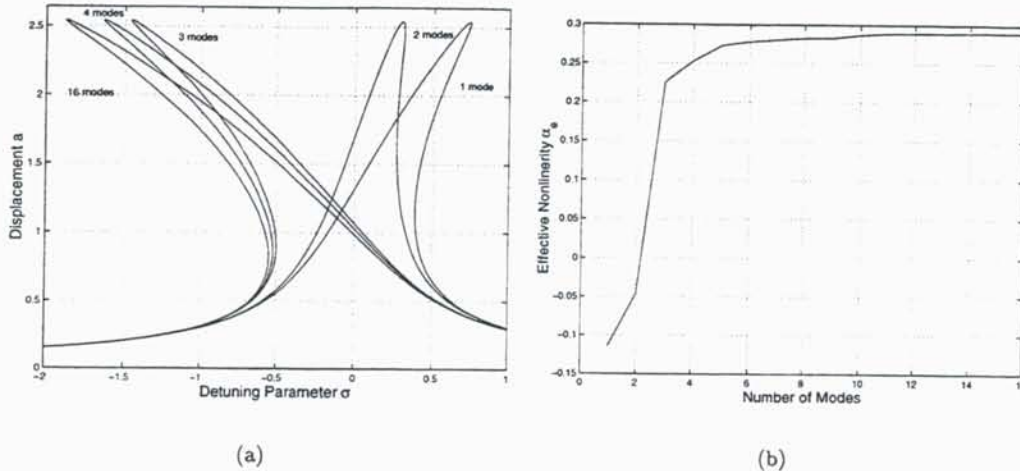


Figure 2: (a) Frequency-response curves of a single-layered shell when $k_x = 0.1$, $k_y = -0.196$, and $\mu_{11} = 0.25$. (b) Effective nonlinearity for a single-layered shell when $k_x = 0.1$ and $k_y = -0.194$.

First, we consider $k_x = 0$ and $k_y = 0.0935$. It follows from Fig. 1a that retaining one or two modes in the approximation predicts frequency-response curves that are bent to the right, indicating a softening-type nonlinearity. However, retaining three modes in the approximation yields a frequency-response curve bent to the left, indicating a softening-type nonlinearity. Increasing the number of retained modes further leads only to quantitative rather than qualitative changes in the predicted response. In Fig. 1b, we show variation of the effective nonlinearity α_e with the number n of the modes retained in the approximation. When $n = 1$ or 2, $\alpha_e < 0$, indicating a softening-type behavior. When $n \geq 3$, $\alpha_e > 0$, indicating a hardening-type behavior. In fact, $\alpha_e \approx -0.068$ when $n = 2$, whereas $\alpha_e \approx 0.55$ when $n = 3$ and $\alpha_e \approx 0.58$ when $n = 4$. The value of α_e converges to 0.62 as n approaches 11.

Second, we consider a doubly-curved single-layered shell with the curvatures $k_x = 0.1$ and $k_y = -0.194$. Again, it follows from Fig. 2a that retaining one or two modes in the approximation predicts frequency-response curves bent to the right, whereas retaining three or more modes in the approximation predicts frequency-response curves bent to the left. It follows from Fig. 2b that α_e changes from -0.046 when $n = 2$ to 0.22 when $n = 3$. As n increases, the predicted α_e continues to increase, indicating a softening-type behavior, and finally converges to 0.29 as n approaches 11.

References

- [1] Nayfeh, A. and Lacarbonara, W., "On the Discretization of Spatially Continuous Systems with Quadratic and Cubic Nonlinearities," *JSME International Journal*, Vol. 4(3), 1988, pp. 2-23.
- [2] Nayfeh, A. and Lacarbonara, W., "On the Discretization of Distributed-Parameter Systems with Quadratic and Cubic Nonlinearities," *Nonlinear Dynamics*, Vol. 13, 1997, pp. 203-220.
- [3] Kobayashi, Y., Yamada, G., and Satoh, M., "Nonlinear Vibration Analysis of Cross-Ply Laminated Shallow Shells," in *Proceedings of the 2nd International Symposium on Vibrations of Continuous Systems*, Grindelwald, Switzerland, July 11-16, 1999, pp. 25-27.
- [4] Bogdanovich, A., *Non-Linear Dynamic Problems for Composite Cylindrical Shells*, Elsevier Applied Science, London, 1991.
- [5] Nayfeh, A. H., *Introduction to Perturbation Techniques*, Wiley, New York, 1981.
- [6] Nayfeh, A. H., *Perturbation Methods*, Wiley, New York, 1973.

Axial Vibration of Compound Bars and Helical Springs

Charles W. Bert
School of Aerospace and Mechanical Engineering
The University of Oklahoma, Norman, OK 73019-1052, USA

The solutions for the free axial vibration of prismatic or tapered bars are well known. However, the present investigator is unaware of any previous analyses of the free vibration of compound bars, i.e., bars arranged in *mechanical series*. The objective of the present investigation is to solve this problem exactly, to present several simple approximate equations for estimating the fundamental frequency, and to apply these results to helical springs.

Exact Solution

The subject system is a compound bar consisting of an arbitrary number (n) of prismatic segments. The governing differential equations of motion are

$$a_i^2 u_{i,xx} = u_{i,tt} ; i = 1, \dots, n \quad (1)$$

where a_i is the acoustic wave velocity of a typical segment i , $u_i = u_i(x, t)$ is the axial displacement of bar i at position x and time t , and $()_{,xx}$ denotes $\partial^2 () / \partial x^2$, etc.

The general solutions of Eqs. (1) are

$$u_i(x, t) = U_i(x) \cos \omega t \quad (2)$$

where $U_i(x)$ is the mode shape of segment i , and ω is the circular natural frequency. The general solutions for the mode shapes are

$$U_i(x) = \alpha_i \cos(\omega x/a_i) + \beta_i \sin(\omega x/a_i) \quad (3)$$

Taking the origin of the coordinate system to be at the left end of segment 1, letting L_i be the length of segment i , and considering the compound bar to be fixed at both ends (for instance), the boundary and junction conditions can be expressed as

$$\begin{aligned} U_1(0) &= 0 \\ U_i(\Sigma L_i) &= U_{i+1}(\Sigma L_i) \\ A_i E_i U_{i,x}(\Sigma L_i) &= A_{i+1} E_{i+1} U_{i+1,x}(\Sigma L_i) \\ &\vdots \\ U_n(\Sigma L_n) &= 0 \end{aligned} \quad (4)$$

where $\Sigma L_i = \sum_{j=1}^n L_j$. For the example of a two-segment bar, Eqs. (4) reduce to

$$\begin{aligned} U_1(0) &= 0; U_1(L_1) = U_2(L_1); \\ A_1 E_1 U_{1,x}(L_1) &= A_2 E_2 U_{2,x}(L_1); U_2(L_1 + L_2) = 0 \end{aligned} \quad (4a)$$

Substitution of Eqs. (3) into Eqs. (4) leads to a set of $2n$ homogeneous algebraic equations in the coefficients α_i and β_i ($i=1, \dots, n$). The determinant of this set must be forced to vanish in order to guarantee a nontrivial solution. This frequency determinant is transcendental in the frequency ω , because the coefficients are of the form of both sine and cosine functions. For a two-segment bar ($n=2$), for instance, the frequency equation consists of two terms containing sines and cosines to the second degree:

$$(A_1 E_1 / a_1) \cos(\omega L_1 / a_1) \sin(\omega L_2 / a_2) + (A_2 E_2 / a_2) \sin(\omega L_1 / a_1) \cos(\omega L_2 / a_2) = 0 \quad (5a)$$

For a three-segment bar, the frequency equation consists of sixteen terms containing sines and cosines to the fifth degree.

Approximate Formulas for the Fundamental Natural Frequency

Due to the complexity of obtaining an exact solution and the need for designers to have relatively simple algebraic formulas, two such formulas are proposed here for the fundamental natural frequency of an n -segment compound bar.

The first formula was motivated by the famous Dunkerley's formula (Dunkerley, 1895) but its exact form was suggested by the actual exact solutions for the case of $n=2$:

$$\omega = \left[\sum_{i=1}^n (1/\omega_i) \right]^{-1} \quad (6)$$

where ω_i is the fundamental natural frequency of segment i . This is different than Dunkerley's formula, which is

$$\omega = \left[\sum_{i=1}^n (1/\omega_i)^2 \right]^{-1/2} \quad (7)$$

The second formula was motivated by the effective *static* stiffness of an n -segment spring:

$$K = \left[\sum_{i=1}^n (1/k_i) \right]^{-1} \quad (8)$$

and the total mass of the system

$$M = \sum_{i=1}^n m_i \quad (9)$$

Then

$$\omega = \pi(K/M)^{1/2} \quad (10)$$

It is noted that for a bar,

$$k_i = A_i E_i / L_i$$

Numerical Results

As a first step toward evaluating the two approximate formulas, the case of a two-segment bar with $k_2 = 1$, $L_1 = L_2 = 1$, and $m_1 = m_2 = 1$ is considered for various values of the ratio k_1/k_2 . The results are tabulated as follows:

Table 1. Values of ω/ω_1

k_1/k_2	Exact	Eq.(6)	% error	Eq. (10)	% error
0.25	0.7323	0.6667	-6.6	0.6325	-13.6
0.49	0.6062	0.5882	-3.0	0.5793	-4.4
0.50	0.6028	0.5858	-2.8	0.5774	+4.2
0.98	0.5023	0.5025	+0.04	0.5025	+0.04
1.00	0.5000	0.5000	0	0.5000	0
1.02	0.4975	0.4975	0	0.4975	0
4.00	0.3662	0.3333	-9.0	0.3162	-13.7
9.00	0.2902	0.2500	-13.0	0.2236	-22.9

It is noted that neither Eq. (6) nor Eq. (10) gives an upper or lower bound, but Eq. (6) is always as good as or better than Eq. (10).

The fundamental frequency of a single cylindrical helical spring is given by

$$\omega = \pi(k/m)^{1/2}$$

where k is the spring rate and m is the active-coil mass (Wahl, 1963). Thus, the present analysis can readily be applied to compound springs.

Reference

Dunkerley, S., 1894, "On the whirling and vibration of shafts", *Philosophical Transactions of the Royal Society, London*, Ser. A, Vol. 185, pp. 279-360.

Wahl, A. M., 1963, *Mechanical Springs*, 2nd ed., McGraw-Hill, New York, chapter 25.

NON-LINEAR DYNAMICS OF AEROELASTIC SYSTEMS

Earl H. Dowell
Duke University

INTRODUCTION

Nonlinear phenomena in aeroelasticity have been known for many years. In the last decade or so, such effects have become of more serious concern to practitioners. And for that reason, and also because of the advance in theoretical and experimental methods, a more substantial and concentrated effort has been made by the research community to understand and pursue how unfavorable nonlinear aeroelastic effects may be diminished and favorable effects exploited.

This paper summarizes several distinct yet related research thrusts that have proven particularly fruitful. While the author draws largely on the experience of the Duke aeroelasticity team, reference is made to the work of many other investigators for the benefit of those who may wish to pursue the ever increasing literature on these topics. However, we do not provide an in depth summary of the total literature, but rather comment selectively on the efforts of the broader community in the recent and not so recent past to provide a context for the work discussed here.

Three topics are considered. The first is an airfoil with a control surface which has freeplay in its attachment to the airfoil. Such a configuration exhibits limit cycle oscillations (LCO) due to freeplay well below the classical linear flutter speed (LFS). The second is a wing with a plate-like structure that undergoes LCO once the LFS is exceeded, but not usually below the LFS. Here, the nonlinearity is a result of the tension induced in the plane of the plate-wing when the wing bending is on the order the wing thickness or greater. The third is a very high aspect ratio wing which exhibits LCO above the LFS, but also exhibits a sensitive to initial disturbances below the LFS that may lead to LCO there as well. Here, the nonlinearity is due to the coupling among flapwise bending, chordwise (or lag) bending and torsion of the wing structure. This coupling is known to be important for rotorcraft blades that are cantilevered at the rotor hub (sometimes called hingeless blades).

For each of the three topics, experiments (conducted in a low speed wind tunnel) are also discussed and correlated with theory. It would be very valuable to have high speed experiments as well. And indeed, the NASA Langley Research Center aeroelasticity team has provided valuable benchmark experiments that are directed toward aerodynamic nonlinearities in the transonic flow regime. And some encouraging correlations with available theory have been made by the Langley team as well. It can be expected that our ability to pursue more such correlations will continue to advance due to the work of the Langley team and the efforts of the aeroelastic community at large.

For a more extensive list of relevant references, the interested reader may contact the author.

I. AIRFOIL PLUS A CONTROL SURFACE WITH FREEPLAY

Many investigators over the last fifty years have considered the effects of a structural stiffness nonlinearity on an airfoil with or without a control surface. Broadly speaking, the literature is characterized by the type of nonlinearity, i.e. continuous or discontinuous (freeplay), whether the nonlinear spring stiffness is for the airfoil or the control surface, and finally the nature of the aerodynamic model. Most of the work has been done at low Mach number using classical Theodorsen aerodynamic theory or approximations thereto or at very high Mach number where piston theory aerodynamics can be applied. Also, most of the studies have been theoretical/numerical, but some interesting experimental work has been done as well. For a more thorough review of the literature, particularly as regards freeplay nonlinearities, see Connor et al [1]. For continuous spring nonlinearities, the recent publication by Lee et al [2] has a nice summary.

Here, we focus on theoretical/experimental correlation as achieved at low Mach number, the theoretical effects of transonic Mach number, and the physical and fundamental insights that have been gained over the years. For another recent study of freeplay in the transonic, low supersonic range, see Kim and Lee [3]. Their results appear comparable to those discussed here [4], although they use different solution methods and do not consider a control surface per se.

II. LOW ASPECT RATIO, PLATE-LIKE WING

The literature for this configuration in the context of nonlinear aeroelasticity is very recent and notably small. However, if one takes a broader view and notes that the basic physical mechanism for the nonlinear effect is that a tension force is induced in the mid-plane of the plate-wing by the out-of-plane bending when the latter deflection is of the order of the plate thickness, then we recall that this is indeed the same physical mechanism that leads to nonlinear effects in general and LCO in particular for "panel flutter" or the flutter of plates and shells. A panel is a local portion of a wing between pairs of spars and stringers. See the monograph by Dowell [5] which gave an early authoritative discussion of the fundamentals of the phenomena and the recent review by Mei [6] that summarizes the recent literature on panel flutter. It is notable that much of the recent panel flutter literature uses the simple piston theory aerodynamic model that is limited to high supersonic Mach number. However it is the subsonic, transonic and low supersonic flow regimes that are often most important for applications. Fortunately, recent theoretical advances make calculations in these Mach number regimes more and more attractive. When such calculations were first done twenty five years ago they were a feat. See Dowell [5]. Today, they do require an understanding of the more sophisticated aerodynamic models, but the calculations themselves are no longer extraordinary in their demand on computer resources. The most recent work for a plate-like wing per se is discussed in [7,8].

III. HIGH ASPECT RATIO, BEAM-LIKE WING

Again, the available literature is small. For very high aspect ratio beams that may bend and twist, it has been known for many years that the flap-wise bending, chord-wise bending (lag) and torsional deformation (twist) may couple among themselves to produce a significant structural nonlinearity. This was first pursued in the context of rotor blades that are often, of course, long and slender. It has not been an issue with fixed wing aircraft for the most part. However, recently and particularly in the context of Uninhabited Air Vehicles (UAV), very high aspect ratio fixed wing configurations are of interest. Thus, researchers have pursued aeroelastic studies of this configuration. Notable work has been done by Patil, Hodges and Cesnik [9]. Their pioneering theoretical studies have shown a number of interesting nonlinear effects including the presence of LCO and also the sensitivity of the onset of classical flutter as well as LCO to temporal disturbances including initial conditions. Their work and that of the Duke team [10] is

discussed here. The latter includes both theoretical and experimental studies.

REFERENCES

1. Conner, M.D., Tang, D.M., Dowell, E.H. and Virgin, L.N., "Nonlinear Behavior of a Typical Airfoil Section with Control Surface Freeplay: A Numerical and Experimental Study," *Journal of Fluids and Structures*, Vol. 11, pp. 89-109, 1997.
2. Liu, L., Wong, Y.S. and Lee, B.H.K., "Application of the Centre Manifold Theory in Non-Linear Aeroelasticity," *Journal of Sound and Vibration*, Vol. 234, No. 4, pp. 641-659, 2000.
3. Kim, D.-H. And Lee, I., "Transonic and Low-Supersonic Aeroelastic Analysis of a Two-Degree-of-Freedom Airfoil With a Freeplay Non-Linearity," *Journal of Sound and Vibration*, Vol. 234, No. 5, pp. 859-880, 2000.
4. Dowell, E.H., Thomas, J.P. and Hall, K.C., "Transonic Limit Cycle Oscillation Analysis Using Reduced Order Modal Aerodynamic Models," presented at the 42nd AIAA/ASME/ASCE/AHS/ASC Structures, Structural Dynamics, and Materials Conference, Seattle, Washington, April 16-19, 2001.
5. Dowell, E.H., "Aeroelasticity of Plates and Shells," Kluwer Publishers, 1975.
6. Mei, C., Abdel-Motagaly, K. and Chen, R.R., "Review of Nonlinear Panel Flutter at Supersonic and Hypersonic Speeds," *Applied Mechanics Reviews*, Vol. 52, No. 10, pp. 321-332, October 1999.
7. Tang, D.M., Henry, J.K. and Dowell, E.H., "Limit Cycle Oscillations of Delta Wing Models in Low Subsonic Flow," *AIAA Journal*, Vol. 37, No. 3, pp. 364-371, 1999.
8. Tang, D.M., Henry, J.K. and Dowell, E.H., "Nonlinear Aeroelastic Response of Delta Wing to Periodic Gust," *Journal of Aircraft*, Vol. 37, No. 1, pp. 155-164, Jan-Feb 2000.
9. Patil, M.J., Hodges, D.H. and Cesnik, C.E.S., "Limit Cycle Oscillations in High-Aspect-Ratio Wings," *Journal of Fluids and Structures*, Vol. 15, No. 1, pp. 107-132, 2001.
10. Tang, D.M. and Dowell, E.H., "Effects of Geometric Structural Nonlinearity on Flutter and Limit Cycle Oscillations of High-Aspect Ratio Wings," submitted to *Journal of Fluids and Structures*.

VIBRATION FREQUENCIES OF VARIABLE THICKNESS RECTANGULAR PLATES

M. Eisenberger

Faculty of Civil Engineering, Technion - Israel Institute of Technology,
Haifa 32000, ISRAEL

The functional of the total potential and kinetic energies for the harmonic vibrations of a variable thickness rectangular thin plate of dimensions $a \times b$ is

$$\begin{aligned} \Pi = & \frac{1}{2} \int_0^b \int_0^a D \{W_{,xx}^2 + 2\nu W_{,xx} W_{,yy} + W_{,yy}^2 + 2(1-\nu) W_{,xy}^2\} dx dy \\ & - \frac{1}{2} \omega^2 \rho \int_0^b \int_0^a h W^2 dx dy \end{aligned} \quad (1)$$

where $W(x, y)$ is the transverse displacement of the plate, $h(x, y)$ is the thickness, ρ is the material density, ω is the frequency of vibration, and $D(x, y)$ is the bending stiffness of the plate. In this work the solution is sought as

$$W(x, y) = X(x) Y(y) \quad (2)$$

with

$$D(x, y) = D_x(x) D_y(y) \quad (3)$$

$$h(x, y) = h_x(x) h_y(y) \quad (4)$$

Substitution of the assumed solution into the functional, and integration by parts yields the following ordinary differential equation with variable coefficients

$$\begin{aligned} A_2 D_y Y'''' + 2A_2 D_y' Y''' + [A_2 D'' + (A_3 - A_4) D_y] Y'' \\ + (A_3 - A_4) D_y Y' + (A_1 D_y + 0.5A_3 D_y'') Y = \omega^2 \rho A_5 h_y Y \end{aligned} \quad (5)$$

with

$$A_1 = \int_0^a D_x (X'')^2 dx \quad (6)$$

$$A_2 = \int_0^a D_x X^2 dx \quad (7)$$

$$A_3 = \int_0^a 2\nu D_x X'' X dx \quad (8)$$

$$A_4 = \int_0^a 2D_x (1-\nu) (X')^2 dx \quad (9)$$

$$A_5 = \int_0^a h_x X^2 dx \quad (10)$$

This procedure enables us to solve the plate vibration problem as a series of beam on elastic foundation problems, by assuming the function $X(x)$. First we solve a beam problem in one direction (here first the y direction), and then in the second direction (in the x direction) using the previously derived solution $Y(y)$, in both cases using the dynamic stiffness method. This defines a cycle of solution. The solution converges very fast and in most cases no more than 2 cycles are required, i.e. very small number of beam vibrational analysis. For different boundary conditions one has only to solve the beam problem with different end restraints.

In the following tables and figures normalized converged vibration frequencies (ω^*) and mode shape plots are given for square plates with linear thickness variation in the x direction and constant in the y direction. The variation is taken as

$$h(x) = h_0(1 - \alpha x) \quad (11)$$

Table 1: Normalized Frequencies and Modes for SSSS plate

α	0.1	0.2	0.3	0.4	0.5	0.6	0.7	0.8
ω^*	18.7469	17.7428	16.7244	15.6883	14.6293	13.5392	12.4032	11.1901
Mode	[1,1]	[1,1]	[1,1]	[1,1]	[1,1]	[1,1]	[1,1]	[1,1]
ω^*	46.8465	44.2692	41.7175	39.0437	36.2769	33.3874	30.3250	26.9917
Mode	[1,2]	[1,2]	[2,1]	[2,1]	[2,1]	[2,1]	[2,1]	[2,1]
ω^*	46.8581	44.3179	66.8249	62.6138	58.2796	33.6469	49.1678	33.8104
Mode	[2,1]	[2,1]	[2,2]	[2,2]	[2,2]	[1,2]	[2,2]	[3,1]
ω^*	93.66353	88.4139		77.9159	72.2655	66.3238	59.9744	44.1420
Mode	[1,3]	[1,3]		[3,1]	[3,1]	[3,1]	[3,1]	[2,2]

and the normalized frequencies are defined as

$$\omega^* = \omega a^2 \sqrt{\frac{\rho H_0}{D_0}} \quad (12)$$

where a is the length of the edge, and h_0 and D_0 are the thickness and bending stiffness at origin of the plate. Results are presented for several combinations of boundary conditions. For all the plates $\nu = 0.25$. In Table 1 results are given for plates with simple support boundary conditions on all four edges. Also given are the modes indicating the number of half waves in the x and y directions, respectively. The modes are plotted in Figure 1, and it is evident that the plate is thinner at the right edge as there the deflections are larger.

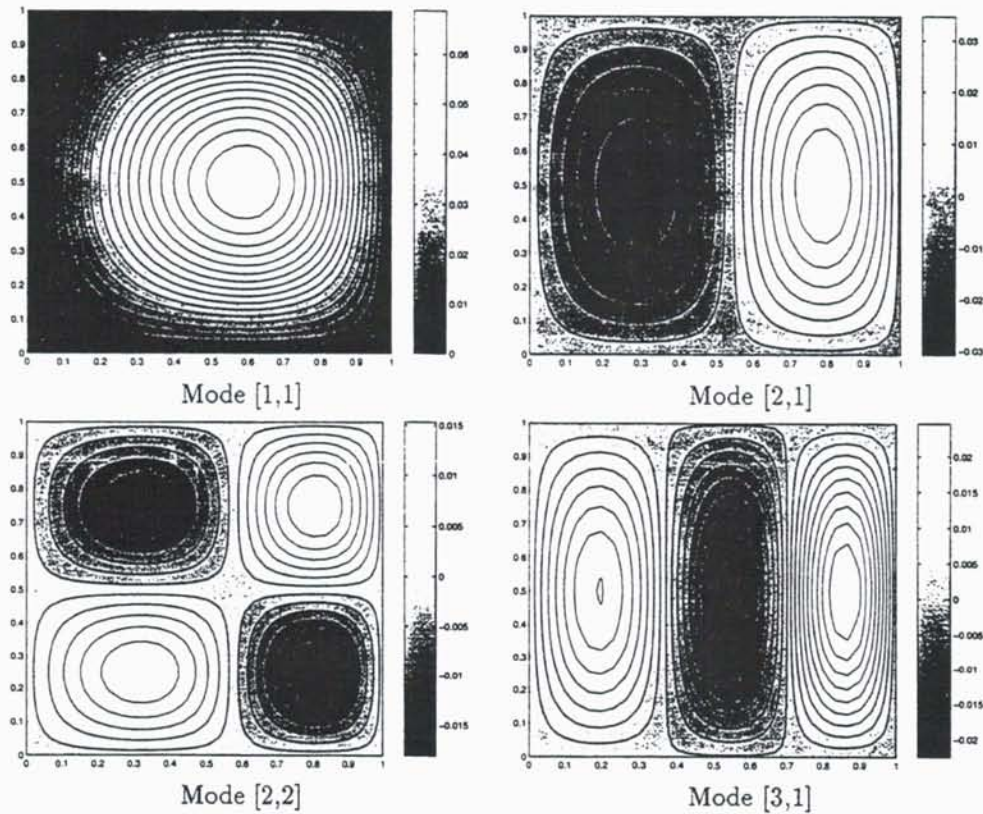


Figure 1: Vibration Modes for SSSS plate with $\alpha = 0.5$

A NONLINEAR ANALYSIS OF A NONIDEAL BEAM-MOTOR SYSTEM

A. Fenili, Faculdade de Engenharia Mecânica, Universidade de Campinas,
Campinas, SP, BRAZIL

J. M. Balthazar, Departamento de Estatística, Matemática Aplicada e Computação, Instituto de Geociências e
Ciências Exatas, Universidade Estadual de São Paulo, Rio Claro, SP, BRAZIL

D. T. Mook, Department of Engineering Science and Mechanics, Virginia Polytechnic Institute and State
University, Blacksburg, VA, USA

The problem of rotating a cantilever beam from one direction to another (often referred to as a slewing motion) is of long-standing interest. It has applications in the field of robotics among other places. For robots in space, the problem is somewhat complicated because of the highly flexible nature of the beam, and theories that include nonlinear inertial and bending terms may be required for an accurate analysis. Moreover, the motor used to rotate the beam may be small with limited power. For such a system, the action of the motor cannot be prescribed, but must be determined interactively with the deflection of the beam as part of the solution. Because of this mutual interaction, which increases the number of unknowns, the system is said to be nonideal. Here we consider the nonideal, nonlinear, slewing problem.

In contrast with earlier approaches, we derive nonlinear equations that govern the time-dependent deflections of a cantilever beam being rotated by applying a moment to its end without assuming that the beam is inextensible. Instead, we find from our analysis that, to the order of the approximations considered here and in the earlier studies, the beam can be considered inextensible. Then we couple the equations that govern the beam to those that govern a weak electric motor, which is used to apply the moment to the end of the beam. Next, we discretize the equations, projecting the response to a prescribed voltage applied to the motor onto the space of linear free-vibration modes.

The rotating, cantilever beam is represented schematically in a top view in Figure 1. The beam rotates around an axis passing through point O with the angular velocity $\dot{\theta}(t)$. Two coordinate systems are used to describe the motion of a point on the beam: (X, Y) denotes the inertial system and (x, y) denotes the one that rotates with the shaft and the undeflected beam. Both the beam and the moving coordinate system are rigidly attached to the shaft, and the motor applies torque to it. The rotating x -axis makes the angle $\theta(t)$ with the X -axis of the inertial system. The undeflected beam lies along the x -axis and has the length L ; its cross section is symmetric with respect to the xy -plane. Gravity acts in the z -direction. Point A on the undeflected beam, which is represented by the heavy dot in Figure 1, is a distance x from the origin of the two coordinate systems at O . During the deflection, A moves to A' ; thus, A and A' represent the position of the same material point in the beam at two different times. The displacement of point A is denoted by \vec{r} . The x - and y -components of \vec{r} are $u(x, t)$ and $v(x, t)$, respectively. The slope of the beam relative to the x -axis at A' is described by the angle $\phi(x, t)$.

We use dimensionless variables (denoted by \sim) to aid in making rational approximations. The time, the arc length of the deformed beam, and the components of the displacements are:

$$\tilde{x} = \frac{x}{L}, \quad \tilde{t} = \frac{t}{T_c}, \quad \tilde{l} = \frac{l}{L}, \quad \tilde{\theta}(\tilde{t}) = \frac{T_c^2 \ddot{\theta}(t)}{\varepsilon}, \quad \tilde{v}(\tilde{x}, \tilde{t}) = \frac{v(x, t)}{\varepsilon L}, \quad \text{and} \quad \tilde{u}(\tilde{x}, \tilde{t}) = \frac{u(x, t)}{\varepsilon^2 L} \quad [1]$$

where L is the length of the undeformed beam, the characteristic time is $T_c = L^2 \sqrt{\frac{\rho}{EI}}$, ρ is the mass per unit of length of the beam, E is the elastic modulus of the beam, I is the moment of inertia of its cross-section area, $\varepsilon \equiv \frac{r^2}{L^2} \ll 1$ is a small dimensionless parameter, and r is the radius of gyration of the cross-

section area. We note that θ is dimensionless; the \sim indicates that $\tilde{\theta}$ is written as a function of dimensionless variables, differentiated with respect to dimensionless variables, and scaled.

Using Hamilton's principle, we obtain after some manipulation and dropping the tildes

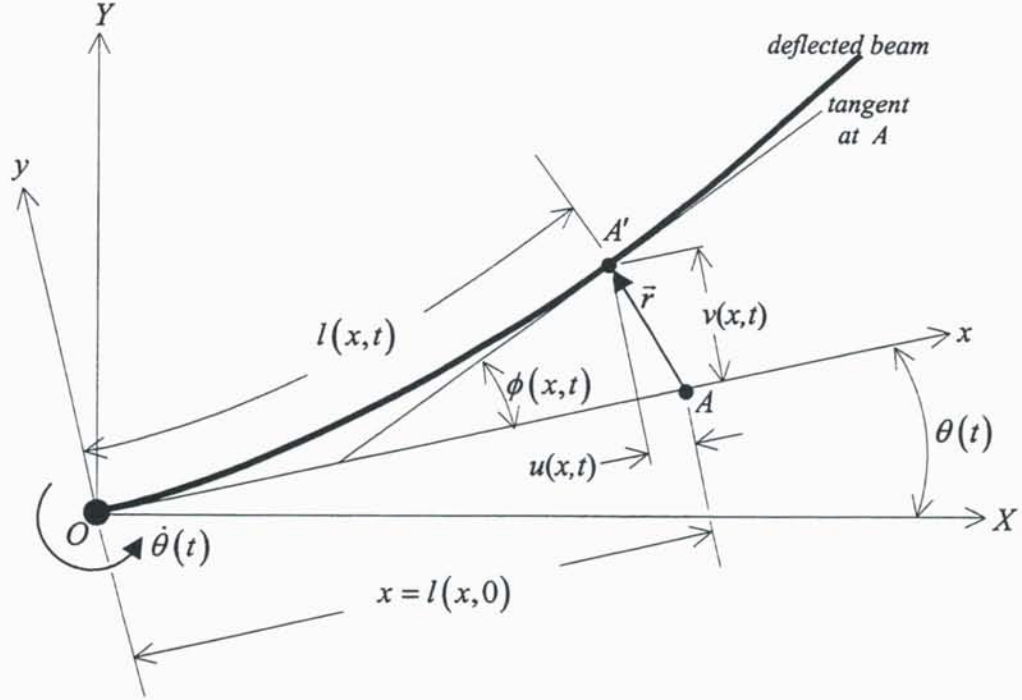


Figure 1. Schematic representation of the deflected beam. The motor-driven shaft is at O .

$$\ddot{v} + v'''' + \ddot{\theta}x + \varepsilon \left[v' \left(u' - \frac{1}{2}v'^2 \right) \right]' - \varepsilon^2 \left(\dot{\theta}^2 v + 2\dot{\theta}\dot{u} + \ddot{\theta}u - 3v'v''v''' - \frac{3}{2}v''^3 \right) = 0 \quad [2]$$

and

$$-\left(u' - \frac{1}{2}v'^2 \right)' + \varepsilon \left(\ddot{u} + \dot{\theta}^2 x + \ddot{\theta}v + 2\dot{\theta}\dot{v} + v'v'''' \right) = 0 \quad [3]$$

where at $x = 0$,

$$v = 0, \quad v' = 0, \quad u = 0 \quad [4]$$

and at $x = 1$,

$$v'' + O(\varepsilon^3) = 0, \quad v''' + O(\varepsilon^3) = 0, \quad \text{and} \quad u' - \frac{1}{2}v'^2 + \varepsilon \left(\frac{1}{2}v''^2 - v'v'''' \right) = 0 \quad [5]$$

where primes and over dots denote the partial derivatives with respect to x and t , respectively. It also follows that the normal strain, e , is given by

$$e = \varepsilon^2 \left(-u' + \frac{1}{2}v'^2 \right) + \varepsilon^4 \left(\frac{1}{2}u'v'^2 - \frac{1}{8}v'^4 \right) + O(\varepsilon^6) = O(\varepsilon^3) \quad [6]$$

Hence, the assumption that the beam is inextensible is justified to this order of approximation.

The equation of motion of the shaft is given by

$$C_1 i_a - C_2 \dot{\theta} + C_3 \left(v'' + 2\varepsilon^2 u' v'' + \dots \right)_{x=0} = \ddot{\theta} \quad [7]$$

where i_a is the current through the armature measured in amperes (the remaining variables are

dimensionless) $C_1 = \frac{\rho L^4 K_t}{\varepsilon EI (J_a + J_s)}$, K_t is the torque constant for the motor ($T_{motor} = K_t i_a$), J_a and

J_s are the polar moments of inertia of the armature and shaft, $C_2 = \frac{CL^2}{J_a + J_s} \sqrt{\frac{\rho}{EI}}$, C is a viscous-drag

coefficient used to model the friction torque acting on the shaft and armature, and $C_3 = \frac{\rho L^3}{J_a + J_s}$. The relationship between the current through the armature, i_a , and the applied voltage, U , is given by the following equation:

$$C_4 \dot{i}_a + C_5 i_a + \dot{\theta} = C_6 U(t) \quad [8]$$

where $C_4 = \frac{L_a}{\varepsilon K_b}$, L_a is the inductance of the armature, K_b is the back-emf constant (it can be shown

that $K_t = K_b$), $C_5 = \frac{R_a L^2}{\varepsilon K_b} \sqrt{\frac{\rho}{EI}}$, R_a is the resistance of the armature (measured in ohms),

$C_6 = \frac{L^2}{\varepsilon K_b} \sqrt{\frac{\rho}{EI}}$, and U is the applied voltage (measured in volts).

We approximate v with an expansion in terms of the linear, dimensionless free-vibration modes for the beam when $\dot{\theta}(t) \equiv 0$, $\varphi_i(x)$:

$$v(x,t) \cong \sum_{i=1}^N q_i(t) \varphi_i(x) \quad [9]$$

where the time-dependent coefficients, $q_i(t)$, are the generalized coordinates. Solving for u in terms of the $q_i(t)$ and the $\varphi_i(x)$ and then substituting the result into the governing equation for v , we obtain the following set of coupled equations for the $q_i(t)$:

$$\ddot{q}_l + \omega_l^2 q_l + \alpha_l \ddot{\theta} + \varepsilon^2 \left\{ \dot{\theta}^2 \sum_{i=1}^N \beta_{il} q_i + \sum_{i=1}^N \sum_{j=1}^N (\lambda_{ijl} \ddot{\theta} q_i q_j + \gamma_{ijl} \dot{\theta} q_i \dot{q}_j) + \sum_{i=1}^N \sum_{j=1}^N \sum_{k=1}^N [\Lambda_{ijkl} (q_i q_j \ddot{q}_k + q_i \dot{q}_j \dot{q}_k) + \Gamma_{ijkl} q_i q_j q_k] \right\} = 0 \quad [10]$$

for $l=1, 2, \dots, N$

where $\Gamma_{ijkl} = \int_0^1 \left[3\varphi_i' \varphi_j'' \varphi_k''' + \frac{3}{2} \varphi_i'' \varphi_j'' \varphi_k'' + \omega_j^2 (\varphi_i' \varphi_j \varphi_k' + W_{ij} \varphi_k'') \right] \varphi_l dx$

$$\alpha_l = \int_0^1 x \varphi_l dx, \quad \beta_{il} = \int_0^1 \left[\varphi_i + x \varphi_i' + \frac{1}{2} (x^2 - 1) \varphi_i'' \right] \varphi_l dx - 1, \quad \gamma_{ijl} = 2 \int_0^1 (V_j \varphi_i'' + \varphi_i' \varphi_j - R_{ij}) \varphi_l dx$$

$$\lambda_{ijl} = \int_0^1 \left(V_j \varphi_j'' + \varphi_i' \varphi_j - \frac{1}{2} R_{ij} \right) \varphi_l dx, \quad \Lambda_{ijkl} = \int_0^1 (S_{jk} \varphi_i'' + R_{jk} \varphi_i') \varphi_l dx$$

Equations [10], [8], and [7] must be solved simultaneously to obtain the response of the system to a prescribed input voltage $U(t)$.

The presentation will consist of some details of the derivation as well as some numerical examples.

Free Vibration Analysis of Bridge Decks Resting on Combinations of Elastic and Inelastic Supports

by
D. J. Gorman
Dep't. of Mech. Eng.
Univ. of Ottawa, Ottawa, Canada

Introduction

In an earlier paper the author described an analytical investigation of the free vibration frequencies and mode shapes of a thin multi-span bridge deck with in-elastic line support at the deck entry and exit locations as well as at interfaces between the spans[1]. Accurate solutions were obtained by the superposition method. The present paper constitutes essentially an extension of the earlier problem. The analysis is extended to cover the case of thin decks with combinations of in-elastic line support as described above and elastic line support. The latter is considered to be provided by rigid massless cross-members running beneath the deck at inter-span locations. Drop-cables, suspended from the main suspension cables, provide vertical elastic support at the outer extremities of the cross-members.

It is recognized that all modes will be symmetric, or anti-symmetric, with respect to the long central axis of the deck. It is found advantageous to analyze these two families of modes separately.

Analysis of Symmetric Modes

For illustrative purposes, and in the interest of brevity, we will describe the analysis of a two-span deck with simple line support at the entrance and exit locations and elastic support as described above at the interface of the spans. It will be seen that the analysis is applicable regardless of the number of spans or their individual lengths.

The deck is analyzed as one full length thin plate with transverse line support applied to it where required. In view of symmetry as described above, only one half of the deck, running its full length, is analyzed. In order to exploit the superposition method three building blocks (forced vibration solutions) as represented schematically in Figure 1 are employed. The dimensionless ξ axis runs along the centre line of the deck of total length 'a' and half-width 'b'. Small pairs of circles adjacent to an edge indicate slip-shear conditions, i.e., vertical edge reaction as well as slope taken normal to the edge are everywhere zero. All other non-driven edges are given simple support.

The first building block is driven by a distributed harmonic edge rotation of circular frequency ω , and is free of vertical edge reaction. Amplitude of the distributed edge rotation, and a Levy type solution for the response, are expressed in dimensionless form, respectively, as,

$$\frac{\partial W(\xi, \eta)}{\partial \eta} = \sum_{m=1,2}^{\infty} E_m \sin m\pi\xi, \quad (1) \quad \text{and, } W(\xi, \eta) = \sum_{m=1,2}^{\infty} Y_m(\eta) \sin m\pi\xi \quad (2)$$

where W equals plate lateral displacement divided by 'a'.

Following well established procedures the prescribed boundary conditions are enforced and exact solutions for the functions $Y_m(\eta)$ are obtained .

The second building block is driven by a distributed harmonic line force of circular frequency ω . This force acts along a line parallel to the η axis and at dimensionless distance α from it. We express amplitude of the driving force in dimensionless form as,

$$\frac{Va^2}{D} = \sum_{n=1,2}^{\infty} E_n \cos n\pi\eta \quad (3)$$

The reason for neglecting the first term in the series ($n=0$) will be explained later. A solution for each segment of the building block, utilizing the segment coordinates of the Figure, is expressed in the form,

$$W(\xi, \eta) = \sum_{n=1,2}^{\infty} Y_n(\xi) \cos n\pi\eta \quad (4)$$

Again, exact solutions for the quantities $Y_n(x)$ are easily obtained by enforcing outer segment boundary conditions as well as continuity conditions at the inter-segment boundaries. In fact, the solutions may be extracted from those of chapter 8 of reference [2].

A solution for the third building block which is driven by a concentrated harmonic force of amplitude P^* is also available following procedures described in reference [2]. The driven edge is considered to be free of bending moment.

In order to generate the eigenvalue matrix established procedures are followed. Upon superimposing the building blocks a condition of zero net bending moment along the deck free edge is enforced. Also, a condition of zero net slope taken along the cross-member - deck line of contact is imposed. These net quantities are expanded in appropriate series and the coefficients thus obtained are set equal to zero. Finally, a condition of elastic equilibrium is enforced at the drop-cable attachment point.

Analysis of Anti-symmetric Modes

This analysis differs only slightly from that described above for symmetric modes. Only these differences will be described.

1) The building blocks will differ from those of Figure 1 in that simple support conditions rather than slip-shear conditions will be imposed along the ξ axis. A solution for the first building block will be expressed, for example, using the trigonometric functions $\sin(2m-1)\pi\xi/2$.

2) Recognizing that attached cross-members can rotate about the ξ axis, in rigid body motion, we enforce a condition of zero second derivative of W with respect to distance along the deck-cross-member interface instead of zero first derivative as was done for symmetric modes.

3) We must now employ a pair of concentrated force driven building blocks, identical to the third building block of Figure 1, for each cross member. The first, driven by a force of dimensionless amplitude P_1^* is utilized to ensure satisfaction of the local elastic force-displacement equilibrium as discussed above. For the second of this pair of building blocks the driving force amplitude P_2^* is so constrained that the net rotational moment about the x axis exerted on the deck by the cross-member will equal zero. The set of $2K+2$ driving coefficients are thus constrained by $2K+2$ equations.

Generation of Eigenvalues and Mode Shapes

Various known limiting free vibration frequencies must be approached as elastic stiffness coefficients approach limits of zero and infinity. Approach to these limits has been verified for multi-span decks.

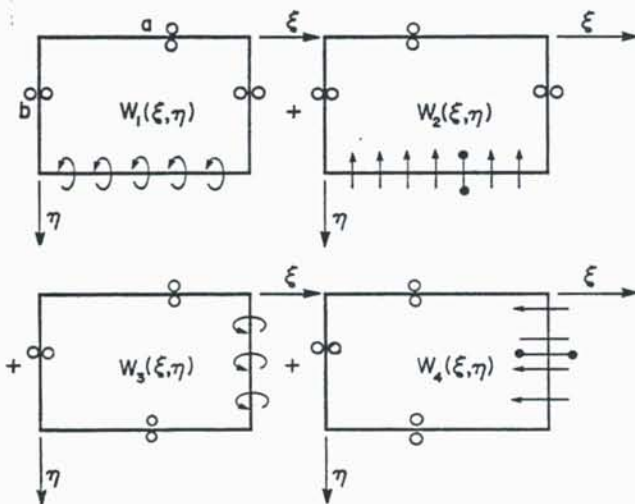


Figure 1. Schematic representation of building blocks employed.

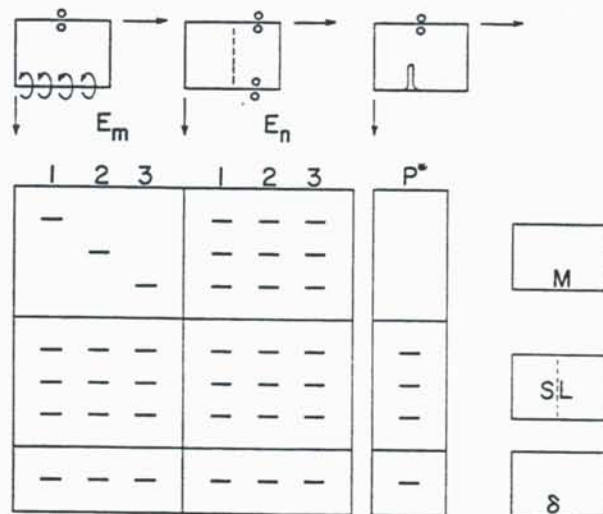


Figure 2. Schematic representation of eigenvalue matrix.

References

[1] Gorman, D. J. and Garibaldi, L. , 'A Study of Multi-Span Bridge Deck Free Vibration by The Method of Superposition', Proceedings, Second Int. Symposium on Vibrations of Continuous Systems, Grindelwald, Switzerland, July 11-16, 1999.

[2] Gorman, D. J., 'Free Vibration of Rectangular Plates', Elsevier North-Holland Co., 1982.

A Mathematical Model for Vibrating Piezoelectric Shells

P.Hagedorn, M. Berg

Department of Applied Mechanics
TU Darmstadt

hagedorn@mechanik.tu-darmstadt.de

Piezoelectric actuators, which have gained in importance during the last two decades, are produced in many geometrical forms depending on their application. In the present paper, the mathematical modeling of the bending vibrations of piezoceramic shells is presented. Piezoceramics are used in this shape for certain ultrasonic piezoelectric travelling wave motors. The aim of this study is to determine the eigenfrequencies and eigenmodes of piezoceramic shells and to examine their efficacy in certain types of actuators.

FLÜGGE'S equations for the bending vibrations of piezoelectric shells are modified by introducing the following constitutive equations for piezoceramic materials

$$\mathbf{T} = \mathbf{c}^E \mathbf{S} - \mathbf{e} \mathbf{E} , \quad (1)$$

$$\mathbf{D} = \mathbf{e} \mathbf{S} + \boldsymbol{\epsilon}^S \mathbf{E} . \quad (2)$$

In this notation, \mathbf{E} is the 3x1 vector of the electric field, \mathbf{S} the strain tensor written in 6x1 vector notation, \mathbf{D} the 3x1 vector of the dielectric displacements and \mathbf{T} the stress tensor written in 6x1 vector notation. Of course, these constitutive relations in which \mathbf{S} and \mathbf{E} are the independent variables, could be substituted by a different but equivalent system of equations.

In addition to the constitutive equations above, MAXWELL'S equations of electrostatics

$$\text{rot } \mathbf{E} = \mathbf{0} \quad (3)$$

$$\text{div } \mathbf{D} = \mathbf{0} , \quad (4)$$

must also be considered. Since dielectrics (such as piezoceramics) normally have no free electric charges, Equation (4) will lead to a differential equation for the

determination of the electric field in the vibrating shells. The electric field \mathbf{E} , which in the case of electrostatics is always irrotational, can be written as a gradient of the potential function Φ :

$$\mathbf{E} = -\text{grad } \Phi(x, \varphi, r) = -\text{grad} [\Phi_x(x) \Phi_\varphi(\varphi) \Phi_r(r)] \quad (5)$$

A kinematic relation is now formulated for the electric displacement vector \mathbf{D} . As a first approximation, it is assumed that the radial component is much larger than the others such that these can be neglected. Thus, Equation (4) can be substituted by

$$\text{div } \mathbf{D} \approx \frac{1}{r} \frac{\partial(rD_r)}{\partial r} = 0. \quad (6)$$

Using Equation (2), this leads to the following expression for the electric displacement:

$$D_r = e_{31} S_1 + e_{31} S_2 + e_{33} S_3 + \epsilon_{33}^S E_3, \quad (7)$$

As part of this first approximation, it will also be assumed that the strain-dependent components of the electric displacement are much smaller than the component given directly by the electric field. This leads to

$$\text{div } \mathbf{D} \approx \frac{1}{r} \frac{\partial(r\epsilon_{33}^S E_3)}{\partial r} = -\frac{1}{r} \frac{\partial(r\epsilon_{33}^S \Phi_{,r})}{\partial r} = -\frac{\epsilon_{33}^S}{r} (\Phi_{,r} + r \Phi_{,rr}), \quad (8)$$

and thus, from Equation (4),

$$\Phi_{,r} + r \Phi_{,rr} = 0. \quad (9)$$

This is a first-order differential equation of EULER's type in Φ . It can be solved using the proper boundary condition in the outer electrodes (where the electric potential is prescribed), leading to

$$\Phi(x, \varphi, r) = \Phi_{\text{Boundary}}(x, \varphi) \frac{\ln \frac{2a-s}{2r}}{\ln \frac{2a-s}{2a+s}}. \quad (10)$$

Therefore, the electric potential over the shell thickness is known and when substituted into the constitutive relation (1), leads to a new form of the dynamical shell equations which can be solved as shown by FLÜGGE. The vibration of the piezoelectric shell can now be studied using an exponential ansatz with respect to time, resulting in three differential equations coupled in the displacement amplitudes. For the free vibration problem, this is a homogeneous system of differential equations. The condition for the existence of non-trivial solution leads to the dispersion relation, which is a polynomial of degree 4 in the square of the axial wavelength, λ , and the circumferential wave number m , and of degree 3 in the square of the circular frequency ω .

For any given ω and circumferential wave number m , eight solutions can be obtained for the axial wave number λ . Eight particular solutions are thus constructed, the superposition of which must fulfill given boundary conditions.

The vibration problem was solved for a free-free shell. Eigenfrequencies and eigenmodes were determined, both numerically computed and experimentally. The agreement was good for a certain range of parameters, however there is need for further improvement. Consequently, the stress-dependent components in Equation (7) were included, leading to a different differential equation for the electric potential in the piezoceramic shell, which had to be solved numerically. Some of these numerical solutions are shown in this paper and compared to experimental data. Particular attention is devoted to the mode shapes and to the features desired in piezoelectric motors.

IDENTIFICATION OF ELASTIC PARAMETERS FOR LAMINATED CIRCULAR CYLINDRICAL SHELLS

Kenji HOSOKAWA
Faculty of Engineering
Chubu University
Kasugai, Aichi 487-8501 Japan

Kin'ya MATSUMOTO
Faculty of Education
Mie University
Tsu, Mie 514-8507 Japan

1. Introduction

To identify the elastic parameters of composite materials, an inverse analysis method has already been applied to the laminated composite plates by the authors [1]. The purpose of this study is to apply the proposed method to a laminated circular cylindrical shell and to compare the estimated elastic parameters with the obtained experimental ones. First, by applying the experimental modal analysis technique to a laminated circular cylindrical shell with free boundary conditions, natural frequencies and mode shapes are obtained. Next, by using the obtained natural frequencies and mode shapes, the elastic parameters for the lamina of the circular cylindrical shell are identified. On the other hand, we obtain the elastic parameters of the lamina experimentally. These experimental elastic parameters were compared, and found to agree well, with the elastic parameters identified using the proposed method.

2. Inverse Analysis Method

Figure 1 shows the flow chart of the identification program. First, the data about the geometrical configuration, initial material properties of the specimen, and natural frequencies obtained by excitation test are given. Secondly, the finite element analysis (eigenvalue analysis) is carried out with initial parameters, where the used element is a shell element. Also, for the relation between stress and strain of a finite shell element model, the first-order shear deformation theory is considered. Thirdly, to identify the elastic parameters appropriately, the analytical modes are compared with the experimental ones by *MAC*. Next, the sensitivity matrix is calculated as the difference of the natural frequencies between analysis and experiment. After the singular value decomposition of the sensitivity matrix is calculated, elastic parameters are identified with the generalized inverse matrix. Finally, if the estimated natural frequencies are converged into the experimental ones, the identification program is terminated.

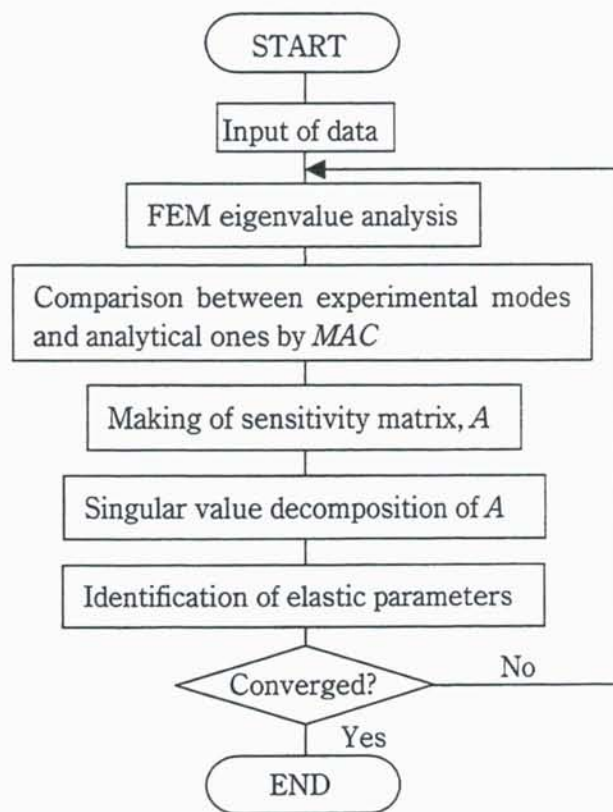


Fig.1 Flow chart of identification program

3. Comparison of Identified and Experimental Elastic Parameters

To identify the elastic parameters for the lamina of the laminated circular cylindrical shell with free boundary conditions, vibration tests were carried out. The stacking sequence of the laminated circular cylindrical shell is $[30^{\circ}_2 / -30^{\circ}_2 / -30^{\circ}_2 / 30^{\circ}_2]$ (See Figure 2). Each layer material, that is lamina, is a carbon fiber reinforced plastic (CFRP). The laminas of the shell are made of the same prepreg sheet. The density of the laminated shell is $1495(\text{Kg}/\text{m}^3)$. The length l of the shell is $0.203(\text{m})$ and the outside radius r is $51.7 \times 10^{-3}(\text{m})$. The thickness h of the laminated shell is $1.63 \times 10^{-3}(\text{m})$.

3.1 Identified Elastic Parameters

The natural frequencies and mode shapes of the laminated circular cylindrical shell were obtained by applying the experimental modal analysis technique. To satisfy the free boundary conditions, the laminated circular cylindrical shell was hung from the ceiling by a fine string. An accelerometer was attached to the laminated circular cylindrical shell and the shell was impacted by an impulse force hammer. The mass of the accelerometer is $0.48(\text{g})$. Figure 3 presents the first three experimental natural frequencies and mode shapes of the laminated circular cylindrical shell. In this figure, the notation “•” represents the location of the attached accelerometer.

From the experimental natural frequencies and mode shapes shown in Figure 3, the elastic parameters for the lamina of the laminated circular cylindrical shell were estimated by the proposed inverse analysis method. For the computation of natural frequencies and mode shapes, the mass of accelerometer was neglected because of it is very small compared to the shell's mass. The identified elastic parameters of the lamina are shown in Table 1. In this table, the elastic moduli E_L , E_T in the

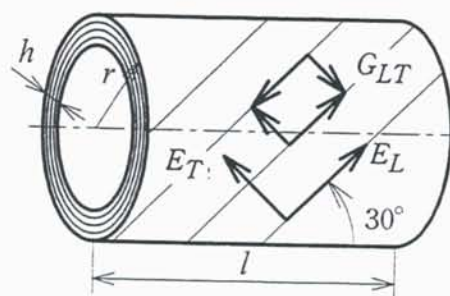


Fig.2 Angle-ply laminated cylindrical shell







Order	Experimental natural frequencies and mode shapes	Calculated natural frequencies and mode shapes
1st mode	 227(Hz)	 225(Hz)
2nd mode	 368(Hz)	 367 (Hz)
3rd mode	 643(Hz)	 650 (Hz)

Fig. 3 Natural frequencies and mode shapes of angle-ply laminated circular cylindrical shell with free boundary conditions ; $[30^{\circ}_2 / -30^{\circ}_2 / -30^{\circ}_2 / 30^{\circ}_2]$, CFRP.

direction of the parallel and normal to the fiber, G_{TV} , G_{VL} , and G_{LT} are shear moduli (where V axis is normal to the L - T plane). Poisson's ratios ν_{TV} and ν_{LT} are 0.32, respectively.

3.2 Justification of Identified Elastic Parameters

To justify the identified elastic parameters for the lamina of the laminated circular cylindrical shell, elastic parameters of the specimens were obtained experimentally. The beam type specimens with fiber orientation angles of 0° , 45° , and 90° were cut from the prepreg sheet which was used as the lamina to make the laminated circular cylindrical shell. The width and thickness of the specimens are 0.025(m) and 0.42×10^{-3} (m), respectively. And the specimens of various lengths ($0.10(\text{m}) \leq l \leq 0.28(\text{m})$) were used. The elastic moduli E_L , E_T , and G_{LT} were estimated numerically from the fundamental natural frequencies obtained by free bending vibration tests of the cantilevered specimen. The Poisson ratio $\nu_{LT} = 0.32$ was estimated from the tensile test of the specimen with the fiber orientation angle of 0° . The measured material properties of the lamina are listed in Table 1. From Table 1, one can see the good agreements between experimental and identified elastic parameters. Furthermore, to confirm the identified elastic parameters, Figure 3 presents the natural frequencies of laminated circular cylindrical shell estimated by the FEM eigenvalue analysis with the identified results. From the comparison of experimental and computational natural frequencies shown in Figure 3, one can see that the difference between the experimental and the numerically calculated natural frequencies is about 1.2% at the most. Also, Figure 3 shows good agreements between experimental and numerical mode shapes of the laminated circular cylindrical shell.

4. Conclusions

The inverse analysis method to identify elastic parameters of the laminated composite materials using the FEM eigenvalue analysis and the sensitivity analysis was applied to the laminated circular cylindrical shell with free boundary conditions. On the other hand, the elastic parameters for the lamina of the shell were obtained experimentally. From the comparison of identified and experimental elastic parameters, one can see the good agreements between these results. Accordingly, it follows that one can accurately estimate elastic parameters for the laminated circular cylindrical shells by using the inverse analysis method proposed by the authors.

Acknowledgement

This study was supported in part by the Nitto Foundation.

References

1. K. HOSOKAWA, K. MATSUMOTO and M. ZAKO 1998 *Fatigue, Environmental factors, and New Materials* PVP-Vol. 374, 325-329. Identification of Elastic Parameters for Laminated Composites Using FEM Eigenvalue Analysis (Comparison of Numerical and Experimental Results)

Table 1 Elastic parameters of lamina

Parameters	E_L [GPa]	E_T [GPa]	G_{TV} [GPa]	G_{VL} [GPa]	G_{LT} [GPa]
Identified	114	7.58	2.93	5.62	5.62
Measured	95.4	6.35	—	—	5.22

Shear Coefficients for Thin-Walled Timoshenko Beams

James R. Hutchinson

Department of Civil and Environmental Engineering
University of California, Davis CA 95616

Introduction

Timoshenko [1] was the first to introduce shear deformation, as well as rotary inertia, into the derivation of vibrating beam theory. He introduced a shear coefficient to account for the variation of the shear stress across the cross section. Timoshenko, in that first paper, used a value of $2/3$ for a rectangular cross section. Many authors have found and used different values for shear coefficients. One of the most accepted of these authors was Cowper [2] who derived shear coefficients for various cross sections for the static problem. In a recent paper [3] a new means of deriving appropriate shear coefficients was found. This new method gave complete agreement with the two three-dimensional solutions which are known. Those are the solution for a circular cylindrical cross-section and for the thin rectangular (plane stress) cross-section. The cross-sections considered in paper [3] were circular, rectangular, elliptical and annular. The only thin-walled cross-section considered was the thin-walled annular cross-section, although, it was pointed out that the procedure could be applied to any thin-walled section. This paper considers all the thin-walled sections considered by Cowper plus two additional ones.

Method of Solution

The approach used in reference [3], to get around the discrepancies inherent in beam theory, was to choose a "best" guess for the stress field and a "best" guess for the displacement field. A variational form was then used in which these two fields can be incompatible. The variational form used was the Hellinger-Reissner principle. The results of this approach were then compared to the Timoshenko Beam solution for long wave lengths, and an expression for the new shear coefficient was found. The displacement field was chosen consistent with the assumption that plane cross-sections remain plane after deformation. The normal stresses and the shear stress τ_{yz} were also chosen consistent with this assumption. The shearing stresses τ_{xy} and τ_{xz} were chosen consistent with the best known solutions for these stresses. The coordinates y and z are in the plane of the cross-section y is the vertical axis and z is the horizontal

axis, x is the axis along the length of the beam. They form a righthanded coordinate system. For solid sections the shear stress distribution is best found from the three-dimensional solution for a tip-loaded cantilever. For thin-walled sections the elementary shear stress theory is best.

Solution Process

The functions f_1 and f_2 express the in-plane distribution of the shearing stresses τ_{xy} and τ_{xz} ,

$$\tau_{xy} = \frac{V}{I_z} f_1(y,z) \quad \tau_{xz} = \frac{V}{I_z} f_2(y,z)$$

where V is the shear force and I_z is the moment of inertia about the z axis. The dynamic shear coefficient is expressed as,

$$k_d = - \frac{2(1+\nu)}{\left[\frac{A}{I_z^2} C_4 + \nu \left(1 - \frac{I_y}{I_z} \right) \right]}$$

where ν is Poisson's ratio, A is the cross-sectional area and C_4 is expressed as,

$$C_4 = - \int_A \left[\nu(f_1 y^2 - f_1 z^2 + 2f_2 yz) + 2(1+\nu)(f_1^2 + f_2^2) \right] dA$$

The static shear coefficient k_s is for the deflection of the original centroidal axis, and the static shear coefficient k_{sc} is for the mean deflection of the cross section, as was done by Cowper.

$$k_s = - \frac{2(1+\nu)I_z^2}{AC_4}$$

$$k_{sc} = - \frac{2(1+\nu)}{\left[\frac{A}{I_z^2} C_4 + \frac{\nu}{2} \left(1 - \frac{I_y}{I_z} \right) \right]}$$

Results

Tabulated results are shown in Table 1 for the six cases which were considered. The cases which were considered by Cowper were cases 1, 3, 4 and 5. In all cases the neutral axis is horizontal and motion takes place in the vertical direction. The I or wide flange beam shown as case 1 is thus

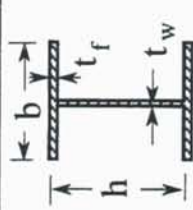
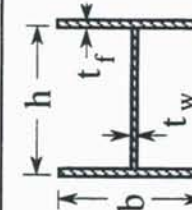
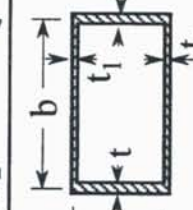
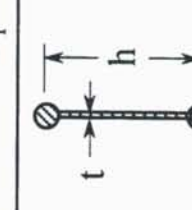
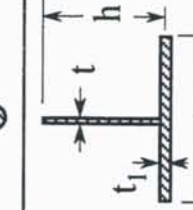
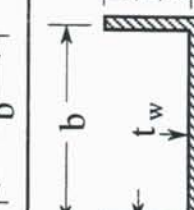
1.		$k_d = \frac{5(1+3m)^2(1+v)}{6+36m+75m^2+45m^3+15n^2(m+m^2)+v(5+30m+60m^2+45m^3)+vn^2(25m+30m^2)}$ $k_s = \frac{10(1+3m)^2(1+v)}{12+72m+150m^2+90m^3+30n^2(m+m^2)+v(15+90m+165m^2+90m^3)+45vn^2(m+m^2)}$ <p>where $m = 2bt_f/ht_w$, $n = b/h$</p>
2.		$k_d = \frac{10(1+v)}{12+12m+v(10+15m-10mn^2)}$ $k_s = \frac{10(1+v)}{12+12m+15v(1+m-n^2-n^2m)}$ <p>where $m = ht_w/2bt_f$, $n = h/b$</p>
3.		$k_d = \frac{5(1+3m)^2(1+v)}{6+36m+75m^2+45m^3+15n^2(m+m^2)+v(5+30m+60m^2+45m^3)+vn^2(10m-15mn-15m^2n)}$ $k_s = \frac{10(1+3m)^2(1+v)}{12+72m+150m^2+90m^3+30n^2(m+m^2)+v(15+90m+165m^2+90m^3)+15vn^2(-1-2m-1m^2-2mn-2m^2n)}$ <p>Box Section where $m = bt_f/ht$, $n = b/h$</p>
4.		$k_d = \frac{5(1+3m)^2(1+v)}{6+36m+75m^2+45m^3+v(5+30m+60m^2+45m^3)}$ $k_s = \frac{10(1+3m)^2(1+v)}{12+72m+150m^2+90m^3+v(15+90m+165m^2+90m^3)}$ <p>Spar and Web Section where $m = 2A_s/ht$, $A_s = \text{Area of one spar}$</p>
5.		$k_d = \frac{5(1+4m)^2(1+v)}{6+48m+138m^2+96m^3+15n^2(m+m^2)+v(5+40m+110m^2+120m^3)+vn^2(25m+35m^2+10m^3)}$ $k_s = \frac{10(1+4m)^2(1+v)}{12+96m+276m^2+192m^3+30n^2(m+m^2)+v(15+120m+300m^2+240m^3)+45vn^2(m+m^2)}$ <p>T - Section where $m = bt_f/ht$, $n = b/h$</p>
6.		$k_d = \frac{20m(2+m)^2n^2(1+v)}{15m+30m^2+n^2(48+138m+96m^2+24m^3)+v(-10-25m-10m^2)+vn^2(60+110m+80m^2+20m^3)}$ $k_s = \frac{20m(2+m)^2n^2(1+v)}{15m+30m^2+n^2(48+138m+96m^2+24m^3)+v(-15-67.5m+90m^2-30m^3)+vn^2(60+150m+120m^2+30m^3)}$ <p>Channel Section where $m = ht_w/t_f b$, $n = h/b$</p>

Table 1 Shear Coefficients for thin walled sections.

vibrating about its major principal axis, whereas, in case 2 it is vibrating about its minor principal axis. In all cases when Poisson's ratio is zero all three shear coefficients agree with the shear coefficient found by Cowper. Plots of the variation of the shear coefficients with Poisson's ratio is shown in Figures 1 - 4. Figure 1 is for a square cross-section with a constant wall thickness. It is a spe-

cial case of the Box Section shown as Case 3 in Table 1. For this case I_z equals I_y so that k_d , k_{s_s} and k_{s_c} are all equal and so are denoted simply as k . In all cases Cowper's shear coefficient is denoted as k_c . Figure 2 is for a typical channel section with $b = 3h$ and $t_f = t_w$. Figures 3 and 4 are for a typical wide flange beam with the flange width $3/4$ of the beam depth and $t_f = 2t_w$.

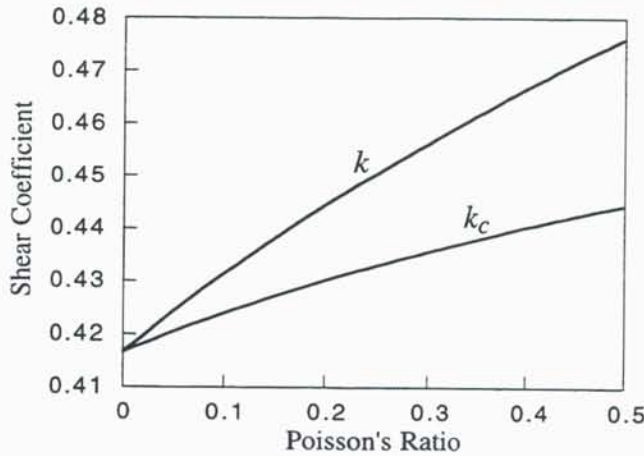


Figure 1. Shear Coefficient versus Poisson's Ratio for a square tube ($m = n = 1$).

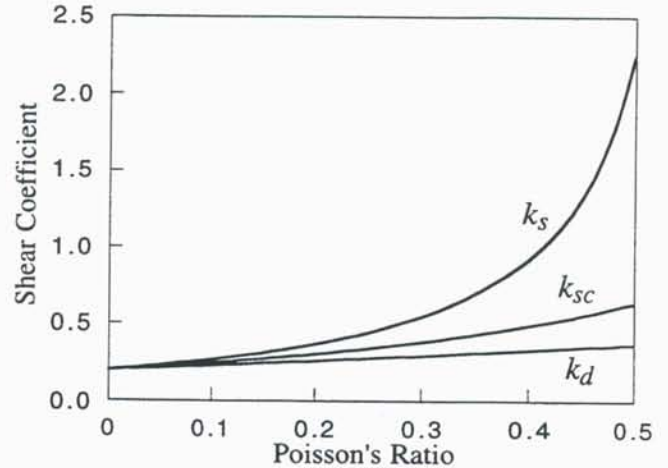


Figure 2. Shear Coefficient versus Poisson's Ratio for a typical channel ($m = n = 1/3$).

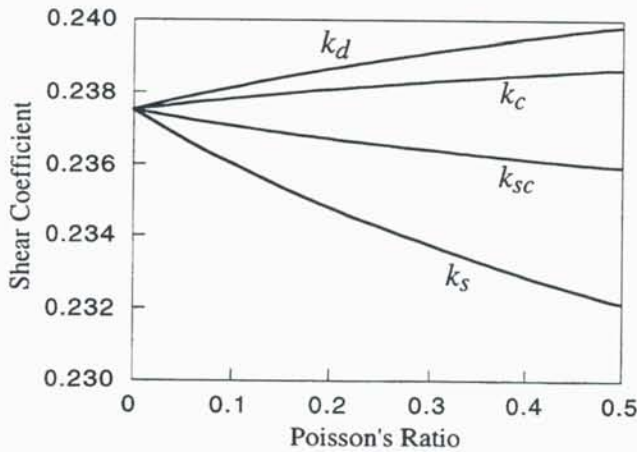


Figure 3. Shear Coefficient versus Poisson's Ratio for an I beam vibrating about its major principal axis ($m = 3, n = 3/4$).

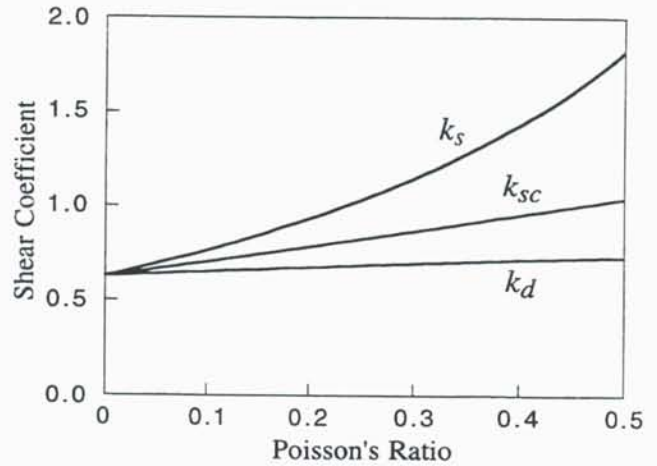


Figure 4. Shear Coefficient versus Poisson's Ratio for an I beam vibrating about its minor principal axis ($m = 1/3, n = 4/3$).

References

- [1] Timoshenko, S. P., 1921, "On the Correction for Shear of the Differential Equation for Transverse Vibrations of Bars of Prismatic Bars," *Philosophical Magazine*, Vol. 41, pp. 744-746.
- [2] Cowper, G. R., 1966, "The Shear Coefficient

in Timoshenko's Beam Theory," *ASME Journal of Applied Mechanics*, Vol. 33, pp. 335-340.

[3] Hutchinson, J. R., 2001, "Shear Coefficients for Timoshenko Beam Theory," *ASME Journal of Applied Mechanics*, Vol. 68, pp. 87-92

VIBRATION INSTABILITY IN CIRCULAR SAWS

Stanley G. Hutton
Department of Mechanical Engineering
University of British Columbia
Vancouver, B.C.
Canada

Abstract

A relatively common problem in the North American primary wood cutting industry (i.e. that part of the industry involved with the production of sawn lumber from logs), is the appearance of a "washboard" pattern on the surface of the wood. Such a pattern is characterized by a sinusoidal like variation in board thickness in both the cutting direction and normal to this direction. Figure 1 shows an example of such a pattern. (A similar phenomenon occurs in metal cutting and is referred to as "chatter" in that context.) In the wood industry, the resulting board thickness variations are subsequently removed by the planing process. This results in higher than necessary sawdust production. The physical mechanisms that give rise to the washboarding phenomenon have not been clearly identified and the problem is dealt with in the industry by trial and error.

The general problem to be solved is that of predicting the self-excited vibrations that are involved in the interaction between a rotating flexible circular saw and a work-piece. The aim of the present work is to present an analysis of the stability characteristics of the blade while subjected to cutting forces and to define those circumstances under which washboarding will occur.

In the dynamics of saw-blade cutting the cutting forces have traditionally been modeled as constant or pulsating in-plane edge forces. The force produced by flank cutting, which is likely the primary cause of the washboarding phenomenon, has been neglected in previous research. An analysis of the instability induced in a rotating saw by multiple moving regenerative cutting forces applied over a given space-fixed sector will be presented in this paper.

Figure 2 shows a diagrammatic representation of rotating circular saw-blade which cuts a work piece over a space-fixed sector. It can be seen from the sectional plot A-A that, if the blade oscillates laterally, there is an extra lateral cutting area between two successive teeth associated with both the transverse response $w(r_0, \theta_j, t)$ of the current tooth (the j th tooth) and the transverse response $w(r_0, \theta_j, t - T)$ of the previous tooth (the $(j-1)$ th tooth) at a given location (r_0, θ_j) on the work-piece. T is the tooth passing period (i.e., the period between successive tooth engagements). Lateral compression between the work-piece and the teeth in this extra cutting area causes the lateral cutting force $f_{cj}(t)$. This type of cutting force is called regenerative.

In actual cutting the saw blade will be subjected to radial and tangential in plane cutting forces as well as lateral forces. Exact modeling of such forces is difficult and is further complicated by the non-homogeneous nature of the wood. In this study the following assumptions are made:

- The only forces acting are lateral forces caused by flank cutting.
- The cutting forces are always normal to the undeformed plane of the saw.

- The cutting forces are a linear function of chip thickness .

Thus, the lateral regenerative cutting forces are assumed in the following linear form:

$$f_c(t) = \sum_{j=1}^{N_t} f_{c_j}(t) = - \sum_{j=1}^{N_t} (1/r) K_r [w(r, \theta, t) - w(r, \theta, t-T)] \delta(r-r_0) \delta(\theta-\theta_j) g(\theta_j) \quad (1)$$

where, N_t is the total number of saw teeth. K_r is a cutting force coefficient, assumed constant, which is determined by the geometry, properties and speeds of the blade, and by the characteristics of the work piece.

The deflection of the present and previous tooth at the location (r_0, θ_j) , respectively are given by:

$$w(r, \theta, t) \delta(r-r_0) \delta(\theta-\theta_j) = w(r_0, \theta_j, t)$$

$$\text{and } w(r, \theta, t-T) \delta(r-r_0) \delta(\theta-\theta_j) = w(r_0, \theta_j, t-T)$$

where $T = 2\pi / (\Omega N_t)$ and:

$$\theta_j = \theta_{st} + \Omega t + (j-1)\theta_p \quad (\theta_1 = \theta_{st} \text{ when } t = 0; \theta_p \text{ is the angular tooth pitch})$$

$$g_j(\theta_j) = 1 \text{ when } \theta_{st} < \theta_j < \theta_{ex} \text{ and } g_j(\theta_j) = 0 \text{ otherwise}$$

θ_{st}, θ_{ex} are the start and exit immersion angles of the cutting range, respectively.

The saw is modeled as an annular circular plate of inner radius a , outer radius b , and thickness h , rotating at a constant angular velocity Ω . The governing equation for transverse vibration in terms of the lateral displacement $w(r, \theta, t)$, with respect to space-fixed coordinates, can be written as:

$$D\nabla^4 w + \rho h (w_{,tt} + 2\Omega w_{,t\theta} + \Omega^2 w_{,\theta\theta}) + L_s(w) = L_n(w) + f_c(t)$$

where D and ρ are the flexural rigidity and mass density of the plate, respectively.

L_s is the membrane operator associated with the axisymmetric stress fields due to the centrifugal force and/or the stress tensioning. L_n is the membrane operator associated with the asymmetric stress fields generated by in-plane edge loads, such as in-plane cutting forces, which, under certain circumstances, may cause instability in such systems. In the present analysis the effect of L_n will be neglected. $f_c(t)$ represents the transverse cutting forces generated by the interaction between the saw-blade and the work-piece.

Substituting Equation (1) into the equation of motion of the rotating disc and applying the Galerkin procedure leads to an equation of motion in the form:

$$[M]\{\ddot{x}(t)\} + [G]\{\dot{x}(t)\} + [K]\{x(t)\} + (1-e^{-TD})[A(t)]\{x(t)\} = \{0\} \quad (2)$$

where, e^{-TD} is a time delay operator (i.e., $e^{-TD}\{x(t)\} = \{x(t-T)\}$). $[M]$, $[G]$ and $[K]$ represent the mass, gyroscopic and stiffness matrices, respectively, which may contain centrifugal stiffening and/or stress tensioning effects. $[A(t)]$ is a periodic (T) time-varying matrix associated with the cutting forces.

The Solution of Equation(2) leads to the prediction of unstable speed zones. A comparison will be made of the instabilities predicted and those that are measured experimentally.

The comparison with experimental results raises the question as to the influence of dissipative effects which have been neglected in the analysis conducted to date. The paper to be presented will address some of the issues that arise in this context



Figure 1 Wasboarding Pattern on a Sawn Board

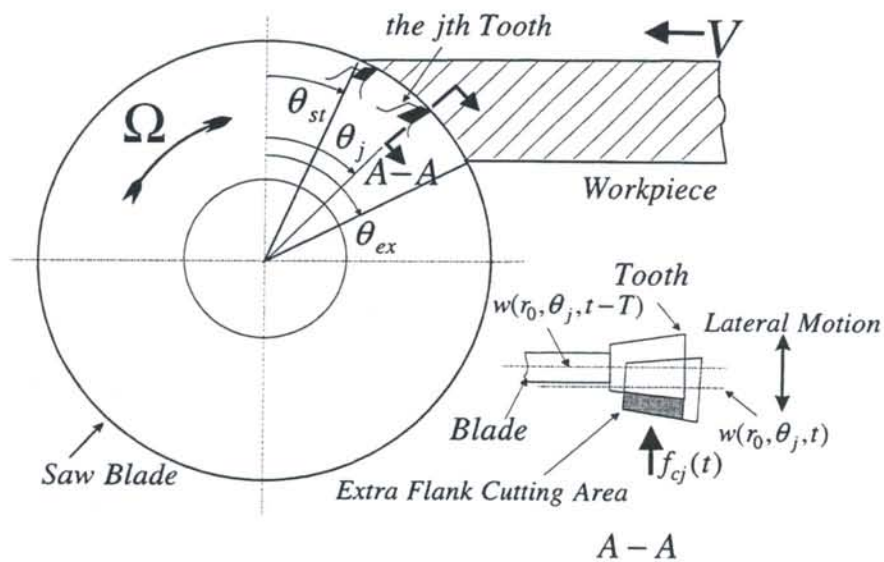


Figure 2 Lateral regenerative cutting force produced in a rotating circular saw

The Rayleigh-Ritz Method without Admissibility Requirements

S. Ilanko
Department of Mechanical Engineering
University of Canterbury
Christchurch
New Zealand

The Rayleigh-Ritz method is a well known and popular method of finding natural frequencies of continuous systems. The major drawback of this procedure has been the need to find admissible functions. For a totally unconstrained system this is not a problem as any continuous function would be admissible as there are no geometric constraints. However, such systems are not common, and for most practical problems, the functions used must be carefully chosen to satisfy the geometric constraint conditions. Since 1941 many researchers have attempted to overcome this problem [1-4], by replacing rigid constraints with artificial partial restraints having very high stiffness coefficients thus effectively causing them to become rigid constraints. This has proved to be a successful technique for finding the lower natural frequencies of continuous systems. A similar approach has also been used more recently to model connected systems [5-9] where the rigid connections are replaced by springs of very large stiffness.

One problem with such modelling is the determination of the magnitude of stiffness to be used in the analysis. In some of the publications, non-dimensional stiffness values of the order of 10^6 were found to be sufficient to calculate the first three natural frequencies of systems consisting of plates, beams and shells to three or more significant figures. However, it can be shown that for determining frequencies corresponding to higher modes, increasing values of stiffness would be needed to ensure that the results obtained are upper-bound estimates of the rigidly constrained system, and one needs to try several values of stiffness until convergence is observed. An interactive computer program to verify this is available at <http://www.geocities.com/ilanko/vibration.htm>. To the author's knowledge, no method for calculating the maximum possible error in modelling rigid constraints with restraints having very large positive stiffness has been reported.

This problem has now been overcome through the use of springs with negative stiffness. In a recent publication [10], results generated for two continuous system models were used to show that by using negative stiffness parameters for springs used in modelling rigid supports and/or joints one can obtain true upper-bound results for natural frequencies, and the difference between the results for systems with constraints modelled using positive and negative stiffness parameters give the maximum possible error due to the asymptotic modelling. A proof for the existence of natural frequencies of negatively or positively restrained systems, and their convergence towards the appropriately constrained systems has also been derived and is currently under review [11].

With these developments, the need to find admissible functions no longer exists and ways of improving the versatility of the Rayleigh-Ritz procedure for systems with irregular boundary conditions may prove to be a useful topic for research. For example, one could

consider whether clamped plates of any arbitrary shape can be analysed by starting with a larger rectangular plate but with continuous elastic foundation of very high stiffness covering all but the area of the plate. Alternatively, lateral and rotational constraints may be imposed on the boundary of an arbitrary shaped plate, and the strain energy of the plate calculated within the plate domain. It is possible that upper-bound estimates of any system may be obtained this way, but if the shapes are irregular some integration may have to be done numerically. The use of imaginary positive and negative restraints with very large magnitude of stiffness eliminates the need to find admissible functions when applying the Rayleigh-Ritz method for determining natural frequencies and modes of vibratory systems. Such asymptotic modelling may also prove to be useful in stress and stability analysis.

REFERENCES

1. R. Courant 1943 *Bulletin of the American Mathematical Society* **49**, 1-23. Variational methods for the solution of problems of equilibrium and vibration.
2. G.B. Warburton and S.L. Edney 1984 *Journal of Sound and Vibration* **95**, 537-552. Vibration of rectangular plates with elastically restrained edges.
3. D.G. Gorman 1989 *Journal of Applied Mechanics*, **56**, 839-899. A comprehensive study of the free vibration of rectangular plates resting on symmetrically-distributed uniform elastic edge supports.
4. C.S. Kim, P.G. Young and S.M. Dickinson 1990 *Journal of Sound and Vibration* **142**, 143-394. On the flexural vibration of rectangular plates approached by using simple polynomials in the Rayleigh-Ritz Method.
5. J. Yuan and S.M. Dickinson 1992 *Journal of Sound and Vibration* **153**, 203-216. On the use of artificial springs in the study of the free vibrations of systems comprised of straight and curved beams.
6. J. Yuan and S.M. Dickinson 1992 *Journal of Sound and Vibration* **159**, 39-55. The flexural vibration of rectangular plate systems approached by using artificial springs in the Rayleigh-Ritz method.
7. L. Cheng and J. Nicolas 1992 *Journal of Sound and Vibration* **155**, 231-247. Free vibration analysis of a cylindrical shell-circular plate system with general coupling and various boundary conditions.
8. J. Yuan and S.M. Dickinson 1994 *Computers and Structures* **53**, 327-334. Natural frequencies of circular and annular plates with radial or circumferential cracks.
9. H.P. Lee and T.Y. Ng 1994 *Applied Acoustics* **42**, 151-163. Natural frequencies and modes for the flexural vibration of a cracked beam.
10. S. Ilanko and S.M. Dickinson 1999 *Journal of Sound and Vibration* **219(2)**, 370-378. Asymptotic modelling of rigid boundaries and connections in the Rayleigh-Ritz Method, doi:10.1006/jsvi.1998.1847
11. S. Ilanko, Existence of natural frequencies of systems with imaginary Restraints and their convergence in asymptotic modelling.

Approximate Methods for the Vibration of Gyroscopic Continua

Rajesh K. Jha and Robert G. Parker

Department of Mechanical Engineering, The Ohio State University
(614) 688-3922, parker.242@osu.edu

Dynamic phenomena in spinning disks, spinning shafts, axially moving media, fluid conveying pipes, and other high-speed systems have led to considerable research on the vibration of gyroscopic systems. These are inherently continuous systems governed by one or more partial differential equations. Analytical solutions are difficult to find in general, and approximate methods are frequently used to obtain the natural frequency spectra and vibration modes. The most common approach has been Galerkin discretization of the configuration space equation of motion (that is, the governing equation for the displacement field) using the corresponding stationary system eigenfunctions. Parker's (1999) results for a moving string on elastic foundation demonstrate the radically incorrect eigenvalue predictions that this discretization basis can give at supercritical speeds. Also considering moving media, Wickert and Mote (1991) showed that use of the complex, speed-dependent eigenfunctions of a related gyroscopic system as basis functions can significantly improve eigenvalue predictions. This study, based on Jha and Parker (2000), presents a systematic analysis of the spatial discretization of gyroscopic continua vibration problems. The problem is examined from the perspectives of configuration and state space form discretizations, stationary versus moving system basis functions, and subcritical versus supercritical speed convergence. Configuration and state space discretizations are shown to yield markedly different results, and the limitations of each are discussed. The moving system eigenfunctions, which are generally thought to be the superior basis for gyroscopic continua problems, can experience potentially severe numerical problems due to their linear dependence. Furthermore, this basis is apparently incomplete at supercritical speeds. In fact, for the moving string problem no acceptable approach was found to analyze supercritical speeds, and published discretization results for such cases should be viewed with caution. While the examples focus on axially moving continua vibration, the findings apply to a broad range of unsolved problems for which discretization might be used. For instance, nonlinear effects that are crucial at high-speed lead to bifurcated, non-trivial equilibria; the results herein identify key issues for eigenvalue problem discretizations about such equilibria.

The linearized equation of motion for free vibration of a gyroscopic continuum is

$$Mw_{tt} + Gw_t + Kw = 0 \quad (1)$$

where M , G and K are linear, time-invariant differential operators and $w(P, t)$ is the displacement field. With the inner product $(u, v) = \int_P u \bar{v} dP$, M and K are self-adjoint while G is skew-self-adjoint. The eigenvalue problem obtained from $w(P, t) = u(P)e^{i\omega t}$ is

$$(-\omega^2 M + i\omega G + K)u = 0 \quad (2)$$

This is referred to as the *configuration space form* in this work. Alternatively, in accordance with Meirovitch (1974), and D'Eleuterio and Hughes (1984), (1) is written in state space form as

$$\mathbf{A}z_t + \mathbf{B}z = 0 \quad (3)$$

$$\mathbf{A} = \begin{bmatrix} M & 0 \\ 0 & K \end{bmatrix}, \quad \mathbf{B} = \begin{bmatrix} G & K \\ -K & 0 \end{bmatrix}, \quad \mathbf{z} = \begin{Bmatrix} w_t \\ w \end{Bmatrix} \quad (4)$$

With the inner product $(z_1, z_2) = \int_P z_1^T \bar{z}_2 dP$ defined on the state space, \mathbf{A} is self-adjoint and \mathbf{B} is skew-self-adjoint. The eigenvalue problem associated with (3) can be formulated in terms of two self-adjoint operator matrices \mathbf{C} and \mathbf{A} (Huseyin, 1976)

$$\mathbf{C} = \begin{bmatrix} iG & K \\ K & 0 \end{bmatrix}, \quad \mathbf{v} = \begin{Bmatrix} \omega u \\ u \end{Bmatrix} \quad (5)$$

$$(\mathbf{C} - \omega \mathbf{A})\mathbf{v} = 0 \quad (6)$$

This is referred to as the *state space form*. The second of (5) relates the state and configuration space eigenfunctions.

Two competing approaches are to apply Galerkin discretization to (2) or (6). While both represent the same dynamic system, discretization of these forms can lead to markedly different results. One must also choose the basis functions. Natural options are the real eigenfunctions for the corresponding stationary system or the complex, moving system eigenfunctions of a simpler, related gyroscopic continuum. Again, the differences in results are striking and call into question the conventional understanding that moving system eigenfunctions are superior bases. Because the configuration and state space discretizations are identical when stationary system bases are used, there are three options to consider: 1) configuration/state space discretizations using eigenfunctions of the stationary system, 2) configuration space discretization using eigenfunctions of a related gyroscopic system, and 3) state space discretization using eigenfunctions of a related gyroscopic system. Further considerations are the distinctly different behavior of these approaches at sub- and supercritical speeds and the nature of convergence (speed and monotonicity).

For sample results, consider the linearized, non-dimensional equation of motion for an axially moving string supported by a distributed elastic foundation

$$w_{tt} + 2\nu w_{xt} - (1 - \nu^2)w_{xx} + \kappa w = 0 \quad (7)$$

where κ is the stiffness density of the foundation. We apply both configuration space and state space discretizations to this problem using the eigenfunctions of the axially moving string as basis functions. Figure 1 compares the rates of convergence for the three approaches mentioned above. Considering first the moving string basis functions, the configuration space form clearly converges faster than the state space form. Note that state space predictions converge *non-monotonically* from *below*. Configuration space predictions always converge monotonically from above. None of the discretization approaches considered here yield correct (or even reasonable) eigenvalue estimates at supercritical speeds for this problem. Parker (1999) showed that spatial discretization at supercritical speeds using the *stationary* system eigenfunctions yields inaccurate and misleading results regardless of the number of terms used. Configuration space discretization using *moving* string eigenfunctions also predicts seriously inaccurate results including flutter instability that does not exist in the continuum model (Figure 2). The state space discretization is even more striking, predicting *infinite* supercritical eigenvalues.

Jha, R. K., and Parker, R. G., 2000, 'Spatial Discretization of Axially Moving Media Vibration Problems,' *ASME Journal of Vibration and Acoustics*, Vol. 122, pp. 290-294.

D'Eleuterio, G. M., and Hughes, P. C., 1984, 'Dynamics of Gyroelastic Continua,' *ASME Journal of Applied Mechanics*, Vol. 51, pp. 415-422.

Huseyin, K., 1976, 'Standard Forms of the Eigenvalue Problems Associated With Gyroscopic Systems,' *Journal of Sound and Vibration*, Vol. 45(1), pp. 29-37.

Meirovitch, L., 1974, 'A New Method of Solution of the Eigenvalue Problem for Gyroscopic Systems,' *AIAA Journal*, Vol. 12, pp. 1337-1342.

Parker, R. G., 1999, 'Supercritical Speed Stability of the Trivial Equilibrium of an Axially Moving String on an Elastic Foundation,' *Journal of Sound and Vibration*, Vol. 221(2), pp. 205-219.

Wickert, J. A., and Mote, C. D. Jr., 1991, 'Response and Discretization Methods for Axially Moving Materials,' *Applied Mechanics Reviews*, Vol. 44, pp. 279-284.

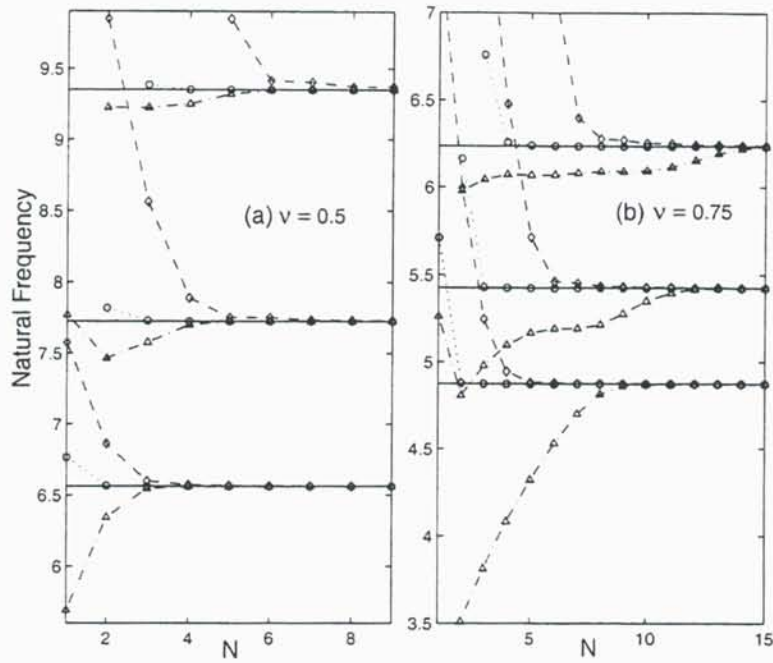


Figure 1: Discretization of an axially moving string on elastic foundation with $\kappa = 50$. Figures (a) and (b) show results for $\nu = 0.5$ and $\nu = 0.75$, respectively. (\diamond) - N terms of stationary string eigenfunctions, (\circ) - configuration space form using N complex conjugate moving string eigenfunction pairs, and (\triangle) - state space form with $2N$ complex conjugate moving string eigenfunction pairs. Horizontal solid lines denote exact eigenvalues.

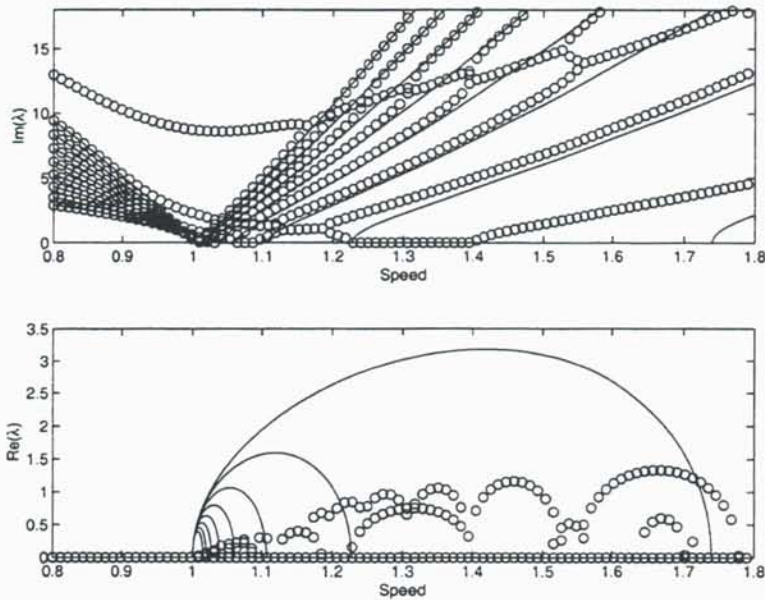


Figure 2: Configuration space discretization of an axially moving string on elastic foundation ($\kappa = 20$) showing incorrect flutter predictions. (\circ) denote eight cc pairs of moving string eigenfunctions and solid lines denote exact eigenvalues.

EQUIVALENCES BETWEEN TRANSCENDENTAL AND LINEAR EIGENVALUE PROBLEMS OF FREE STRUCTURAL VIBRATION

D. Kennedy

Cardiff School of Engineering, Cardiff University, Cardiff CF24 0YF, U.K.

F. W. Williams

Department of Building and Construction, City University of Hong Kong, Kowloon, Hong Kong

M.S. Djoudi

Cardiff School of Engineering, Cardiff University, Cardiff CF24 0YF, UK

S. Yuan

Department of Civil Engineering, Tsinghua University, Beijing 100084, P.R. China

INTRODUCTION

A companion paper¹ explains how the hypothetical, infinite order, finite element eigenvalue problem, which explicitly retains the infinite number of degrees of freedom between the joints (i.e. connection nodes) of the structure, can be reduced to the exactly equivalent finite order transcendental eigenvalue problem

$$\mathbf{K}(\lambda) \mathbf{D}_c = \mathbf{0} \quad (1)$$

where $\mathbf{D}_c \sin \omega t$ is the modal displacement vector of the freedoms at the joints and the dynamic stiffness matrix \mathbf{K} , which implicitly allows for the infinite number of degrees of freedom between joints, varies transcendently with $\lambda = \omega^2$. The natural frequencies ω can be calculated to any required accuracy using the Wittrick-Williams (WW) algorithm^{2,3} and usually correspond to singularities of \mathbf{K} (i.e. $|\mathbf{K}| = 0$), so that the corresponding mode shapes can be found, to somewhat less accuracy, by solving equation (1) with the null right-hand side replaced by a random force vector.⁴ Exceptional modes for which equation (1) is instead satisfied by $\mathbf{D}_c = \mathbf{0}$ can be found by the retrospective introduction of additional joints.⁵ Attempts to locate natural frequencies by following a plot of $|\mathbf{K}|$ fail to find those frequencies associated with modes for which $\mathbf{D}_c = \mathbf{0}$, and are also hindered by the presence of poles where $|\mathbf{K}|$ becomes infinite.

Recent preliminary work⁶⁻⁸ has identified the need to improve the accuracy of mode finding methods. This is the principal objective of a 3 year grant for collaboration between Cardiff and Tsinghua Universities (which commenced in January 2001) to explore analogies between transcendental eigensolutions and the numerous solution methods available for linear eigenproblems. This should lead to improved WW eigensolutions for civil⁹ and aerospace^{10,11} structures.



Figure 1. Rigidly connected two bar example. Boundary conditions: F = free; C = clamped.

2. SPECIAL CASES ILLUSTRATED BY SIMPLE BAR EXAMPLES

Analysis of the exact dynamic stiffness formulation for a uniform bar with one end free and the other end clamped (denoted F-C) shows that the natural frequencies occur when $|\mathbf{K}| = 0$. In contrast, the natural frequencies of a C-C bar occur when $\mathbf{D}_c = \mathbf{0}$ and coincide with those of a F-F bar, for which the previously neglected possibility of $|\mathbf{K}| \neq 0$ and $\mathbf{D}_c \neq \mathbf{0}$ occurs. All these natural frequencies and their mode shapes are found successfully using the WW algorithm with the random force vector method.

For the example of two rigidly connected bars shown in Figure 1, two special cases are identified where the properties of bars a and b are such that natural frequencies occur for which both $|\mathbf{K}| \neq 0$ and $\mathbf{D}_c \neq \mathbf{0}$. Although the WW algorithm successfully locates such eigenvalues, use of the random force vector method can lead to ill conditioning in the vicinity of these special cases so that incorrect mode shapes are found.

3. SOLUTION OF INFINITE ORDER EIGENVALUE PROBLEM BY MULTI-LEVEL SUBSTRUCTURING

Figure 2 illustrates a multi-level substructuring approach, in which uniform members of length $l/2^N$ are repeatedly "doubled up" using the WW algorithm¹² in order to assemble a uniform member of length l . At each of the levels $(N-1), (N-2), \dots, 0$, two members from the previous level are connected to form a structure with three collinear nodes and the freedoms at node 1 are eliminated to produce a new member connecting nodes 2 and 3. If exact dynamic stiffnesses are used for the member defined at level N , this procedure yields the exact transcendental stiffness matrix for the resulting member at level 0.

It is shown that the exact stiffnesses can also be obtained, to any required accuracy, by choosing N large enough and making appropriate finite element approximations at level N , for example using the usual static stiffness matrix and consistent mass matrix. This approach permits the calculation and normalization of the determinant of the stiffness matrix corresponding to the hypothetical, infinite order, eigenvalue problem referred to in the Introduction. The natural frequencies of the structure are all given by zeros of this determinant, which has no poles. It is believed that the development of this method will improve the calculation of natural frequencies and their mode shapes, and also assist in further transfers of technology from linear to transcendental eigensolution methods.

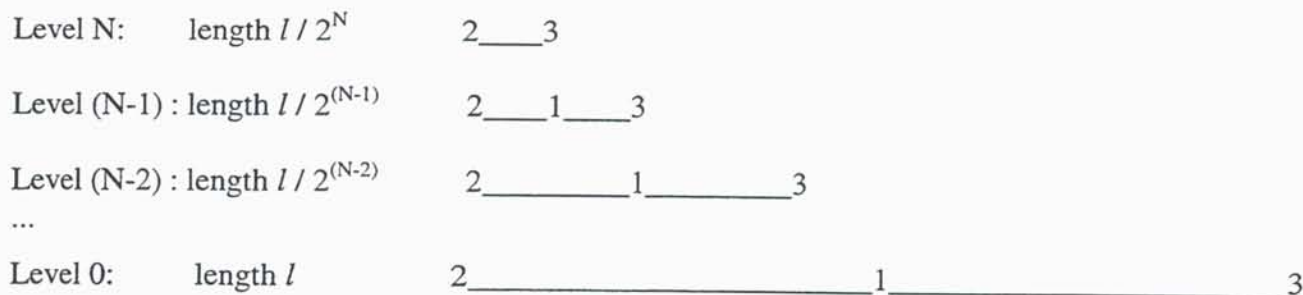


Figure 2. Assembly of a member of length l by substructuring to N levels.

ACKNOWLEDGEMENTS

This work is funded by the Engineering and Physical Sciences Research Council (grant GR/R05406/01) and the Royal Academy of Engineering.

REFERENCES

1. F.W. Williams, W.X. Zhong, W.P. Howson and A. Watson, Useful analogies with finding natural frequencies of structures from dynamic stiffness matrix formulations, *3rd International Symposium on Vibrations of Continuous Systems*, Grand Teton, WY, 2001 (to appear).
2. F.W. Williams and W.H. Wittrick, An automatic computational procedure for calculating natural frequencies of skeletal structures, *International Journal of Mechanical Sciences*, **12** (9), 1970, 781-791.
3. W.H. Wittrick and F.W. Williams, A general algorithm for computing natural frequencies of elastic structures, *Quarterly Journal of Mechanics and Applied Mathematics*, **24** (3), 1971, 263-284.
4. C.T. Hopper and F.W. Williams, Mode finding in non-linear structural eigenvalue calculations, *Journal of Structural Mechanics*, **5** (3), 1977, 255-278.
5. H.R. Ronagh, R. Lawther and F.W. Williams, Calculation of eigenvectors with uniform accuracy, *ASCE Journal of Engineering Mechanics*, **121** (9), 1995, 948-955.
6. S. Yuan, K.S. Ye and F.W. Williams, Towards exact computation of vibration modes in dynamic stiffness matrix methods, *5th International Symposium on Structural Engineering for Young Experts: Theories and Practices of Structural Engineering*, Shenyang, China, 1998, 11-19.
7. S. Yuan, K.S. Ye and F.W. Williams, From "random" to "precise": on exact computation of vibration modes in dynamic stiffness matrix methods, *2nd Symposium for Universities of Mainland China, Taiwan and Hong Kong area on Civil and Structural Engineering*, Taipei, Taiwan, 1998, 9-17.
8. F.W. Williams and S. Yuan, Calculating the modes from dynamic stiffness matrix analysis of piecewise continuous structures, *7th International Conference on Enhancement and Promotion of Computational Methods in Engineering and Science*, Macao, 1999, 89-99.
9. W.P. Howson, J.R. Banerjee and F.W. Williams, Concise equations and program for exact eigensolutions of plane frames including member shear, *Advances in Engineering Software*, **5** (3), 1983, 137-141.
10. M.S. Anderson and F.W. Williams, BUNVIS-RG: exact frame buckling and vibration program, with repetitive geometry and substructuring, *Journal of Spacecraft and Rockets*, **24** (4), 1987, 353-361.
11. F.W. Williams, D. Kennedy, R. Butler and M.S. Anderson, VICONOPT: program for exact vibration and buckling analysis or design of prismatic plate assemblies, *AIAA Journal*, **29** (11), 1991, 1927-1928.
12. F.W. Williams, Natural frequencies of repetitive structures, *Quarterly Journal of Mechanics and Applied Mathematics*, **24** (3), 1971, 285-310.

Reduced-Order Model for Nonlinear Vibration Analysis Using the Finite-Element Method

Yukinori KOBAYASHI, Gen YAMADA and Akira HARADA
Division of Mechanical Science, Hokkaido University, Sapporo, 060-8628 Japan

INTRODUCTION

There are many researches based on the finite element method (FEM) that takes geometrical nonlinearity into account, such as Rao *et al.*[1]. Recently Ribeiro and Petyt[2][3] used the hierarchical finite element method in order to possess an accurate spatial model with a small number of d.o.f. Iwatsubo *et al.*[4] used the substructure synthesis method to reduce the order of the nonlinear finite element model. But they have simplified the nonlinear model roughly so that there is a limitation of application. By using FEM, we can obtain the solution under any kinds of boundary conditions. It is however difficult to know the physical meaning of the solution. In this paper, the nonlinear finite element model is reduced by using the procedure of the modal analysis. Considering dominant modes on the nonlinear vibration, we can obtain accurate results using a few modes that are selected properly. The present method is applied to the nonlinear vibration of a straight beam and numerical results are shown in figures and tables.

ANALYSIS

Considering geometrical nonlinearity, finite element formulation is generally expressed as

$$[\mathbf{M}] \{\ddot{\mathbf{V}}\} + ([\mathbf{K}_1] + [\mathbf{K}_2(\mathbf{V})] + [\mathbf{K}_3(\mathbf{V}, \mathbf{V})]) \{\mathbf{V}\} = \{\mathbf{F}\}. \quad (1)$$

where $[\mathbf{M}]$, $[\mathbf{K}_1]$ and $[\mathbf{K}_i]$ ($i = 2, 3$) are, respectively, mass, linear stiffness and nonlinear stiffness matrices. $\{\mathbf{V}\}$ and $\{\mathbf{F}\}$ are node value and force vectors, respectively. Matrix $[\mathbf{K}_2]$ depends on $\{\mathbf{V}\}$ linearly, $[\mathbf{K}_3]$ depends on $\{\mathbf{V}\}$ quadratically.

Consider harmonic excitation and the response of fundamental harmonics, equation (1) can be rewritten as

$$(-\omega^2 [\mathbf{M}] + [\mathbf{K}_1] + [\mathbf{K}_2(\mathbf{V})] + [\mathbf{K}_3(\mathbf{V}, \mathbf{V})]) \{\mathbf{V}\} = \{\mathbf{F}\}. \quad (2)$$

Eigenvalue equation of the linear free vibration is given by

$$(-\omega^2 [\mathbf{M}] + [\mathbf{K}_1]) \{\mathbf{V}\} = 0. \quad (3)$$

Using a modal co-ordinate vector $\{\xi\}$ and the modal matrix $[\phi]$ which consists of eigenvectors of equation (3), the node value vector $\{\mathbf{V}\}$ is assumed to have the form

$$\{\mathbf{V}\} = [\phi] \{\xi\}. \quad (4)$$

Substituting equation (4) into equation (1) results in

$$[\mathbf{M}] [\phi] \{\ddot{\xi}\} + ([\mathbf{K}_1] + [\mathbf{K}_2(\xi)] + [\mathbf{K}_3(\xi)]) [\phi] \{\xi\} = \{\mathbf{F}\}. \quad (5)$$

Multiplying equation (5) by $[\phi]^T$, we obtain

$$[\mathbf{m}] \{\ddot{\xi}\} + ([\mathbf{k}] + [\mathbf{K}_{m2}(\xi)] + [\mathbf{K}_{m3}(\xi, \xi)]) \{\xi\} = [\phi]^T \{\mathbf{F}\} \quad (6)$$

or

$$(-\omega^2 [\mathbf{m}] + [\mathbf{k}] + [\mathbf{K}_{m2}(\xi)] + [\mathbf{K}_{m3}(\xi, \xi)]) \{\xi\} = [\phi]_s^T \{\mathbf{F}\}, \quad (7)$$

where

$$\begin{aligned} [\mathbf{m}] &= [\phi]^T [\mathbf{M}] [\phi], \quad [\mathbf{k}] = [\phi]^T [\mathbf{K}_1] [\phi], \\ [\mathbf{K}_{m2}(\xi)] &= [\phi]^T [\mathbf{K}_2(\xi)] [\phi], \quad [\mathbf{K}_{m3}(\xi, \xi)] = [\phi]^T [\mathbf{K}_3(\xi, \xi)] [\phi]. \end{aligned} \quad (8)$$

RESULTS AND DISCUSSION

Though we can obtain results by numerical integration of equation (1), it takes a lot of computation time. It is desirable to obtain the accurate results from equation (6) using modes as few as possible. Nonlinearity of an out-of-plane mode of continuous systems comes from the coupling with some in-plane modes because of geometrical nonlinearity. It is expected that one of in-plane modes is dominantly affected on the corresponding out-of-plane mode. If we can find the combination of out-of-plane and in-plane modes, accurate results are obtained by using only two modes.

We investigate about the nonlinear response of a clamped-clamped beam around the fundamental natural frequency in detail. Table 1 shows the specification of the beam treated here. To obtain the nonlinear response of the fundamental mode, we use the fundamental out-of-plane mode and an in-plane mode in equation (6). In order to determine the using in-plane mode, we examine the qualitative effect of the mode by applying Newton-Raphson method to equation (7) in advance. When we apply Newton-Raphson method to equation (7), vector $\{\xi\}$ is treated as constant for each frequency. Though this procedure is not exact because vector $\{\xi\}$ is dependent of time, it is enough accurate to know the effect of in-plane mode on the nonlinear vibration and we can save computation time very much.

When we use one of in-plane modes ξ and one of out-of-plane modes η , equation (6) is rewritten in the form

$$\begin{bmatrix} m_i & 0 \\ 0 & m_o \end{bmatrix} \begin{Bmatrix} \ddot{\xi} \\ \ddot{\eta} \end{Bmatrix} + \left(\begin{bmatrix} k_{1i} & 0 \\ 0 & k_{1o} \end{bmatrix} + \begin{bmatrix} 0 & k_2\eta \\ 2k_2\eta & k_3\eta^2 \end{bmatrix} \right) \begin{Bmatrix} \xi \\ \eta \end{Bmatrix} = \begin{Bmatrix} 0 \\ f \end{Bmatrix}. \quad (9)$$

Neglecting the in-plane inertia and eliminating ξ from equation (9), we obtain

$$m\ddot{\eta} + k\eta + \beta\eta^3 = f, \quad (10)$$

where

$$m = m_o, \quad k = k_{1o}, \quad \beta = k_3 - 2\frac{k_2^2}{k_{1i}}. \quad (11)$$

Equation (10) is thought to be equivalent to Duffing equation. Figure 1 shows frequency resonance functions (FRF) obtained by the single-mode analysis and two-mode analysis by using the fundamental out-of-plane mode and an in-plane mode. Numbers i in the figure denote the order of the in-plane mode ξ_i that is used in the calculation as well as the fundamental out-of-plane mode η_1 . In the case of $i=0$, the in-plane mode is not used. The results obtained by present method show nonlinearity stronger than that by the nonlinear FEM (NLFEM). But the result using ξ_4 makes good agreement with NLFEM because the in-plane mode shape of ξ_4 is similar to the actual in-plane displacement. We can obtain good results by using a suitable

Table 1: Specification of the beam

Length	0.313[m]
Width	30.5×10^{-3} [m]
Height	0.6×10^{-3} [m]
Young's Modulus	210[GPa]
Density	7870[kg/m ³]
Number of Element	100

Table 2: Coefficients of equation (10)

	Yamaki <i>et al.</i> [5]	present
m	1.7873×10^{-2}	1.7873×10^{-2}
k	7.4615×10^2	7.4617×10^2
β	1.4909×10^9	1.5336×10^9

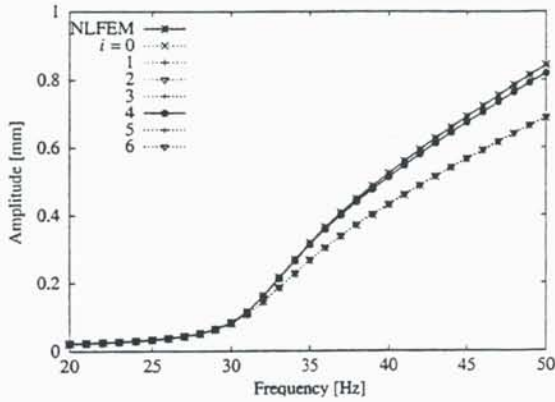


Figure 1: FRF obtained by FEM, single-mode(η_1) and two-mode($\eta_1 + \xi_i : i = 1, 2, \dots, 6$) analyses.

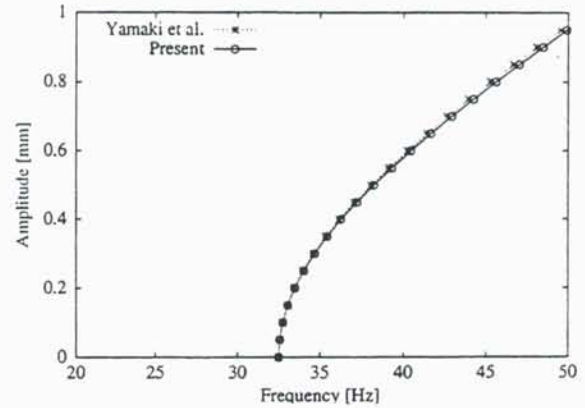


Figure 2: Comparison between the backbone curve obtained by the present method and that by Yamaki *et al.*[5].

in-plane mode that has a similar distribution to the actual in-plane displacement. On this calculation, $\eta_1 + \xi_4$ is the best combination of the mode. Figure 2 shows that the backbone curve obtained by the present method, equation (10), makes good agreement with the backbone curve obtained analytically by Yamaki *et al.*[5]. Table 2 shows the coefficients of equation (10) obtained by the present method and those by Yamaki *et al.* As seen in the table, the coefficient of nonlinear term β is approximated very well by the present method.

CONCLUSIONS

In this paper, a single d.o.f. model for the steady-state vibration of a uniform, slender beam with the geometrical nonlinearity is obtained by using FEM with modal co-ordinates. If we choose a suitable in-plane mode, results by the present method have enough accuracy. The present method may be extended to the nonlinear vibration analysis of continuous systems under any kinds of boundary conditions and then we can derive the low order Duffing type equations on dominant modes.

REFERENCES

- [1] Rao, G. V., Raju, I. S., and Raju, K. K., (1979) Finite Element Formulation for Large Amplitude Free Vibrations of Beams and Orthotropic Circular Plates, *Computer and Structures*, **6**, 169-172.
- [2] Ribeiro, P., and Petyt, M., (1999) Nonlinear Vibration of Beams with Internal Resonance by Hierarchical Finite-Element Methods, *J. Sound Vib.*, **224**(4), 591-624.
- [3] Ribeiro, P., and Petyt, M., (1999) Nonlinear Vibration of Plate by Hierarchical Finite Element and Continuation Methods, *Int. J. Mech. Sci.*, **41**, 437-459.
- [4] Iwatsubo, T., Kawamura, S., and Moon, B., (1998) Non-Linear Vibration Analysis of Rotor System Using Substructure Synthesis Method (Analysis with Consideration of Non-Linearity of Rotor), *JSME Int. J.*, **41**(4), C, 727-733.
- [5] Yamaki, N., and Mori, A., (1980) Non-Linear Vibration of a Clamped Beam with Initial Deflection and Initial Axial Displacement, Part I: Theory, *J. Sound Vib.*, **71**(3), 333-346.

Responses of Nonlinear Asymmetric Forced Vibrations of a Circular Plate

M. H. YEO and W. K. LEE

School of Mechanical Engineering, Yeungnam University
Gyongsan 712-749, Korea

A clamped circular plate experiences mid-plane stretching when deflected. The influence of this stretching on the dynamic response increases with the amplitude of the response. This situation can be described with nonlinear strain-displacement equations and a linear stress-strain law which give us the dynamic analogue of the von Karman equations with geometric nonlinearity. Nonlinear dynamic responses of a clamped circular plate subjected to harmonic excitations have been investigated by two approaches. The one is to include symmetric vibrations and the other asymmetric vibrations. For symmetric responses, Sridhar et al. [1] and Hadian and Nayfeh [2] studied primary resonance of a circular plate with three-mode interaction. Lee and Kim [3] studied combination resonance of the plate. In these studies the steady-state response can only have the form of a standing wave.

For asymmetric responses, Sridhar et al. [4] considered four-mode interaction of a circular plate shown in Fig. 1. They expected that the steady-state response can only have the form of standing wave unless the frequency of excitation is near the highest frequency involved in the internal resonance. In this case, they concluded that it is possible for a traveling wave component of the highest mode to appear in the steady-state response. They, however, didn't present any illustration on the responses by using numerical example.

After examining their work, we found that they had misderived the solvability conditions in applying the method of multiple scales. We corrected therefore their solvability conditions (31) in [4] as follows:

$$\begin{aligned}
 & -2i\omega_{kl}(D_1 A_{kl} + c_{kl} A_{kl}) + A_{kl} \left\{ \sum_{n=-\infty}^{\infty} \sum_{m=1}^{\infty} \gamma_{klnm} (A_{nm} \bar{A}_{nm} + B_{nm} \bar{B}_{nm}) - \gamma_{klkl} A_{kl} \bar{A}_{kl} \right\} \\
 & + 2(1 - \delta_{k0}) B_{kl} \left\{ \sum_{m=1}^{\infty} \hat{\gamma}_{klkm} A_{km} \bar{B}_{km} - \hat{\gamma}_{klkl} A_{kl} \bar{B}_{kl} \right\} + N_{kl}^A + R_{kl}^A = 0
 \end{aligned} \tag{1a}$$

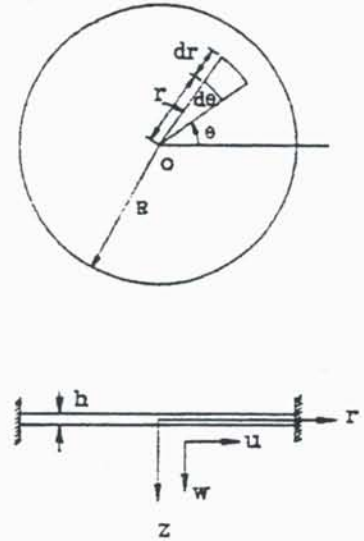


Fig. 1 A schematic diagram of a clamped circular plate

$$2i\omega_{kl}(D_1 \bar{B}_{kl} + c_{kl} \bar{B}_{kl}) + \bar{B}_{kl} \left\{ \sum_{n=-\infty}^{\infty} \sum_{m=1}^{\infty} \gamma_{kinm} (A_{nm} \bar{A}_{nm} + B_{nm} \bar{B}_{nm}) - \gamma_{klkl} B_{kl} \bar{B}_{kl} \right\} \\ + 2(1 - \delta_{k0}) \bar{A}_{kl} \left\{ \sum_{m=1}^{\infty} \hat{\gamma}_{klkm} A_{km} \bar{B}_{km} - \hat{\gamma}_{klkl} A_{kl} \bar{B}_{kl} \right\} + N_{kl}^B + R_{kl}^B = 0 \quad (1b)$$

where, $R_{kl}^{A,B}$ are terms due to internal resonances, if any, $N_{kl}^{A,B}$ are terms due to the external resonance, if any, and γ_{kinm} and $\hat{\gamma}_{kinm}$ are constants.

In this study we consider a primary resonance in the absence of internal resonance. The frequency of excitation λ is near natural frequency ω_{11} (=21.2604) corresponding to the mode with one nodal diameter and no other nodal circle but the boundary. We introduce a detuning parameter, σ , defined as follows:

$$\lambda = \omega_{11} + \varepsilon\sigma, \quad (2)$$

where ε is a small parameter. In this case equations (1) give a system of four autonomous ordinary differential equations for amplitudes and phases as follows:

$$a_{11}' = -c_{11}a_{11} + \frac{P_{11}}{4\omega_{11}} \sin \mu_{11}^a, \quad b_{11}' = -c_{11}b_{11} + \frac{P_{11}}{4\omega_{11}} \sin \mu_{11}^b \quad (3a, b)$$

$$a_{11}\mu_{11}^{a'} = \sigma a_{11} + \frac{\gamma_{1111}}{8\omega_{11}} a_{11}(a_{11}^2 + 2b_{11}^2) + \frac{P_{11}}{4\omega_{11}} \cos \mu_{11}^a = 0 \quad (3c)$$

$$b_{11}\mu_{11}^{b'} = \sigma b_{11} + \frac{\gamma_{1111}}{8\omega_{11}} b_{11}(b_{11}^2 + 2a_{11}^2) + \frac{P_{11}}{4\omega_{11}} \cos \mu_{11}^b = 0 \quad (3d)$$

The steady-state solution is given by equations (3) when $a_{kl}' = b_{kl}' = \mu_{11}^{a'} = \mu_{11}^{b'} = 0$. Then the steady-state response can be written as follows:

$$w = \phi_{11} \{ a_{11} \cos(\lambda t - \mu_{11}^a + \theta + \tau_{11}) + b_{11} \cos(\lambda t - \mu_{11}^b - \theta - \tau_{11}) \} + O(\varepsilon), \quad \text{or} \quad (4a)$$

$$w = Z_1 \cos(\lambda t + \varepsilon_1) \phi_{11}(r) \cos \theta + Z_2 \cos(\lambda t + \varepsilon_2) \phi_{11}(r) \sin \theta + O(\varepsilon), \quad (4b)$$

which is the superposition of two traveling waves. This response gives traveling wave unless $a_{11} = b_{11}$ and $\mu_{11}^a = \mu_{11}^b$. When $a_{11} = b_{11}$ and $\mu_{11}^a = \mu_{11}^b$, the form can be reduced to the standing wave of the form

$$w = 2\phi_{11} a_{11} \cos(\lambda t - \mu_{11}^a) \cos(\theta + \tau_{11}) + O(\varepsilon), \quad (5)$$

which is similar to the natural mode corresponding to ω_{11} .

In Fig. 2 the amplitudes a_{11} , b_{11} are plotted as functions of detuning parameter $\varepsilon\sigma$ when $\{\nu, \varepsilon, \varepsilon c, \varepsilon P_{11}\} = \{1/3, 0.001067, 0.01, 8\}$. Branches SS1, SS2, US1, and US2 represent the standing waves, while branches ST1, UT1, and UT2 represent traveling waves. Solid and dotted lines denote, respectively, stable and unstable responses. Except for the instability of branch US1, the response in the form of standing wave is essentially that of Duffing equation. The stable response in the form of traveling wave, $\{ST1_A, ST1_B\}$ represents $\{a_{11}, b_{11}\}$ or $\{b_{11}, a_{11}\}$. When $\varepsilon\sigma < 0.025$ and

$0.025 < \varepsilon\sigma < 0.095$, respectively, standing and traveling waves exist in reality. While standing and traveling waves coexist when $0.095 < \varepsilon\sigma < 0.42$, standing wave only exists when $0.42 < \varepsilon\sigma$. This result is remarkably different from one by Sridhar et al. [4]. They expected that the response is in the form of standing wave, which is that of Duffing equation. We believe that this difference comes from the correction of solvability conditions.

Acknowledgment: This research was supported by the Yeungnam University research grants in 2000.

References

- [1] Sridhar, S. Mook, D. T. and Nayfeh, A. H., 1975, *Journal of Sound and Vibration*, 41(3), 359-373, Non-Linear Resonances in the Forced Responses of Plates, Part I: Symmetric Responses of Circular Plates.
- [2] Hadian, J. and Nayfeh, A. H., 1990, *Journal of Sound and Vibration*, 142(2), 279-292, Modal Interaction in Circular Plates.
- [3] Lee, W. K. and Kim, C. H., 1995, *ASME Journal of Applied Mechanics*, 62, 1015-1022, Combination Resonances of a Circular Plate with Three-Mode Interaction.
- [4] Sridhar, S. Mook, D. T. and Nayfeh, A. H., 1978, *Journal of Sound and Vibration*, 59(2), 159-170, Non-Linear Resonances in the Forced Responses of Plates, Part II: Asymmetric Responses of Circular Plates.

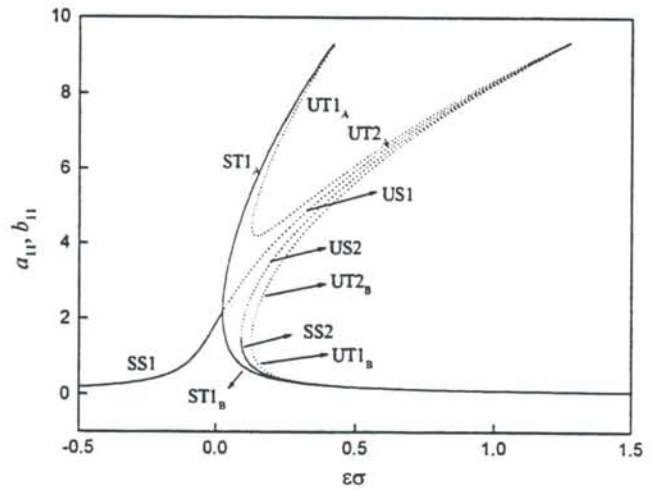


Fig. 2 Variations of the amplitudes with detuning parameter $\varepsilon\sigma_2$ when $\varepsilon P_{22}=8$. —, stable; - - -, unstable.

Exact Solutions for the Free Vibrations of Rectangular Plates with Linearly Varying In-Plane Loading

Arthur W. Leissa
Professor Emeritus
Ohio State University
Columbus, Ohio USA

Hundreds of research papers have been published on the free vibrations of rectangular plates, and dozens of them consider the effects of static, in-plane stresses applied while the plate is vibrating. However, almost all of these deal with the situation when the in-plane loading causes uniform normal stresses (tensile or compressive) throughout the plate. The few results (frequencies and mode shapes) that have been presented for nonuniform loadings have been obtained by approximate procedures, such as the Ritz method.

Consider a rectangular plate which is subjected to a linearly varying normal stress along two opposite edges, $x = 0$ and $x = a$, as shown in Fig. 1. The stress (σ_x) causes in-plane stress resultants, $N_x = \sigma_x h$ (force/length), which may be written as

$$N_x = -N_0(1 - \alpha y/b) \quad (1)$$

where N_0 is the intensity of the compressive force at the edge $y = 0$ and α is an arbitrary constant. Assuming the in-plane shear stress to be zero along $x = 0, a$ and that no stresses act upon the other two plate edges ($y = 0, b$), one easily sees that the exact solution of the plane elasticity problem is that the normal stress σ_x varies as Eq. (1) throughout the plate, and the other two stress components (σ_y and τ_{xy}) are zero everywhere.

Using this stress field in the transverse equation of motion for the plate yields a partial differential equation having coefficients which vary with x . An exact solution of this equation may be obtained as

$$w(x, y, t) = Y(y) \sin(m\pi x/a) \sin \omega t \quad (2)$$

where w is the transverse displacement, Y is a function only of y , m is an integer, and ω is a natural frequency. Such a displacement function yields zero w and zero out-of-plane bending moment (M_x) along the edges $x = 0, a$. That is, these edges are hinged or supported by knife edges (i.e., simply supported).

Substituting Eq. (2) into the equation of motion results in an ordinary differential equation in $Y(y)$ having a coefficient which varies linearly with y . An exact solution of it is obtained by the classic method of Frobenius, which assumes an infinite power series function for Y . This results in four independent coefficients of the power series for the lowest degree terms, with the higher degree coefficients obtained from them by recursion relations. Having an exact solution to the governing differential equation, this is applied to the two remaining plate edges ($y = 0$ and b) with appropriate boundary conditions (clamped, simply supported, or free) to yield a standard eigenvalue problem for the nondimensional frequencies, requiring finding the roots of a fourth order characteristic determinant.

Extensive results have been obtained for all possible combinations of edge conditions at $y = 0, b$, and for several useful and interesting values of α in Eq. (1), as depicted by the in-plane edge loads shown in Fig.2. As shown there, as α varies from 0 to 2, the edge loading varies from being uniform to a pure in-plane moment (i.e., couple) at the edges $x = 0, a$. Frequency data and some interesting mode shapes are presented in Ref.1 for SS-F-SS-F plates having in-plane end moments ($\alpha = 2$) acting.

One finds that the convergence of the power series is erratic, and a rather large number of terms must be used to obtain accurate frequencies. This is demonstrated by convergence tables for frequencies. Changes in frequency due to increasing end loads are examined for all nine distinct combinations of clamped, simply supported and free conditions along the unloaded edges, especially for the case of in-plane moment loading ($\alpha = 2$). It is found that for three of these nine cases, in-plane moments cause increases in the fundamental frequencies. Some interesting mode shapes are also exhibited.

1. Kang, J.-H. and Leissa, A.W. (2001). Vibration and buckling of rectangular plates loaded at two simply supported opposite edges by in-plane moments, free along the other two edges. *International Journal of Structural Stability and Dynamics* (to appear).

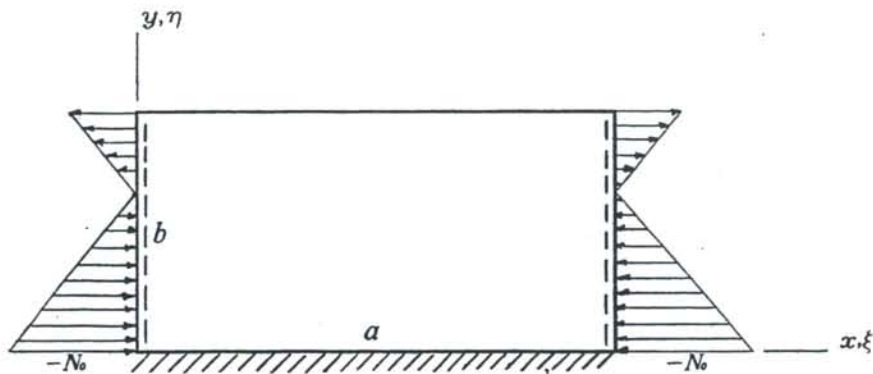


FIG. 1. An SS-C-SS-F Rectangular Plate Loaded by Linearly Varying In-Plane Stresses, with Coordinate Convention.

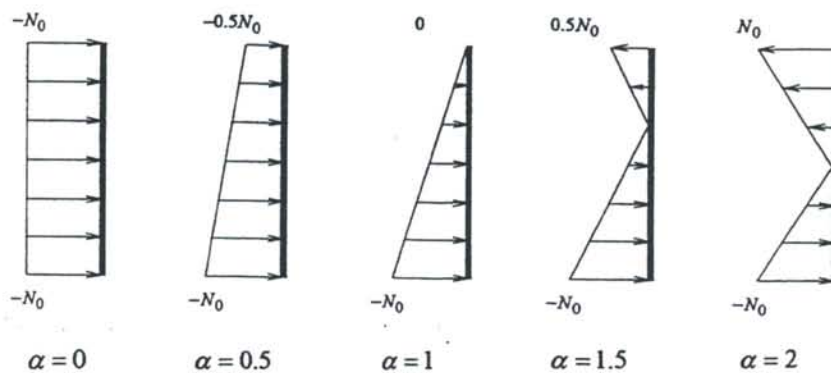


FIG. 2. Examples of In-Plane Loading N_x along the Edge $x=0$

Development of Fourier- p Shape Functions For Vibration of Plates

C. W. Lim, and A. Y. T. Leung

Department of Building and Construction, City University of Hong Kong,

Tat Chee Avenue, Kowloon, Hong Kong

bccwlim@cityu.edu.hk, Andrew.Leung@cityu.edu.hk

Abstract

A new approach is presented to incorporate the commonly well-behaved Fourier series with polynomials in representing the shape functions for vibration of plates using the Ritz Method. It significantly improves (i) *accuracy* and (ii) *convergence* of the common Ritz method using polynomials as shape functions. As polynomials tends to induce numerical instability, ill-conditioning and insolvability, the development of this Fourier- p Ritz approach helps to resolve these problems. Exhausting numerical computation can also be alleviated.

Introduction

Plate and shell structures have been widely used as engineering design components in civil, structural, mechanical, aerospace and building constructions. Although the finite element method (FEM) has been a useful numerical method in analyzing the engineering behaviour of these structures, other numerical methods has also been of much interest especially at a research level. Among them are the Ritz method and Galerkin method which are often the basis of finite element formulation.

Over years of research and development, researchers had found that the Ritz method is a powerful tool for the vibration analysis of plate structures. However it is very difficult to find exact solutions having an admissible shape function that satisfies both the geometric and natural boundary conditions except for plates with opposite sides simply supported (Leissa, 1969, 1973). Although polynomial admissible functions for plates with opposite sides clamped are available (Lim and Liew, 1994), these polynomials functions do not satisfy the governing differential equation and thus do not render exact solutions. Thus a number of polynomial terms have to be included in the numerical Ritz method to obtain converged solutions. Very frequently these approximate methods, including FEM, using polynomials as shape functions run into numerical insolvabilities, or yields suspicious results due to numerical instability and ill-conditioning. Users of the FE packages may face difficulties in justifying the FE solutions.

In an attempt to remedy the shortcomings of polynomial shape functions, a Fourier- p Ritz approach for vibration of plates is proposed here. It is based on the concept of Leung (1979) where the standard beam FE was enriched by means of eigenfunctions and

increased accuracy was predicted before the name p -version was used by Babuska *et al.* (1981). This involves the integration of products of polynomials and beam functions. Although closed form integration formulae can be found (Leung, 1990), the complexity increased rapidly when the products of beam functions are involved in nonlinear analysis. The product of polynomials and Fourier series is introduced here is to construct the shape function in plate vibration analysis (Leung and Chan, 1998). Because Fourier series are well behaved, the limitation caused by numerical instability, ill-conditioning and insolvability using polynomial functions disappears. When applied to the free vibration analysis of plates, solutions converge much faster than when using polynomials alone.

References

- Babuska, I, B.A. Szabo and I.N. Katz (1981), "The p -version of the finite element method," *SIAM Journal on Numerical Analysis*, **18**, 515-545.
- Leissa, A.W., (1969), *Vibration of plates*, NASA SP-160.
- Leissa, A.W., (1973), "The free vibration of rectangular plates," *Journal of Sound and Vibration*, **31**(3), 257-293.
- Leung, A.Y.T. (1979), "An accurate method of dynamic substructuring with simplified computation," *International Journal for Numerical Methods in Engineering*, **14**, 1241-1256.
- Leung, A.Y.T. (1990), "Recurrent integration of beam functions", *Computers and Structures*, **37**, 277-282.
- Leung, A.Y.T. and J.K.W. Chan (1998), "Fourier p -element for the analysis of beams and plates", *Journal of Sound and Vibration*, **212**(1), 179-185, 1998.
- Lim, C.W. and K.M. Liew (1994), "A pb -2 Ritz formulation for flexural vibration of shallow cylindrical shells of rectangular planform," *Journal of Sound and Vibration*, **173**(3), 343-375.
- Lim, C.W. and K.M. Liew (1995), "Vibrations of perforated plates with rounded corners," *ASCE Journal of Engineering Mechanics*, **121**(2), 203-213.
- Lim, C.W (1999), "Three dimensional vibration analysis of a cantilevered parallelepiped: Exact and approximate solutions, *Journal of the Acoustical Society of America*, **106**(6), 3375-3383.
- Rao, J.S. (1999), *Dynamics of Plates*, Narosa Publishing House, New Delhi.

Chaotic Oscillations of a Cylindrical Shell-Panel with Concentrated Mass under Gravity and Cyclic Load

Ken-ichi NAGAI, Takao YAMAGUCHI

Department of Mechanical Engineering,
Gunma University, 1-5-1 Tenjincho, Kiryu, Gunma, 376-8515, JAPAN
nagai@eng.gunma-u.ac.jp, yamagme4@me.gunma-u.ac.jp

Takeshi MURATA

Matsushita Refrigeration Co.,Ltd., Osaka, JAPAN

1. Introduction

Both analytical and experimental results are presented for chaotic oscillations of a shallow cylindrical shell-panel carrying a concentrated mass. The shell with square boundary is simply supported along all edges. In-plane displacement of the shell is elastically constrained at the edges. Concentrated mass is located at the center of the shell. The shell is subjected to gravitational and cyclic acceleration. The Donnell type equation is used with modification of a lateral inertia force. Assuming a solution of multiple modes of vibration, nonlinear coupled differential equations are reduced by the Galerkin procedure. Chaotic responses are obtained by numerical integration. Experiment is conducted to reinforce the analytical results. Frequency response curves are measured where chaotic responses are generated. The chaotic response are testified by the Fourier spectrum, the Poincaré map and the maximum Lyapunov exponent. The maximum Lyapunov exponent of the experiment is compared with the results of analysis. Fairly well agreements are obtained, moreover, the chaos of the shell involves four modes of resonance vibration simultaneously.

2. Governing Equation of Motion

As shown in Figure 1, shell with Young's modulus E , Poisson's ratio ν and mass density ρ is excited laterally by acceleration $g + a_d \cos \Omega t$. g is gravitational acceleration, a_d and Ω are exciting amplitude and frequency, respectively. Denoting w , w_0 and f as the non-dimensional total deflection, initial deflection and stress function, the non-dimensional governing equation is given by

$$[1 + \gamma \delta(\xi - \xi_1) \delta(\eta - \eta_1)] w_{,\tau\tau} + \nabla^4 (w - w_0) - \alpha f_{,\xi\xi} - \beta^2 (f_{,\xi\xi} w_{,\eta\eta} - 2f_{,\xi\eta} w_{,\xi\eta} + f_{,\eta\eta} w_{,\xi\xi}) - (p_s + p_d \cos \omega\tau) = 0$$

$$\nabla^4 f = \beta^2 (w_{,\xi\xi} w_{,\eta\eta} - w_{,\xi\eta} w_{,\xi\eta} + w_{0,\xi\xi} w_{0,\eta\eta}) - \alpha (w - w_0)_{,\xi\xi}, \quad (1)$$

where $\xi = x/a$ and $\eta = y/b$ are non-dimensional coordinates. $\nabla^2 \equiv \partial^2/\partial\xi^2 + \beta^2 \partial^2/\partial\eta^2$ is the Laplace operator. $\delta(\xi - \xi_1)$ is the Dirac's delta function. Subscript following a comma stands for partial differentiation. $\alpha = a^2/Rh$ is the non-dimensional shell curvature. $\beta = a/b$ is the aspect ratio of the length of the rectangular boundary, the concentrated mass is located at $\xi_1 = 0.5$ and $\eta_1 = 0.5$. $\gamma = m/\rho abh$ is the mass ratio. $p_s = g\rho a^4/D$ and $p_d = a_d \rho a^4/D$ ($D = Eh^3/12(1-\nu^2)$) correspond to the non-dimensional load intensities. The shell boundary is simply supported for deflection. For the condition of in-plane boundary, the edges are considered to be constrained by elastic springs. The springs have non-dimensional elastic coefficients k_x and k_y along the curved edge and straight edge, respectively. In-plane displacements $u = Ual/h^2$ and $v = Val/h^2$ relate with the stress function f .

3. Procedure of Analytical Solution

The lateral displacement w and w_0 are assumed as

$$[w, w_0] = \sum_m \sum_n [\hat{b}_{mn}(\tau), \hat{a}_{mn}] \sin m\pi\xi \sin n\pi\eta, \quad (m, n = 1, 2, 3, \dots) \quad (2)$$

where \hat{b}_{mn} is unknown time function and \hat{a}_{mn} is constant representing an initial imperfection of the shell. Inserting the foregoing equation to equation (1), stress function f is derived with the

function of \hat{b}_{mn} and \hat{a}_{mn} . The Galerkin method reduced the resulting governing equation (1) to nonlinear ordinary differential equations in terms of \hat{b}_{mn} :

$$\sum_{m,n} \hat{B}_{rsmn} \hat{b}_{mn} + \tau \tau + \sum_{m,n} \hat{C}_{rsmn} \hat{b}_{mn} + \sum_{k,l,m,n} \hat{D}_{rsklmn} \hat{b}_{kl} \hat{b}_{mn} \hat{b}_{kl} \hat{b}_{mn} + \sum_{i,j,k,l,m,n} \hat{E}_{rsijklmn} \hat{b}_{ij} - \hat{F}_{rs} - (p_s + p_d \cos \omega \tau) \hat{G}_{rs} = 0 \quad (r, s, i, j, k, l, m, n = 1, 2, 3, \dots) \quad (3)$$

The equations including a damping terms are integrated using the Runge-Kutta-Gill method. Nonlinear responses are obtained in specific frequency ranges.

4. Experimental Procedure

A sheet of phosphor bronze with mass density $\rho=7.52 \times 10^3 [\text{kg/m}^3]$, Young's modulus $E=62.4 [\text{GPa}]$ and Poisson's ratio $\nu=0.33$ is used as a test shell. The shell with thickness $h=0.24 [\text{mm}]$ is rolled to shallow cylindrical surface. The shell is cut out to a close square of $a=139.5 [\text{mm}]$ and $b=139.8 [\text{mm}]$. To satisfy the simply supported boundary of the cylindrical shell-panel, the edges are connected to inner walls of the rectangular frame by thin flexible films. Elastic property of the film acts as the in-plane elastic constraint to the shell boundary. Rise of the cylindrical shell is $0.48 [\text{mm}]$ in average, and curvature of the shell is calculated as $R=5190 \pm 710 [\text{mm}]$. To reinforce both analytical and experimental results of nonlinear dynamic responses, the shell curvature and the in-plane spring coefficients are determined by the characteristics of static deformation and the linear natural frequencies. The shell is excited by the electro-magnetic shaker. Dynamic responses of the shell are recorded by non-contact laser displacement sensors.

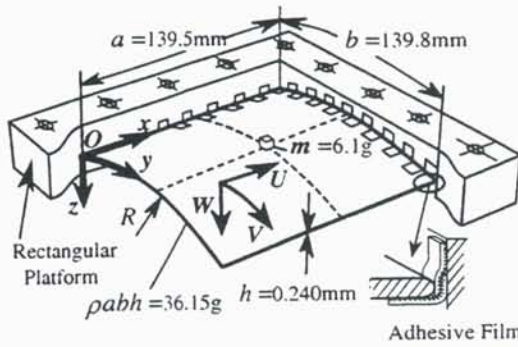
5. Results and Discussions

Figure 2 shows characteristics of static deflection under concentrated force acted on the center. The shell has spring characteristics with a soft-hardening type including negative gradient. The shell curvature is found to be $\alpha=15$ and in-plane spring contents are regarded as $k_x=0.01$, $k_y \neq 0$. Figure 3 shows the frequency response curve. w_{rms} is the root mean square value of periodic response. ω is the non-dimensional exiting frequency. Figures (a) and (b) show results of the shell without mass and with mass, respectively. In the figure, the regions of the chaotic vibration are assigned by the named $C_{(m,n;j)}$, in which (m,n) is generated mode of vibration, while, j indicates the type of resonance. The integers m and n imply predominant half wave number of deflection in x -direction and y -direction, respectively. Chaotic responses of the shell without mass appears in wide frequency ranges. On the contrary, chaotic response hardly appears in the restricted narrow range. The inertia force due to concentrated mass results in the generation of periodic response rather than the chaos. In Figure 4, Poincaré maps of the chaos are recorded in a phase delay θ rad. Compared with the result of analysis, both results coincide very well. The maximum Lyapunov exponent λ_{max} is identified from experimental data. Lyapunov dimension and λ_{max} are calculated numerically. Figure 5 shows that λ_{max} of experimental data converges to $\lambda_{max}=2$ where embedding dimension $e=8$, and the result has good agreement with the analytical result $\lambda_{max}=2.6$. In Figure 6, (a) and (b) show the λ_{max} of experimental results in the frequency ranges $C_{(1,1;1/2)}$ and $C_{(1,1;3/4)}$, respectively. Lyapunov exponents of the shell without mass show higher magnitude than those of the shell with mass.

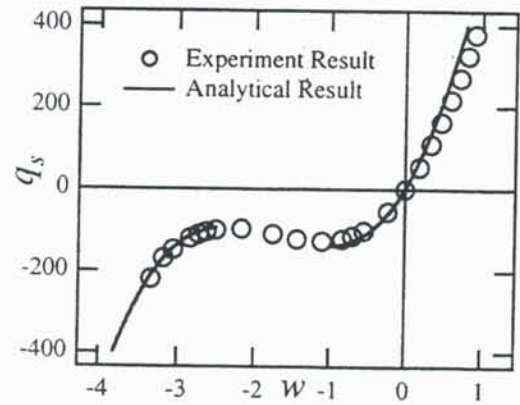
References

- (1) Nagai, K. and Yamaguchi, T., "Chaotic oscillations of a shallow cylindrical shell with rectangular boundary under cyclic excitation", High Pressure Technology, ASME,PVP-Vol. 297,(1995),pp.107-115.
- (2) Yamaguchi, T. and Nagai, K., "Chaotic vibration of a cylindrical shell-panel with an in-plane elastic-support at boundary", Nonlinear Dynamics Vol.13,(1997), pp.259-277.
- (3) Nagai, K., Kasuga, K., Kamada, M., Yamaguchi, T. and Tanifuji, K., "Experiment on chaotic oscillations of a post-buckled reinforced beam constrained by an axial spring", International Journal of Japan Society of Mechanical Engineers Vol.41, (1998), No.3, pp.563-569.

The authors would like to thank graduate student Dai Yanagisawa for discussions and helpful typing of the manuscript.



Figure,1 Shallow shell-panel with concentrated mass



Figure,2 Deflection of the shell-panel under concentrated load on $\xi=0.5, \eta=0.5$

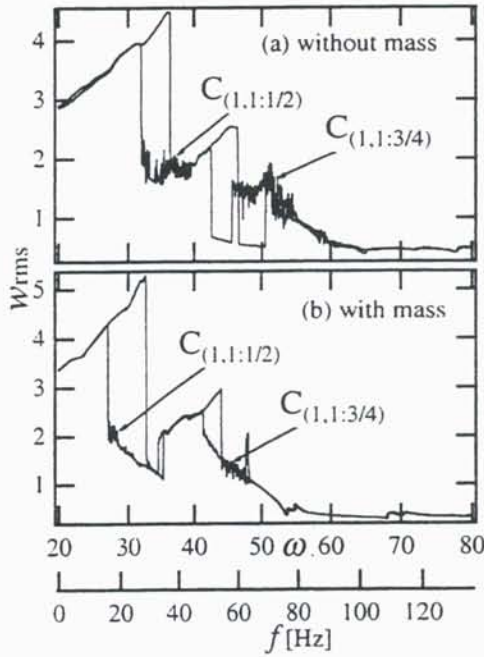


Figure.3 Frequency response curve $P_d=490$

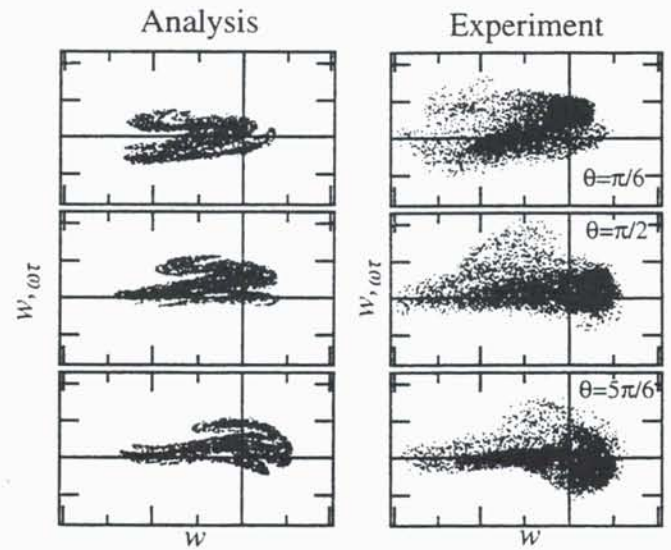
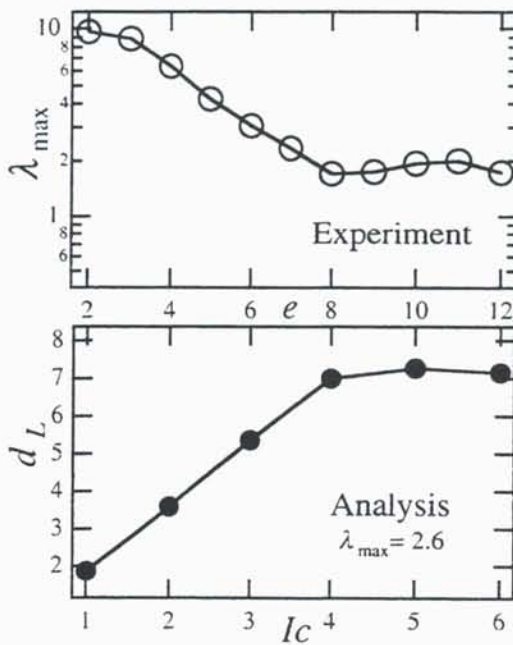


Figure.4 Poincaré map of the chaotic response



Figure,5 Maximum Lyapunov related embedding dimension (Experiment) & Lyapunov dimension related I_c (Analysis)

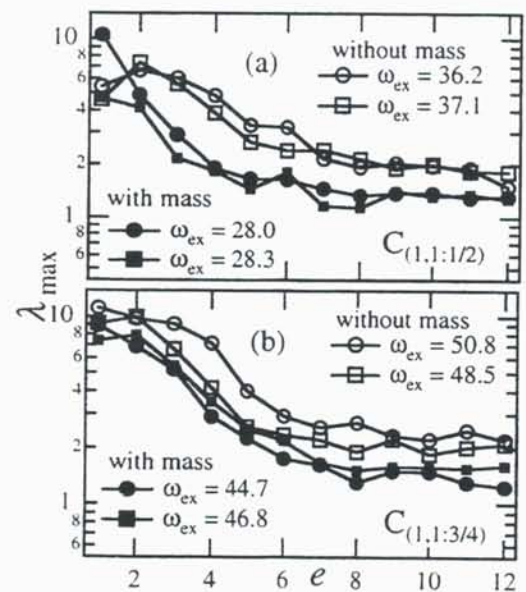


Figure.6 Maximum Lyapunov exponent related to embedding dimension (Experiment)

Applicability of the Donnell-type Theory to Open Cylindrical Shells

Composed of Composite Materials

Yoshihiro Narita

Hokkaido Institute of Technology

7-15 Maeda, Teine-ku, Sapporo 006-8585, Japan

1. Introduction

Open shell structures are often found in structural applications. The Donnell (-Mushtari) type shell theory is usually applied to vibration analysis of the open shells, while higher-order shell theories, such as Flügge, Love and Sanders, are used to analyze closed shell structures.

The Donnell theory makes use of the *shallowness* assumption that excludes some curvature effects in the formulation but the range of applicability of the theory has not been clarified enough in the past literature. Also composite material is increasingly used in weight sensitive structures and anisotropy of the material makes the range of applicability of the theory more complicated.

In this presentation, the free vibration of laminated composite open shells is analyzed by using the Flügge theory with tracing parameters that can be simplified to the Donnell theory as a special case. Numerical examples show various effects of the assumptions used in the theory upon accuracy of the natural frequencies.

2. Summary of the Analysis

Figure 1 shows an open shell with cylindrical curvature and the coordinate system. The u , v and w denote displacements in x , θ and z directions, respectively. The b is length measured along the curved surface. Assuming the laminated unidirectional composite, each lamina has a constitutive relation

$$\begin{Bmatrix} \sigma_x \\ \sigma_\theta \\ \tau_{x\theta} \end{Bmatrix}^k = \begin{bmatrix} \bar{Q}_{11} & \bar{Q}_{12} & \bar{Q}_{16} \\ \bar{Q}_{12} & \bar{Q}_{22} & \bar{Q}_{26} \\ \bar{Q}_{16} & \bar{Q}_{26} & \bar{Q}_{66} \end{bmatrix}^k \begin{Bmatrix} \varepsilon_x \\ \varepsilon_\theta \\ \gamma_{x\theta} \end{Bmatrix} \quad (1)$$

The displacements at (x, θ, z) are expressed in terms of the displacements on the middle surface.

$$u^* = u - z \frac{\partial w}{\partial x}, \quad v^* = \frac{R + \delta_1 z}{R} v - z \frac{\partial w}{R \partial \theta}, \quad w^* = w \quad (2)$$

where δ_1 is a tracing parameter (or tracer) that expresses difference of shell theories. For $\delta_1=0$ it represents the relation used in the Donnell theory and for $\delta_1=1$ it does that in the Flügge theory.

The strain-displacement relations are

$$\varepsilon_x = \frac{\partial u^*}{\partial x}, \quad \varepsilon_\theta = \frac{1}{R + \delta_2 z} \left(\frac{\partial v^*}{\partial \theta} + w^* \right), \quad \gamma_{x\theta} = \frac{1}{R + \delta_2 z} \frac{\partial v^*}{\partial x} + \frac{\partial w^*}{\partial \theta} \quad (3)$$

with $\delta_2=0$ for the Donnell theory and $\delta_2=1$ for the Flügge theory.

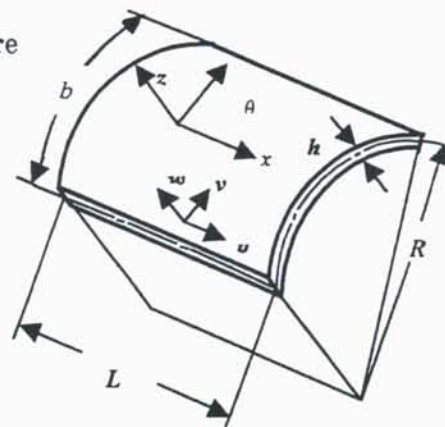


Fig.1 Open cylindrical shell

The stress and moment resultants are obtained by integrating through the thickness as

$$\begin{aligned} N_x &= \int_{-h/2}^{h/2} \sigma_x \left(1 + \delta_3 \frac{z}{R}\right) dz, & N_\theta &= \int_{-h/2}^{h/2} \sigma_\theta dz, & N_{x\theta} &= \int_{-h/2}^{h/2} \tau_{x\theta} \left(1 + \delta_3 \frac{z}{R}\right) dz, & N_{\alpha x} &= \int_{-h/2}^{h/2} \tau_{x\theta} dz \\ M_x &= \int_{-h/2}^{h/2} \sigma_x z \left(1 + \delta_3 \frac{z}{R}\right) dz, & M_\theta &= \int_{-h/2}^{h/2} \sigma_\theta z dz, & M_{x\theta} &= \int_{-h/2}^{h/2} \tau_{x\theta} z \left(1 + \delta_3 \frac{z}{R}\right) dz, & M_{\alpha x} &= \int_{-h/2}^{h/2} \tau_{x\theta} z dz \end{aligned} \quad (4)$$

with $\delta_3=0$ for the Donnell theory and $\delta_3=1$ for the Flügge theory.

The equilibrium equations are

$$N_x^* + \frac{1}{R} N_{\alpha x}^* = I\ddot{u}, \quad N_{x\theta}^* + \frac{1}{R} N_\theta^* + \delta_4 \frac{1}{R} \left(M_{x\theta}^* + \frac{M_\theta^*}{R} \right) = \bar{v}, \quad \left(M_x^* + \frac{1}{R} M_{\alpha x}^* \right) + \frac{1}{R} \left(M_{x\theta}^* + \frac{1}{R} M_\theta^* \right) - \frac{N_\theta^*}{R} = I\ddot{w} \quad (5)$$

where $\bullet = \frac{\partial}{\partial x}$, $\circ = \frac{\partial}{\partial \theta}$ and $\delta_4=0$ is for the Donnell theory and $\delta_4=1$ is for the Flügge theory.

Substitution of Eqs.(1)-(4) into (5) yields a set of differential equations in terms of u, v and w . Setting $\delta_1 = \delta_2 = \delta_3 = \delta_4 = 0$ gives the equations based on the Donnell theory and $\delta_1 = \delta_2 = \delta_3 = \delta_4 = 1$ does on the Flügge theory. Furthermore, shell theories possibly existing between the two theories can be examined by defining each tracing parameter independently (i.e., for various combinations of $\delta_1, \delta_2, \delta_3$ and δ_4).

Assuming an open shell with rectangular planform, the equations can be solved by assuming

$$u(x, \theta, t) = u_{mn} \cos \frac{m\pi x}{L} \sin n\theta \sin \omega t, \quad v(x, \theta, t) = v_{mn} \sin \frac{m\pi x}{L} \cos n\theta \sin \omega t, \quad W(x, \theta, t) = w_{mn} \sin \frac{m\pi x}{L} \sin n\theta \sin \omega t \quad (6)$$

for the simply supported (shear diaphragms) shell, where the boundary conditions of $v=w=M_x=N_x=0$ at $x=0$, are satisfied along the four edges. The u_{mn}, v_{mn} and w_{mn} are unknown coefficients given for each part of wave numbers m and n , where m is an integer but n is not necessarily an integer here.

The resulting eigenvalue equation is written as

$$\left([K] - \Omega^2 [M] \right) \begin{Bmatrix} u_{mn} \\ v_{mn} \\ w_{mn} \end{Bmatrix}^T = 0 \quad (7)$$

where a frequency parameter is $\Omega^2 = \omega L^2 (\rho / D_0)^{1/2}$ with a reference stiffness $D_0 = E_2 h^3 / 12(1 - \nu_{LT} \nu_{TL})$.

3. Numerical examples

Numerical study has been done for both isotropic and anisotropic open shells supported by shear diaphragms. The aspect ratio is taken for $\alpha=1$ and 4, and the curvature ratio is $\beta=0.2, 0.5, 1$ and 2. The thickness ratio is kept constant as $h/L=0.01$.

Table 1 and 2 present two sets of the first four frequency parameters obtained by the two theories for *isotropic* open shells. The errors between the two theories are written that are given by

$$\text{error}(\%) = (\Omega_{Donnel} - \Omega_{Flügge}) / \Omega_{Flügge} \times 100 \quad (8)$$

Generally speaking, the errors become greater as the shells get deeper (b/R is increased). For isotropic square shells in Table 1, the errors are less than 3 percent, but for isotropic rectangular shells ($L/b=4$) in Table 2, errors are not negligible particularly for the deeper shells ($b/R > 1$). The maximum error is found 23.2 percent for the fundamental frequency of the shell with $b/R=2$.

Table 3 and 4 present the frequency parameters of unidirectional single layer open shells having the fiber orientation angles $\theta=0$ deg and $\theta=90$ deg, respectively. The material

constants

$$E_L=138 \text{ GPa}, E_T=8.96 \text{ GPa}, \nu_{LT}=0.3, G_{LT}=7.1 \text{ GPa},$$

are used in these examples.

It is found here that introduction of material anisotropy does not affect much on the difference between the shell theories, and conversely the errors become less for orthotropic shells ($\theta = 0$ deg) in Table 3 than for isotropic shells in Table 1. Apparently the aspect ratio has more pronounced effects on the use of shell theories.

Table 1. Difference of frequency parameters between Donnell and Flügge theories ($L/b=1$, $h=0.01$) (Isotropic material)

b/R		1st	2nd	3rd	4th
0.2	Donnell	38.44	51.16	72.30	85.56
	Flügge	38.42	51.01	72.28	85.53
	error(%)	0.1	0.1	0	0
0.5	Donnell	59.18	84.18	99.91	114.0
	Flügge	58.96	84.12	99.65	113.8
	error(%)	0.4	0.1	0.3	0.2
1	Donnell	81.35	103.4	160.6	162.8
	Flügge	80.72	102.4	160.5	161.9
	error(%)	0.8	1.0	0.1	0.6
2	Donnell	115.9	133.8	169.9	234.3
	Flügge	112.5	132.4	165.9	230.8
	error(%)	3.0	1.1	2.4	1.5

Table 2. Difference of frequency parameters between Donnell and Flügge theories ($L/b=4$, $h=0.01$) (Isotropic material)

b/R		1st	2nd	3rd	4th
0.2	Donnell	168.1	203.9	263.9	341.2
	Flügge	167.5	203.2	263.3	341.3
	error(%)	0.4	0.3	0.2	0.2
0.5	Donnell	169.9	234.3	338.7	453
	Flügge	165.9	230.8	335.7	450.3
	error(%)	2.4	1.5	0.9	0.6
1	Donnell	175.6	312.8	511.6	633.6
	Flügge	161.5	303.2	504.3	617.7
	error(%)	8.7	3.2	1.4	2.6
2	Donnell	190.9	467.9	611.7	654
	Flügge	155	451.4	550.3	592.9
	error(%)	23.2	3.7	11.2	10.3

Table 3. Difference of frequency parameters between Donnell and Flügge theories ($L/b=1$, $h=0.01$) (Single layer, GFRP, [0 deg])

b/R		1st	2nd	3rd	4th
0.2	Donnell	63.59	72.15	113.8	170.9
	Flügge	63.57	72.11	113.8	170.9
	error(%)	0	0.1	0	0
0.5	Donnell	94.91	121.0	123.5	183.0
	Flügge	94.75	120.7	123.4	182.7
	error(%)	0.2	0.2	0.1	0.2
1	Donnell	139.2	146.0	187.8	228.7
	Flügge	138.5	145.6	186.8	228.7
	error(%)	0.5	0.3	0.5	0
2	Donnell	199.2	211.5	265.2	278.9
	Flügge	197.1	208.1	264.4	275.0
	error(%)	1.1	1.6	0.3	1.4

Table 4. Difference of frequency parameters between Donnell and Flügge theories ($L/b=1$, $h=0.01$) (Single layer, GFRP, [90 deg])

b/R		1st	2nd	3rd	4th
0.2	Donnell	63.48	124.4	160.5	182.9
	Flügge	63.37	124.4	160.3	182.8
	error(%)	0.2	0	0.1	0.1
0.5	Donnell	120.7	163.7	210.1	268.1
	Flügge	120.4	162.7	209.2	267.9
	error(%)	0.2	0.6	0.4	0.1
1	Donnell	174.3	220.1	284.9	353.1
	Flügge	170.7	219.4	282.5	349.1
	error(%)	2.1	0.3	0.8	1.1
2	Donnell	208.1	352.1	378.0	432.3
	Flügge	197.4	337.0	376.9	419.4
	error(%)	5.4	4.5	0.3	3.1

CONTINUUM REPRESENTATIONS FOR THE VIBRATION OF VEHICLE TRACKS

N. C. Perkins
C. Scholar

Mechanical Engineering and Applied Mechanics
University of Michigan
Ann Arbor, MI 48109-2125
USA

Heavy vehicles driven by tracks include construction vehicles, mining equipment, agricultural vehicles, military tanks and others. Regardless of their use, all tracked vehicles are subject to very substantial vibration levels; partly from the rough terrain that they frequently traverse and partly from the construction and motion of their track systems. This vibration limits the service life of many components and adversely affects vehicle performance. For instance, the vibration environment found inside military vehicles can be so severe as to seriously degrade the performance of on-board instrumentation, electronics and personnel. In addition, the associated acoustic emissions can themselves compromise the missions of these vehicles. This presentation will focus on a model used to examine the vibration response of the tracks that drive these vehicles. In doing so, we discuss the merits of viewing the track as an equivalent continuum.

Prior models of vehicle tracks have considered them to be large dimensional, multi-body systems composed of individual rigid links (pitches). This approach invariably leads to models of tracked vehicles possessing hundreds of degrees of freedom resulting in considerable computational effort to deduce even relatively simple responses. The novel approach discussed here is to model the track as an equivalent elastic continuum which is then coupled to the (rigid body) elements forming the remainder of the vehicle suspension system. To this end, a continuum model will be presented which describes the dynamic deformation of a track element within the vertical plane. This element model accounts for 1) the stretching of the track and resulting dynamic track tension, 2) the transverse vibration of the track spans, and 3) the static track sag. The element model is then extended in forming a model for the entire track system including typical suspension elements. The natural frequencies and mode shapes associated with this system model are then employed to evaluate the forced response of the track system using classical modal analysis methods. Figure 1 presents an example of this calculation and illustrates the first four vibration modes of a military vehicle. The forced responses considered derive from dominant sources of excitation for tracked vehicles including rough terrain and drive train excitation.

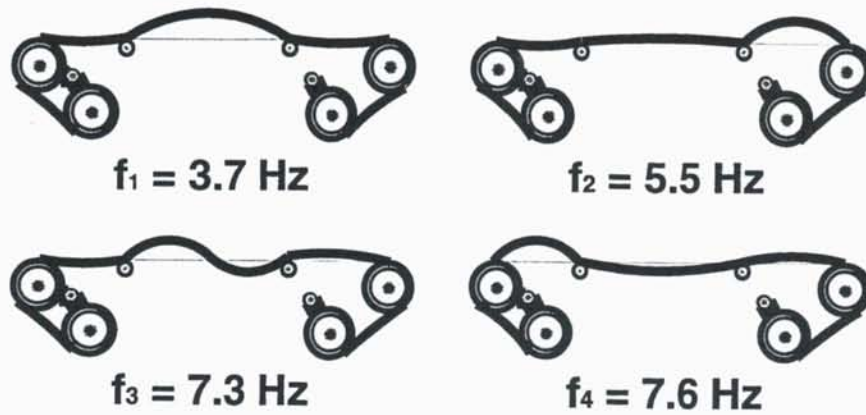


Figure 1: Track system modes.

The modeling of a vehicle track as a continuum is unique and requires justification. As a means towards this end, we shall review experimental results on the vibration response of track segments and critically compare these with predictions from the continuum model. Figure 2 illustrates experimentally measured frequency response functions for a sample track from which the natural frequencies are quite apparent. Once the accuracy and limits of the continuum model have been established, we shall then review how it is employed in the simulation of entire tracked vehicles traversing rough terrain.

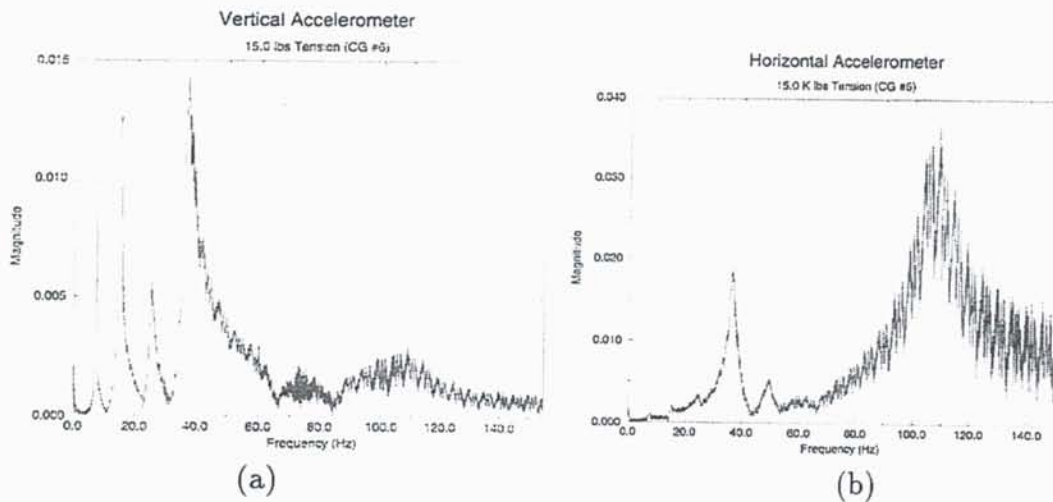


Figure 2: Experimental frequency responses; (a) Vertical accelerometer; (b) Horizontal accelerometer.

Vibrations of Ballooning Strings

Christopher D. Rahn

Associate Professor

The Pennsylvania State University
University Park, PA 16802

Introduction

Many textile processes (*e.g.* yarn spinning, twisting, and unwinding) require high-speed rotation of lightweight, flexible yarns, filaments, and fibers. To an inertial observer, the rotating yarn blurs to produce a balloon or surface of revolution formed by the rotating yarn. Relative to a frame that rotates with the string, a steady balloon is stationary. For the heavy yarns with negligible air drag studied in this research, the steady yarn displacement resembles a planar catenary relative to the rotating frame. The dynamic response of the balloon to varying rotation speed, boundary excitation, and disturbances govern the quality of the textile product. Resonance, in particular, can cause large tension variations that reduce product quality and may cause yarn breakage.

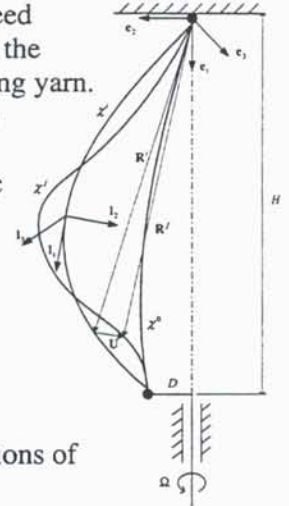


Figure 1: Schematic Diagram of the Ballooning String Model

Dynamic Model

Figure 1 shows a schematic diagram of the ballooning string model. Under assumptions of perfect flexibility and negligible air drag, the nondimensional equations of motion can be written

$$\frac{\partial}{\partial s} \left(\frac{p \mathbf{e}_2}{\varepsilon_1 (1 + \varepsilon_2)} \right) \left(\frac{\partial \mathbf{r}}{\partial s} + \frac{\partial \mathbf{u}}{\partial s} \right) = \mathbf{e}_1 \times (\mathbf{e}_1 \times (\mathbf{r} + \mathbf{u})) + 2 \mathbf{e}_1 \times \frac{\partial \mathbf{u}}{\partial t} + \frac{\partial^2 \mathbf{u}}{\partial t^2} \quad (1)$$

where s is the arc length coordinate, t is time, $\mathbf{r}(s) = x\mathbf{e}_1 + y\mathbf{e}_2 + z\mathbf{e}_3$ is the steady state displacement, $p(s)$ is the steady state tension, $\mathbf{u}(s, t) = u_1\mathbf{e}_1 + u_2\mathbf{e}_2 + u_3\mathbf{e}_3$ is the displacement relative to steady state, and ε_1 and ε_2 are the strains relative to the unstressed and steady state, respectively. The boundary conditions are

$$\mathbf{r}(0) = \mathbf{u}(0, t) = \mathbf{u}(l_0, t) = 0, \quad \mathbf{r}(l_0) = \mathbf{e}_2 + h\mathbf{e}_1$$

where l_0 and h are the unstretched string length and balloon height, respectively.

Steady State Balloon Shapes

Substitution of $\mathbf{u} = \mathbf{0}$ into Eq. (1) yields the steady state balloon shapes and tension

$$p = \gamma \sqrt{(1 + p_e / \gamma)^2 - x^2 / \gamma - \gamma}$$

where $p_e = p(0)$ is the fixed eyelet tension and γ is the axial string stiffness. A shooting technique solves the nonlinear ODEs to produce the results shown in Fig. 2. The solid, dashed, and dash-dotted lines show the tension versus string length for the relatively extensible $\gamma = 100$, $\gamma = 1000$, and an inextensible string. The inset boxes show the corresponding, planar balloon shapes. The height of the balloon is fixed at $h = 10$, so increasing Δ_l indicates increasing increasing balloon length. The top curves in Fig. 2 correspond to single loop balloons. Taut balloons with small Δ_l have high tension. With increasing Δ_l , the eyelet tension reduces to a minimum near $\Delta_l = 0.06$ and then increases. As the tension decreases, the balloons acquire more loops. The balloons corresponding to the next lower curves change shape from one and

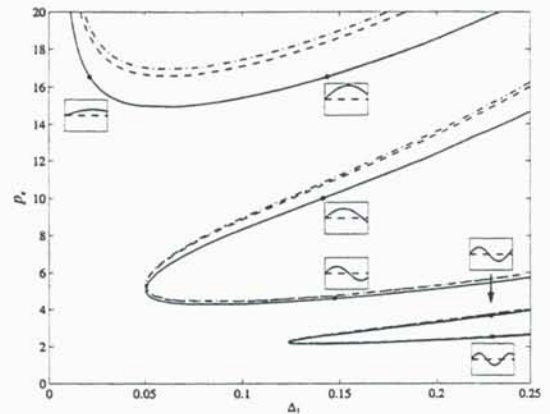


Figure 2: Steady state tension and balloon shapes (insets) versus string length $\Delta_l = (l_1 - h)/l_1$.

a half loop to double loop at the turning point near $p_e = 5.5$. The tension increases with increasing Δ_l for these balloons except for a small region near the turning point. The balloons on the bottom curves have two and a half loops and triple loops. The maximum difference between the $\gamma = 1000$ and inextensible cases, however, is less than 0.5%, so the inextensible assumption appears reasonable for strings with $\gamma > 1000$.

Vibration Analysis

Linearization of Eq. (1) about the steady state produces the vibration equations

$$\frac{\partial}{\partial s} \left(p \frac{\partial \mathbf{u}}{\partial s} + \gamma \left(\frac{\partial \mathbf{r}}{\partial s} \bullet \frac{\partial \mathbf{u}}{\partial s} \right) \frac{\partial \mathbf{r}}{\partial s} \right) = \mathbf{e}_1 \times (\mathbf{e}_1 \times \mathbf{u}) + 2\mathbf{e}_1 \times \frac{\partial \mathbf{u}}{\partial t} + \frac{\partial^2 \mathbf{u}}{\partial t^2}$$

The displacement field is represented by a separable series of comparison functions and Galerkin's method approximates the natural frequencies, mode shapes, and stability. It is found that single loop balloons are stable with purely imaginary eigenvalues, half loop balloons are divergent unstable, and double loop balloons are flutter unstable except for low stiffness and long string length cases. The solid lines in Fig. 3 shows the single loop balloon natural frequencies ω versus the string stiffness. The dashed lines indicate frequencies calculated using the inextensible steady state solution. For small γ , the dashed lines differ significantly from the corresponding solid lines. For $\gamma > 1000$, however, the first six frequencies obtained from the two approaches match to within 3%.

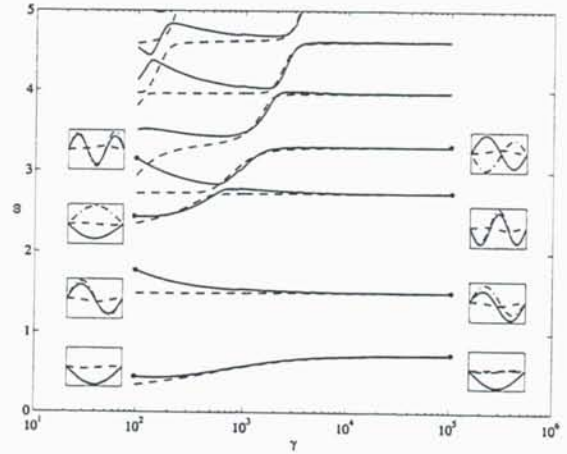


Figure 3: Single balloon natural frequencies versus string stiffness, extensible (solid), inextensible (dashed).

Inextensible, Small Curvature, Quasistatic Analysis

The previous analysis shows that extensibility effects can be neglected for axially stiff ($\gamma > 1000$) strings. Thus, we neglect the small string stretch between the unstressed and steady state configurations and assume that axial vibration propagates infinitely fast (quasistatically). Assumption of small curvature allows the development of a simple model that enables physical insight into the vibration natural frequencies and mode shapes of single loop balloons. Small curvature implies that the steady state balloon shapes and curvature $k(s)$ are sinusoidal

$$y(s) = \frac{d \sin \omega s}{\sin \omega}, \quad k(s) = \frac{d \omega^2 \sin \omega s}{\sin \omega}$$

with d and ω ($< \pi$ for single loop) the eyelet length and rotation speed using a slightly different nondimensionalization scheme. We linearize the equations of motion about the small curvature steady state to produce the scalar equations

$$u_{2,tt} - 2\omega u_{3,tt} + \omega^2 u_2 + \gamma \omega^2 k \int_0^1 k u_2 ds - u_{2,ss} = 0 \quad (2)$$

$$u_{3,tt} + 2\omega u_{2,tt} - \omega^2 u_3 - u_{3,ss} = 0$$

where comma subscripts indicate partial differentiation and $u_2(s,t)$ and $u_3(s,t)$ are displacements in the normal (in-plane) and binormal (out-of-plane) directions.

Figure 4 shows how the natural frequencies and mode shapes change with nondimensional rotation speed ω for fixed d and $\gamma = 10^5$. At $\omega = 0$ the balloon is taut and the in-plane and out-of-plane vibration frequencies repeat at the pinned string natural frequencies $\omega_n = n\pi$. As ω increases, the frequencies separate into forward and backward whirling modes. The forward whirling modes move faster relative to a ground observer and thus have higher frequency. The mode shapes for the first three modes at $\omega = 0.3\pi$ shown in Fig. 4(a) have identical in-plane and out-of-plane amplitudes, indicating circular whirling. Above $\omega = 0.4\pi$, the curvature

begins to become significant and the stiffening integral term in Eq. (2) increases the frequency of modes that are not orthogonal to $k(s)$. As $k(s)$ is approximately a half-sine, the first two modes are most affected by increasing curvature. The other modes, being essentially sinusoids with spatial wavelengths equal to integral divisors of the first mode wavelength, are orthogonal to $k(s)$ and are not as sensitive to increasing curvature. At $\omega = 0.6\pi$ (Fig. 4(b)), the first forward whirling mode and the second backward whirling mode exchange order due to an eigenvalue curve veering near $\omega = 0.5\pi$. The first backward whirling mode frequency increases slightly from $\omega = 0.5\pi$ to $\omega = 0.7\pi$ due to curvature stiffening that reduces the in-plane modal amplitude, producing elliptical whirling. At $\omega = 0.9\pi$ (Fig. 4(c)), the first backward whirling mode is almost entirely confined to the out-of-plane with the small in-plane component having a full sine shape. The first forward whirling mode has veered up off the graph. The second and third modes are the second and third backward whirling modes, respectively. At $\omega = \pi$, the first backward whirling mode buckles and the first forward whirling mode veers to infinity. The other forward and backward whirling modes change by $\pm\pi$ from their values at $\omega = 0$, respectively.

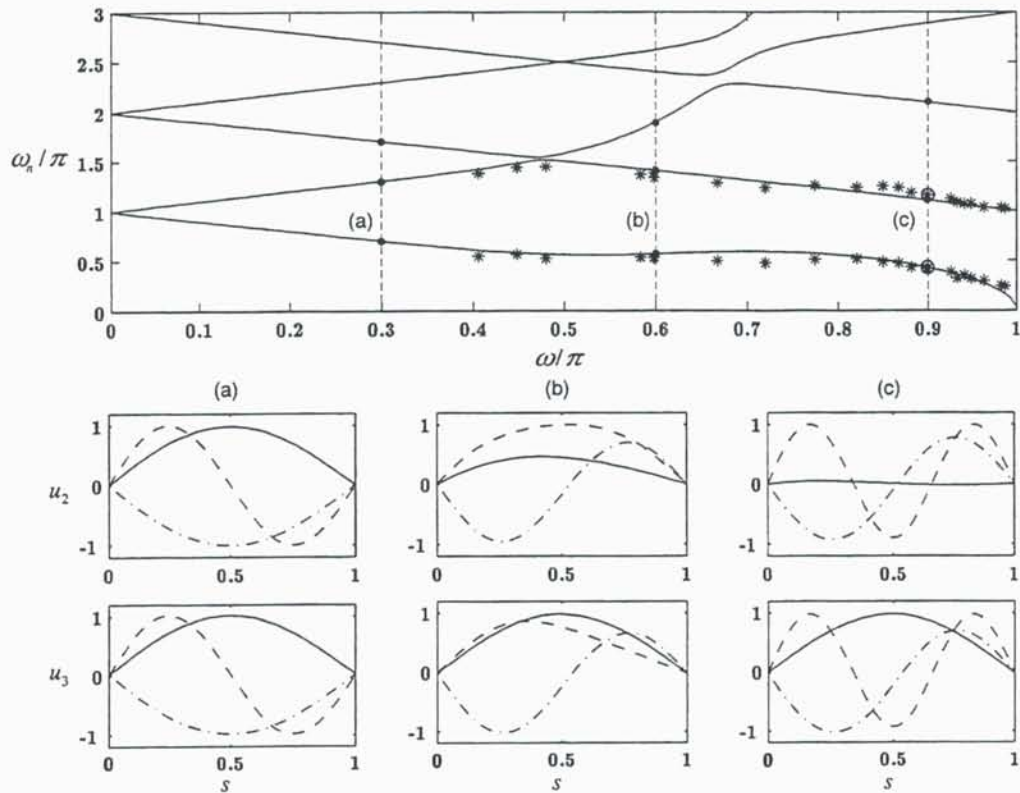


Figure 4: Theoretical (solid) and experimental (*) natural frequencies. Mode shapes (1st solid, 2nd dash-dotted, 3rd dashed): (a) $\omega = 0.3\pi$, (b) $\omega = 0.6\pi$, (c) $\omega = 0.9\pi$.

Vibrations of a Flexible Rod Induced by Friction

Yuichi SATO

Department of Mechanical Engineering
Saitama University
Urawa, Japan
ysato@mech.saitama-u.ac.jp

Observed phenomena

A soot-blower shown in Fig. 1 is used to blow off soot on tubes in a tubular heat exchanger, or a gas heater. High frequency vibrations and noises occurred in operation. A soot-blower has a long slender pipe called a lance, 8m long and 76mm in diameter, which is put slowly into a gas heater. Steam flows through the lance and is discharged at the free end to blow off soot. In operation the lance rotates about its axis at 12 rpm. At an intermediate position the lance is supported by a support bearing, called a lance bearing (shown in Fig. 1(b))

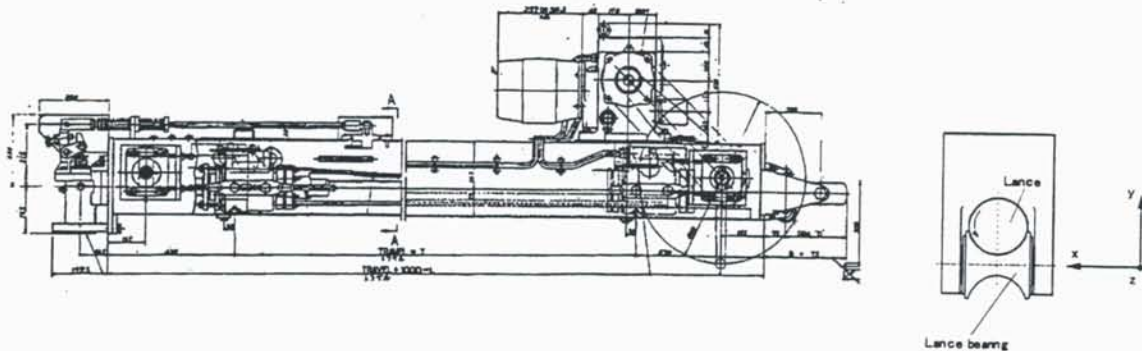
From frequency analysis the observed frequencies are the eighth to the eleventh natural frequencies. Figure 2 shows the relation between the observed dominant frequencies and inserted length S from the support bearing to the free end of the lance. As the inserted length becomes longer, the dominant frequency decreases and then increases abruptly. Since a lance bearing can rotate about the x -axis (Fig. 1(b)) and not about the z -axis, and the lance rotates about its axis parallel to z -axis, the vibrations was considered to be induced by the tangential friction force between the lance and the lance bearing.

Experiment

Fig. 3 shows the test apparatus. The rod is held by four ball bearings and a support, which is located at a distance S from the free end of the rod. A slender rod of 3 mm in diameter and 2 m long is rotated about its axis by an electric motor up to a speed of 300 rpm. Three semi-cylindrical supports are used which have inner diameters of 3.4, 4.0 and 6 mm, and axial length of 10 mm.

Figure 4 shows an example of experimental results. The lower frequency component has the same frequency as the rotational speed. At 2.6 rps or 156 rpm a resonance occurs. For the rotational speeds higher than 2 rps or 120 rpm, the frequency components of approximately 20 Hz always appear. They are considered self-excited vibrations. By comparing the observed and calculated mode shapes, we conclude that the third mode is dominant.

Figures 5 show the relation between the observed frequency components and support position. Higher modes appear as the gap between the rod and the semi-circular support is reduced. Vibrations occur only in the range where natural frequency increases with the decrease in S or the increase in L (Fig. 2).



(a) Outline

(b) Lance bearing

Fig.1 Schematic of a soot-blower

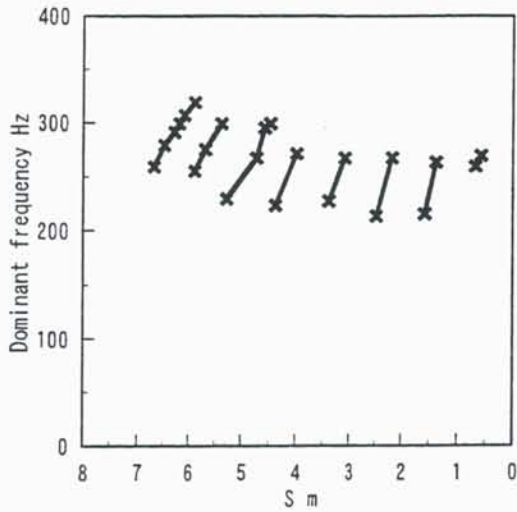


Fig. 2 Observed frequencies

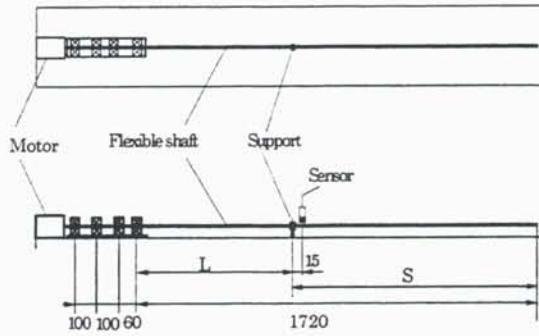
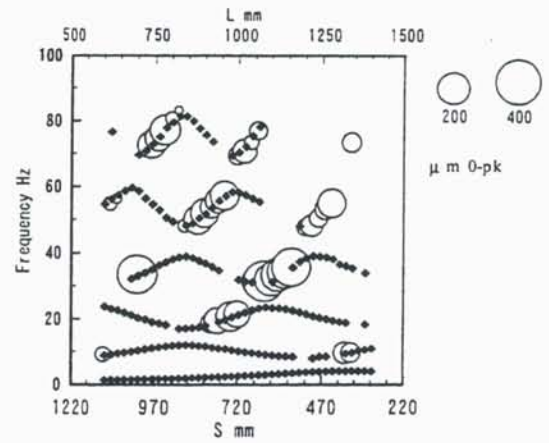
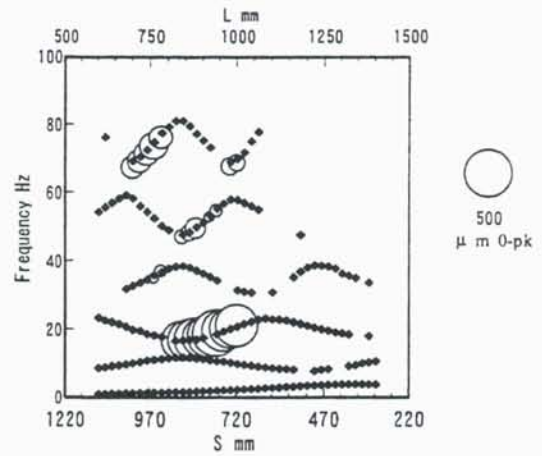


Fig. 3 Experimental apparatus



(a) Bearing diameter $d=3.4\text{mm}$



(b) Bearing diameter $d=4\text{mm}$

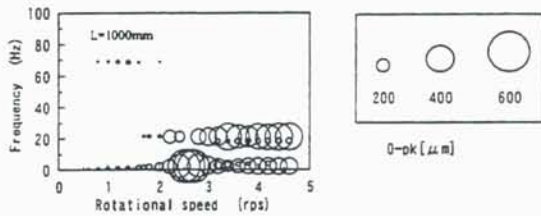
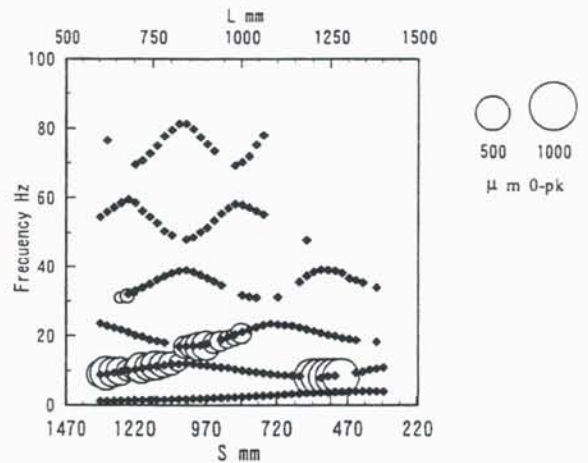


Fig. 4 Campbell diagrams (support bearing diameter $d=4\text{mm}$, $S=720\text{ mm}$ or $L=1000\text{mm}$)



(c) Bearing diameter $d=6\text{mm}$

Fig. 5 Observed nonsynchronous vibration

Forced Linear and Non-Linear Vibration of a Piezoceramic Transformer

Wolfgang Seemann and Rainer Gausmann
University of Kaiserslautern
Post Box 3049
67653 Kaiserslautern
Germany
Seemann@mv.uni-kl.de

Since long it is known that electric voltage can be transformed mechanically by using piezoceramic devices. This presentation describes a device, which consists of two piezoceramic elements and three metal parts. The configuration is such that the system has the form of a slender rod. The first, third and last section of this rod are made of metal and the second and the fourth section are made of piezoceramic material, which is polarized in longitudinal direction.

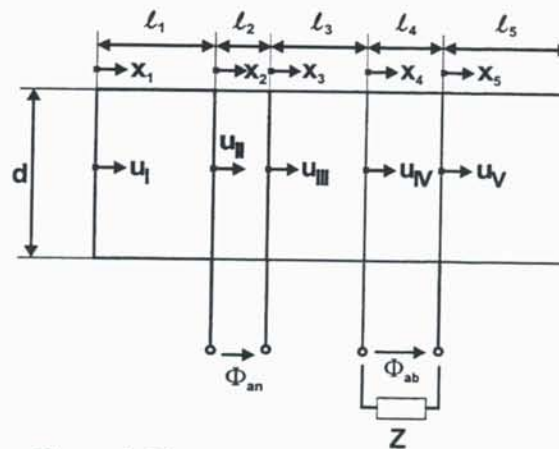


Figure 1: Piezoceramic-based transformer

To use the system as a voltage transformer a time harmonic electric field is applied at one of the piezoceramic elements so that the rod is vibrating in longitudinal direction. Due to the strain, which occurs during vibration, an electric field is generated at the second piezoceramic element. An integration of this electric field leads to the voltage which can be measured at the second ceramic. The electric field, however, depends on the electric impedance which is connected to the electrodes. If the electrodes are short-circuited, the voltage between the two electrodes is zero. If the electrodes are open circuited the charge between the electrodes is zero. These are the two limiting cases. As either the voltage or the current is zero, no energy is dissipated so that this leads to undamped forced vibration of the whole system. If an impedance in the form of a resistor, a capacitance or a combination of both is connected to the electrodes, energy may be dissipated.

In a first step a linear model of the whole system is presented. In this model all the sections are modeled as rods. The metal parts are assumed to undergo elastic longitudinal vibration as well as the ceramic parts. In the ceramics, however, the mechanical field and the electric field are coupled. This coupling is assumed to be linear leading to linear constitutive equations. In general, linear constitutive equations are used especially if the electric field in the ceramic is weak. Between the sections transition conditions are formulated: Continuity of the longitudinal displacement and continuity of the longitudinal stress. The boundary conditions at the ends of the system are assumed to be: vanishing longitudinal stress.

The equations of motion are then given by five wave equations for the different sections. The electric field and thus the exciting voltage enters the equations through the boundary conditions. As the main interest is on the forced vibration it can be shown that for a time harmonic excitation a particular solution can be found if

all displacements and the electric field are also time harmonic. This leads to ordinary differential equations for the displacements in the sections. One problem is that the electric field and the strain are coupled and that the electric field in the ceramic has to be integrated in order to get the voltage amplitude. This is even more a problem for the second ceramic as the voltage between the electrodes is not known a priori. Instead, due to the impedance only a relation between the voltage amplitude and the current amplitude is given.

For several configurations the displacement amplitudes and the voltage amplitudes at the second ceramic are shown. As was to be expected for the open and short circuited electrodes no damping occurs. If a resistor is connected to the electrodes, the maximum amplitude is limited and the resonance frequency lies between the resonance frequencies of the open and short circuited frequencies.

The results of the theoretical model are compared with measurements of a real system. It can be seen that the results agree very well, especially if the transverse contraction is also taken into account in the theoretical model. Due to the fact that in real systems there is always some damping, the amplitudes of the real system are finite near the resonance. In the theoretical model this can be taken into account by introducing a complex Young's modulus.

Significant differences, however, occur if the voltage at the exciting ceramic is increased slightly. The electric field within the ceramic is then in the range below 100 V/mm. Normally, for such electric fields the ceramic is assumed to behave quite linear. Nevertheless, the experiments show that for such moderate electric fields within the ceramic strong nonlinearities may occur. In the experiments this was such that near resonance for a time harmonic voltage the current signal was only periodic but not harmonic. But not only a distortion of the current signal was observed. Also the voltage at the second ceramic showed the same behavior like the current at the exciting ceramic. The distortion could be such strong that the frequency of the current was twice the frequency of the exciting voltage. This gives a hint that in these frequency ranges non-linear constitutive models for the piezoceramic should be used. Some non-linear constitutive equations and their effects on the results are currently under investigation and will be presented during the presentation.

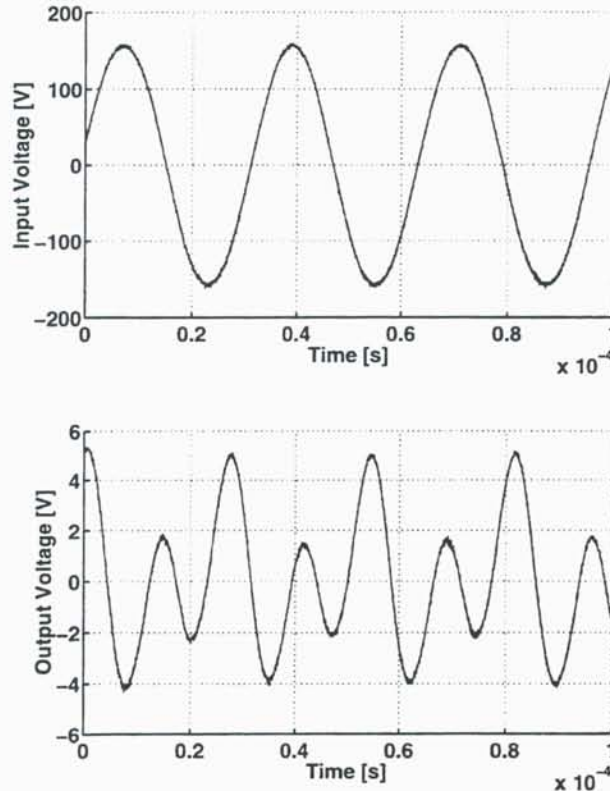


Figure 2: Experimental results showing the strong non-linear behavior

VIBRATION CHARACTERISTICS OF THIN FGM CYLINDRICAL SHELLS

C.B. Sharma and M.N. Naeem

Department of Mathematics, UMIST, Manchester, M60 1QD UK

Introduction

Many biological materials found in nature have special material properties as variables of geometrical parameters and shapes. It is especially true of load sustaining structures like bones of living beings, branches and trunks of trees and various biological hard tissues, etc. Much research has been done to study the principles of designs and processes abundant in the biological world. The concept of functionally graded materials (FGM) is a small step in the direction of developing new, smart materials for engineering and technological applications based on the concept of the smart material characteristics present in nature as a consequence of continuous process of intelligent optimization. FGMs are advanced materials with special mechanical and heat resistant material properties. Recently [1] powder metallurgy techniques have been used in the FGM fabrication. The composition is multi-constituent and materials are distributed continuously in the thickness direction in accordance with a volume fraction law. The most well known FGM is compositionally graded from a ceramic to a metal to incorporate such diverse properties as heat, wear and oxidation resistance of ceramics with the high toughness, strength, machinability and bending capability of metals.

FGMs concept and its applications in practice have been studied extensively e.g. in cutting tool technology, machine and engine components. In such applications diverse qualities of metals such as heat, wear, corrosion resistance, toughness, durability and machinability are brought together. Most research work has been confined to thermal stress analysis and deformation due to their heat shielding properties. The use of FGMs can also be made in the field of structural vibration where the inherent properties can be tailored to suit the problem under consideration. Cylindrical shells can be structured from FGMs and their stability characteristics such as vibration and buckling etc., can be studied. Although an extensive amount of research work has been carried out to study the vibration characteristics of isotropic as well as composite cylindrical shells, there is not much evidence of work on vibration of FGM shells. In a recent paper Loy et al [2] have analysed frequency characteristics of FGM cylindrical shells for simply supported boundary conditions.

In this paper vibration frequencies for FGM shells are analysed and influence of boundary conditions is analysed. The simplest form of FGM has been used where two material constituents (stainless steel and nickel in the present case) change gradually from one to the other through the shell thickness. Since closed form solutions are limited to simple cases so approximate method of solution is employed here and numerical evaluation of frequencies is carried out. The analysis is capable of dealing with arbitrary end conditions but the important ones like SS, CF, CS, CC are studied here. Axial modal dependence is given in terms of Ritz polynomials for a rapid convergence of Ritz method used here and Sanders [3] thin shell theory equations are utilised. To study the FGM characteristics for the constitutive materials a *volume fraction law* is used to take into account for the variation in the materials compositions. Frequency parameters calculated here are compared with some available cases in the literature concerning the stability of shells and related structures. An excellent agreement was achieved for the natural frequency parameters.

Theoretical Considerations

Functionally graded materials (FGMs) are fabricated from two or more material ingredients. Strong heat resistant materials are specifically used for the structures exposed to high temperature conditions. Clearly the material properties of FGMs are functions of material properties and volume fractions of the constituent materials.

For a FGM fabricated from k constituent materials a particular property P can be expressed in the form

$$P = P_i V_i \quad (i = 1, 2, \dots, k) \quad (1)$$

Where P_i and V_i are the material property and volume fraction of the i th constituent and for the repeated index i in equation (1) summation convention is implied. It is also obvious from the volume fraction

assumption that $\sum_{i=1}^k V_i=1$. Volume fraction for a cylindrical shell is defined by the expression

$$V=((2z+h)/2h)^p \quad (2)$$

Where h is uniform thickness of the shell with the reference middle surface and p is the power law exponent, $0 \leq p \leq \infty$. Here a circular cylindrical shell fabricated using the simplest FGM consisting of two material constituents is considered. With E_1, E_2, ν_1, ν_2 and ρ_1, ρ_2 as Young's moduli, Poisson's ratio and mass densities for the materials 1 and 2 respectively, the corresponding material properties, E, ν and ρ of the FGM are expressed as

$$\begin{aligned} E &= (E_1 - E_2) ((2z+h)/2h)^p + E_2 \\ \nu &= (\nu_1 - \nu_2) ((2z+h)/2h)^p + \nu_2 \\ \rho &= (\rho_1 - \rho_2) ((2z+h)/2h)^p + \rho_2 \end{aligned} \quad (3)$$

The material properties of the shell vary continuously from the material 2 at the inner surface to material 1 at the outer surface. It is obvious that at the inner surface, $z=h/2$, $E=E_2, \nu = \nu_2$ and $\rho = \rho_2$ (material 2) and at the outer surface $z=h/2$, $E=E_1, \nu = \nu_1$ and $\rho = \rho_1$ (material 1), where $z=0$ corresponds to the middle surface of the shell. A cylindrical shell fabricated of functionally graded material is essentially an inhomogeneous shell consisting of a mixture of isotropic materials. Unlike shells laminated of fibre-reinforced material where transverse shear deformation effects can be significant, for a FGM shell a classical thin shell theory is applicable if radius-to-thickness ratio is ≤ 20 .

In this paper a formulation based on Sanders thin shell theory [2] is carried out for a FGM shell. Strain and kinetic energy expressions are evaluated taking into account asymmetry of material properties about the shell mid-surface due to the presence of coupling stiffness, which do not exist for a homogeneous isotropic shell. Displacement vector is written down in usual manner where axial modal dependence is assumed in the form of Ritz polynomial functions. Application of energy method results in a generalized eigenvalue problem which is then solved using a Matlab package. Eigenvalues and eigenvectors correspond to natural frequency parameters and modal forms respectively.

Results and Discussion

Due to space limitation only results discussed here are for a cylindrical shell with SS and CC boundary conditions only. Table 1 lists the frequency parameters for an isotropic SS shell evaluated by the method in [2] and also the present analysis. An excellent agreement is evident. FGM shells are of two types: Type I with steel used for the inner surface and nickel for the outer surface and in type II where the roles of these two materials are reversed. In Table 2 frequencies are listed for an SS shell of type I for a given set of geometrical parameters and a given power law exponent p . Agreement between the two sets of corresponding results is once again excellent with present results slightly underestimating the results in [2]. Given in Table 3 are the results for a type II shell. Pattern being the same as in Table 2. It is obvious that the general vibratory behaviour for a FGM shell is similar to an isotropic shell as regards frequency variation with circumferential wave number. From Table 2 and 3 it is also obvious that as p increases for the type I the frequencies descend from steel shell in the inner surface to nickel shell in the outer surface and for a shell of type II the converse is true. Tables 4 and 5 correspond to a CC shell of type I and II respectively. Pattern is the same as for the SS case given in Tables 2 and 3. Only difference being that the corresponding frequencies in CC case are higher than those for SS case as expected. This analysis can be extended to other boundary conditions.

References

1. Yamanouchi M, Koizumi M, Hirai T and Shiota I. Proceedings of the First International Symposium on Functionally Graded Materials, Japan, 1990.
2. Loy C T, Lam K Y and Reddy J N. Vibration of functionally graded cylindrical shells. International Journal of Mechanical Sciences **41**, pp 309-324, 1999.

3. Sanders J L. An improved first-approximation theory for thin shells. NASA TR-24, National Aeronautics and Space Administration, Washington, D.C., 1959.

4. Loy C T, Lam K Y and Shu K Y. Analysis of cylindrical shells using generalized differential quadrature, Shock and Vibration, 4, pp 193-198, 1997.

Table 1. Comparison of frequency parameters for various boundary conditions ($m=1$) for an isotropic case. Shell parameters: $L/R=20$, $R/h=100$, $\nu=0.3$.

n	SS		CS		CC	
	I	II	I	II	I	II
1	0.016101	0.016101	0.023987	0.023988	0.032885	0.032915
2	0.009382	0.009381	0.011225	0.011236	0.013932	0.013934
3	0.022105	0.022105	0.022310	0.022310	0.022672	0.022673
4	0.042095	0.042095	0.042139	0.042139	0.042208	0.042208

I. Loy C.T., Lam K.Y., Shu C. [4]

II. Present method.

Table 2. Comparison for natural frequencies (Hz) for FGM cylindrical shell with SS conditions ($m=1$) Type I. Shell parameters: $L/R=20$, $R/h=500$, $\nu=0.3$.

n	Steel ($p=0$)		$p=0.5$		$p=1$		$p=5$	
	I	II	I	II	I	II	I	II
1	13.548	13.548	13.321	13.321	13.211	13.211	12.998	12.988
2	4.592	4.5916	4.5168	4.5118	4.4370	4.474	4.4068	4.4024
3	4.263	4.2628	4.1911	4.1839	4.1150	4.148	4.0891	4.0828
4	7.225	7.2247	7.0976	7.0926	6.9760	7.033	6.9251	6.9211

I. Loy C.T., Lam K.Y., Reddy [2]

II. Present Method.

Table 3. Comparison for natural frequencies (Hz) for an FGM cylindrical shell with SS conditions ($m=1$) Type II. Shell parameters: $L/R=20$, $R/h=500$, $\nu=0.3$.

n	Nickel ($p=0$)		$p=0.5$		$p=1$		$p=5$	
	I	II	I	II	I	II	I	II
1	12.894	12.894	13.103	13.103	13.211	13.211	13.433	13.433
2	4.3690	4.3687	4.4382	4.4425	4.4742	4.4797	4.5504	4.5542
3	4.0489	4.0484	4.1252	4.1214	4.1486	4.1565	4.2191	4.2247
4	6.8577	6.8574	6.9754	6.9794	7.0330	7.0381	7.1510	7.1546

I. Loy C.T., Lam K.Y., Reddy [4]

II. Present Method.

Table 4. Natural frequencies (Hz) of a CC FGM cylindrical shell Type I ($m=1$) Shell parameters: $L/R=20$, $R/h=500$, $\nu=0.3$. Present method.

n	Steel ($p=0$)	Nickel ($p=0$)	$p=0.5$	$p=0.7$	$p=1$	$p=2$	$p=5$	$p=15$
1	27.666	26.351	27.212	27.107	26.969	26.772	26.565	26.430
2	9.814	9.331	9.639	9.615	9.5606	9.482	9.406	9.361
3	5.976	5.679	5.871	5.844	5.819	5.772	5.7263	5.698
4	7.623	7.237	7.485	7.455	7.422	7.362	7.3038	7.265

Table 5. Natural frequencies (Hz) of a CC FGM cylindrical shell Type II ($m=1$) Shell parameters: $L/R=20$, $R/h=500$, $\nu=0.3$. Present method.

n	Steel ($p=0$)	Nickel ($p=0$)	$p=0.5$	$p=0.7$	$p=1$	$p=2$	$p=5$	$p=15$
1	27.666	26.351	26.771	26.875	26.992	27.208	27.445	27.592
2	9.814	9.331	9.484	9.523	9.563	9.644	9.736	9.771
3	5.976	5.679	5.778	5.801	5.827	5.874	5.923	5.955
4	7.623	7.237	7.367	7.395	7.427	7.490	7.551	7.594

FREE VIBRATION ANALYSIS OF THICK SHELLS OF REVOLUTION

A.V.Singh

Department of Mechanical and
Materials Engineering
The University of Western Ontario
London, Ontario, Canada, N6A 5B9

Figure 1 shows the sectional view of an axially symmetric solid, bounded by four curved edges in $r - z$ plane. The geometry of the problem is defined by prescribing the (r, z) coordinates of the eight points shown in the figure. The natural coordinates $(\xi$ and $\eta)$ are used to map this area into a square. The relationship between the two coordinate systems $(r - z)$ and $(\xi - \eta)$ respectively is well known, as this type of mapping is done in the formulation of an eight node isoparametric finite element (Weaver and Johnston, 1984). The coordinates (r, z) of an arbitrary point within the cross sectional area are represented by

$$r(\xi, \eta) = \sum_{i=1}^8 N_i(\xi, \eta) r_i \quad z(\xi, \eta) = \sum_{i=1}^8 N_i(\xi, \eta) z_i \quad (1)$$

Here, $N_i(\xi, \eta)$ and (r_i, z_i) ; for $i = 1, 2, 3, \dots, 8$; are respectively the shape functions and the coordinates of the eight points defining the geometry. The infinitesimal volume dV with reference to the cylindrical coordinates (r, θ, z) can be written as:

$$dV = r d\theta dr dz = r(\xi, \eta) |J(\xi, \eta)| d\xi d\eta d\theta \quad (2)$$

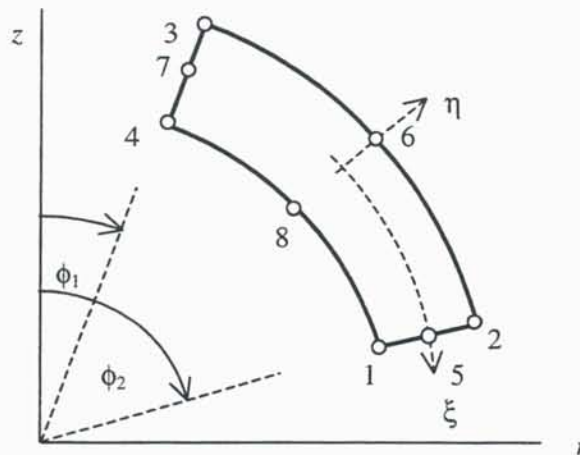


Figure 1. Sectional View of an Axially Symmetric Solid

In order to develop the numerical procedure for the free vibration analysis, the basic equations for axially symmetric solids from the theory of elasticity in (r, θ, z) coordinates are used. These equations include strain displacement relations, stress strain relations and energy expressions.

For example the strain-displacement relationships used in the present study are:

$$\begin{aligned}
 \varepsilon_r &= \frac{\partial u}{\partial r}; & \varepsilon_z &= \frac{\partial v}{\partial z}; \\
 \varepsilon_\theta &= \frac{u}{r} + \frac{1}{r} \frac{\partial w}{\partial \theta}; & \gamma_{rz} &= \frac{\partial u}{\partial z} + \frac{\partial v}{\partial r}; \\
 \gamma_{z\theta} &= \frac{1}{r} \frac{\partial v}{\partial \theta} + \frac{\partial w}{\partial z}; & \gamma_{r\theta} &= \frac{1}{r} \frac{\partial u}{\partial \theta} + \frac{\partial w}{\partial r} - \frac{w}{r}
 \end{aligned} \tag{3}$$

Where, u , v and w represent the displacement components along r , z and θ (circumferential) directions respectively.

The solution procedure is based on the Rayleigh-Ritz method, which requires pre-defined displacement fields with fully satisfied geometric (essential) boundary conditions. To define the displacement fields, the following form of the simple algebraic polynomial is chosen.

$$f(\xi) = a_0 (1 - \xi)^n + a_1(1 - \xi)^{n-1}(1 + \xi) + \dots + a_{n-1}(1 - \xi)(1 + \xi)^{n-1} + a_n(1 + \xi)^n \tag{4}$$

The advantages of using such a polynomial, in the solution procedure, are that the polynomial is complete and the enforcement of the geometric boundary conditions are simple and straightforward. The admissible displacement fields are generated by multiplying the polynomial $f(\xi)$ by its counterpart $f(\eta)$. The coefficients resulting from the product of the polynomials are denoted by a set of two-dimensional arrays: a_{jk} , b_{jk} and c_{jk} for u , v and w respectively. For illustration purpose, the displacement component u is represented by the following double summation series in which n denotes the Fourier harmonic mode of vibration.

$$u = \sum_{k=1}^p \sum_{j=1}^q a_{jk} f_j(\xi) f_k(\eta) \cos n\theta \tag{5}$$

The dimensionless frequency parameter is represented by: $\Omega = \sqrt{(\rho/E)} \omega a$, where ρ = mass density of the material; E = the modulus of elasticity; ω = natural frequency in radian/second; and a = a length parameter. Typically a prominent dimension pertaining to the main characteristics of the problem is selected for a .

One should note that the numerical procedure developed herein is valid for a general solid of revolution generated by rotating a planar section bounded by four straight or curved edges. Therefore; by changing parameters, it is possible to analyze problems having a wide range of shapes and sizes. Values of E and ρ are already attached to the non-dimensional frequency parameter Ω . The value of the Poisson's ratio ν is taken to be 0.3 in all of the following results. In the calculations using the Ritz method, the accuracy of the results depends upon the number of terms used in polynomials $f_j(\xi)$ and $f_k(\eta)$, which are complete functions in the sense that there is no term missing between the first and last terms. If sufficiently large number of terms is used, the method is expected to yield exact results. The selection of the number of terms depends upon the geometry of the solid of revolution. In the present study, numerical computation has been carried out with eight terms (i.e. $q = 8$) in $f_j(\xi)$ and four term (i.e. $p = 4$) in $f_k(\eta)$. With these values of p and q , the order is 96 for each of the stiffness and mass matrices, which are computed numerically by Gaussian quadrature, with eight and four integration points in ξ and η directions respectively. The convergence study has been conducted during this study and results for many additional cases have been generated, but are not included in this paper due to the page limitation. To establish the applicability and validation of the present formulation, some results for the free vibration of a cylindrical solid and moderately thick spherical shell are presented in Tables 1 and 2 respectively. The results are compared with the published data by Leissa and So (1995) and Singh and Mirza (1985).

REFERENCES

Leissa, A. W. and So, J., (1995), Accurate vibration frequencies of circular cylinders from three dimensional analysis, Journal of the Acoustical Society of America, v. 98, p. 2316-2141.

Singh, A. V., and Mirza, S., (1985), Asymmetric Modes and Associated Eigenvalues for Spherical Shells, Journal of Pressure Vessel Technology, vol. 107, p. 77-82.

Weaver, W. and Johnston, P. R., (1984), Finite Elements for Structural Analysis, Prentice Hall, Inc., Englewood Cliffs, New Jersey.

Table 1. Comparison of the frequencies for cylindrical solid clamped at the bottom.

Mode	L/a = 2.0							
	n = 0		N = 1		n = 2		n = 3	
	Present	Leissa and So (95)	Present	Leissa and So (95)	Present	Leissa and So (95)	Present	Leissa and So (95)
1	0.7980	0.7975	0.3140	0.3138	1.3410	1.3408	2.0234	2.0205
2	1.8365	1.8357	0.8958	0.8955	1.5628	1.5616	2.2961	2.2934
3	1.9660	1.9653	1.6069	1.6050	2.1424	2.1400	2.6657	2.6600
4	2.5951	2.5936	1.7702	1.7700	2.3352	2.3320	2.8923	2.8844
5	2.6719	2.6650	2.0770	2.0751	2.7103	2.6960	3.3396	3.3180

Table 2. Comparison of the frequencies for the spherical shell clamped at the open edge $\phi = 60^\circ$.

Mode	h/R = 0.05							
	n = 1		n = 2		n = 3		n = 4	
	Present	Singh and Mirza (85)	Present	Singh and Mirza (85)	Present	Singh and Mirza (85)	Present	Singh and Mirza (85)
1	0.9007	0.8990	1.0916	1.0790	1.2264	1.2140	1.3998	1.3931
2	1.2071	1.2092	1.4750	1.4756	1.7741	1.7657	2.2122	2.1028
3	1.7884	1.7596	2.2329	2.1842	2.7676	2.6141	3.3418	3.0760
4	2.2592	2.2397	3.2212	3.0864	4.1377	3.6792	5.0005	4.2431
5	3.0291	2.7194	3.8304	3.3194	4.5975	4.1620	5.5276	5.0022

Vibration Studies of Composite Laminated Structural Components

Kostas P. Soldatos

University of Nottingham, Pope Building, Nottingham NG7 2RD, UK

Arcangelo Messina

Dipartimento di Ingegneria dell 'Innovazione, Università di Lecce, Via Monteroni, 73100 Lecce, Italy.

This paper summarises the progress that its authors (Soldatos and Messina, 1998, 2000; Messina and Soldatos, 1999a-d; Messina and Soldatos, in preparation) have recently made in studying the free vibrations of a certain type of laminated composite structural components. The geometric configuration of the components considered is that of a rectangular plate, an open cylindrical panel with rectangular plan-form or a closed cylindrical shell. In the most general case, each layer of such a structural component is assumed as made of a linearly elastic monoclinic material, so that all possible kinds of relevant cross-ply and angle-ply material lay-ups are particular cases. Moreover, the study can consider any possible set of variationally consistent set of boundary conditions applied at the edges of the structural component.

The mathematical model is based on a generalised, five-degrees-of-freedom, shear deformable laminated cylindrical shell theory (Soldatos and Timarci, 1993) but for simplicity its Love-type classical shell theory analogue (Timarci and Soldatos, 1995) is only considered. The theory involves two general functions of the transverse co-ordinate parameter, the *a-posteriori* specification of which can reduce it into anyone of the conventional five-degrees-of freedom theories, like the so-called uniform- and parabolic-shear deformable laminate theories. An important feature of the present theory is however the fact that, unlike the aforementioned conventional shell theories, appropriate choices of the shape functions involved enable the satisfaction of the interlaminar stresses continuity at the component material interfaces, without increasing the number of the degrees of freedom involved.

The mathematical analysis is based on the Ritz method, which is applied on the energy functional of the aforementioned generalised shell theory. The resulting formulation is general enough to incorporate into the Ritz-type analysis any set of basis functions but only simple power series and orthogonal polynomials have so far been used in the numerical applications performed. Both of these sets of basis functions are complete in the appropriate Hilbert functional space. As a result, their conjunction with the Ritz method can lead, in an asymptotic sense, to numerical results that are practically equivalent to those that could be obtained through the exact solution of the corresponding set of governing differential equations. The fact that, for any given set of edge boundary conditions, both sets of basis functions lead to practically identical numerical results (Messina and Soldatos, 1999d) is only a verification of this theoretical result.

This research study started with the free vibration analysis of laminated structural components having all their edges free of traction (Soldatos and Messina, 1998; Messina and Soldatos, 1999a), namely a class of structural elements which is privileged for laboratory tests. It also started with the relatively simple material configuration of the cross-ply lay-up (Soldatos and Messina, 1998; Messina and Soldatos, 1999b-d) before proceeds further with more complicated angle-ply material arrangements (Messina and Soldatos, 1999a; Soldatos and Messina, 2000). The simpler cross-ply material arrangement has already allowed the incorporation into the theoretical analysis of shape functions that enable the satisfaction of the interlaminar stresses continuity at the component material interfaces (Timarci and Soldatos, 1995; Soldatos and Messina, 1998; Messina and Soldatos, 1999c).

The interlaminar stresses continuity was not implemented in the initial relevant studies that dealt with the more complicated angle-ply material arrangement (Messina and Soldatos, 1999a; Soldatos and Messina, 2000). The manner however has recently been found to handle this problem successfully and some relevant numerical results that have already been obtained are in the process of classification and physical interpretation (Messina and Soldatos, in preparation).

It should be noted that the efficiency and the accuracy of the described analysis were always carefully tested before, gradually, each one of its different pieces was brought into publicity. This was achieved by means of successful numerical comparisons with corresponding results that, dealing with particular cases, had already been obtained on the basis of other theoretical/analytical approaches (Leissa, 1973; Gorman, 1978; Leissa and Narita, 1984; Khdeir and Reddy, 1990; Narita *et al.* 1992; Qatu, 1991, 1992; Qatu and Leissa, 1991; Frederiksen, 1995; Soldatos and Ye, 1995; Timarci and Soldatos, 1995; Xavier *et al.* 1995; Anderson and Nayfeh, 1996; So and Leissa, 1997; Singh and Kumar, 1998a, 1998b; Timarci and Soldatos, 2000) and/or experimental methods (Anderson and Nayfeh, 1996; Jones *et al.*, 1996).

ACKNOWLEDGEMENTS

The described investigation was initially supported by the Italian National Research Council (CNR) and later by the Royal Society of London.

REFERENCES

- Anderson, T.J. and Nayfeh, A.H. (1996) Natural frequencies and mode shapes of laminated composite plates: experiments and FEA, *J. Vibr. Contr.* **2**, 381-414.
- Bhat, R.B. (1985) Natural frequencies of rectangular plates using characteristic orthogonal polynomials in Rayleigh-Ritz method, *J. Sound Vibr.* **102**, 493-499.
- Gorman, D.J. (1978) Free vibration analysis of the completely free rectangular plate by the method of superposition, *J. Sound Vibr.* **57**, 437-447.
- Frederiksen, P.S. (1995) Single-layer plate theories applied to the flexural vibration of completely free thick laminates, *J. Sound Vibr.* **186**, 743-759.
- Jones, I.A., Williams, E. and Messina, A. (1996) Theoretical, experimental and finite element modelling of laminated composite shells, *Proc. 2nd Int. Conf. Struct. Dyn. Model., NAFEM, Cumbria*, 267-279.
- Khreir, A.A. and Reddy, J.N. (1990) Influence of edge conditions on the modal characteristics of cross-ply laminated shells, *Comput. Struct.* **34**, 817-826.
- Leissa, A.W. (1973) The free vibration of rectangular plates, *J. Sound Vibr.* **31**, 257-293.
- Leissa, A.W. and Narita, Y. (1984) Vibrations of completely free shallow shells of rectangular planform, *J. Sound Vibr.* **96**, 207-218.
- Messina, A. and Soldatos, K.P. (1999a) Vibration of completely free composite plates and cylindrical shell panels by a higher order theory, *Int. J. Mech. Sci.* **41**, 819-918.
- Messina, A. and Soldatos, K.P. (1999b) Ritz-type dynamic analysis of cross-ply laminated circular cylinders subjected to different boundary conditions, *J. Sound Vibr.* **227**, 749-768.
- Messina, A. and Soldatos, K.P. (1999c) Influence of edge boundary conditions on the free vibrations of cross-ply laminated circular cylindrical panels, *J. Acoust. Soc. Am.* **106**, 2608-2620.
- Messina, A. and Soldatos, K.P. (1999d) Application of the Ritz method for the vibration of symmetric laminates by different functional bases, *Proc. 2nd Int. Conf. Ident. Engng Syst. – Univ Wales Swansea*, March 29-31, 1999).
- Messina, A. and Soldatos, K.P. (in preparation) A general vibration model of angle-ply laminated plates that accounts for the continuity of interlaminar stresses.

- Narita, Y., Ohta, Y., Yamada, G. and Kobayashi, T. (1992) Analytical method for vibration of angle-ply cylindrical shells having arbitrary edges, *AIAA J.* **30**, 790-796.
- Qatu, M. (1991) Free vibrations of laminated composite rectangular plates, *Int. J. Solids Struct.* **28**, 941-954.
- Qatu, M. (1992) Mode shape analysis of angle-ply laminated composite shallow, *J. Acoust. Soc. Am.* **92**, 1509-1520.
- Qatu, M. and Leissa, A.W. (1991) Free vibrations of completely free doubly curved laminated composite shallow shells, *J. Sound Vibr.* **151**, 9-29.
- Singh, A.V. and Kumar, V. (1998a) On the free vibrations of fiber reinforced doubly curved panels, Part 1: Formulation/Convergence study, *J. Vibr. Acoust.* **120**, 287-294.
- Singh, A.V. and Kumar, V. (1998b) On the free vibrations of fiber reinforced doubly curved panels, Part 2: Applications, *ASME J. Vibr. Acoust.* **120**, 295-300.
- So, J. and Leissa, A.W. (1997) Free vibrations of thick hollow circular cylinders from three-dimensional analysis, *J. Vibr. Acoust.* **119**, 79-85.
- Soldatos, K.P. and Timarci, T. (1993) A unified formulation of laminated composite shear deformable five-degrees-of-freedom cylindrical shell theories, *Compos. Struct.* **25**, 165-171.
- Soldatos, K.P. and Ye, J.Q. (1995) Axisymmetric static and dynamic analysis of laminated hollow cylinders of monoclinic elastic layers, *J. Sound Vibr.* **184**, 245-259.
- Soldatos, K.P. and Messina, A. (1998) Vibration studies of cross-ply laminated shear deformable circular cylinders on the basis of orthogonal polynomials, *J. Sound Vibr.* **218**, 219-243.
- Soldatos, K.P. and Messina, A. (2000) The influence of boundary conditions and transverse shear on the vibration of angle-ply laminated plates, circular cylinders and cylindrical panels, *Comput. Meth. Appl. Mech. & Engng.* **accepted**.
- Timarci, T. and Soldatos, K.P. (1995) Comparative dynamic studies for symmetric cross-ply circular cylindrical shells on the basis of a unified shear deformable shell theory, *J. Sound Vibr.* **187**, 609-624.
- Timarci, T. and Soldatos, K.P. (2000) Vibrations of angle-ply laminated circular cylindrical shells subjected to different sets of edge boundary conditions, *J. Engng Math.* **37**, 211-230.
- Xavier, P.C., Chew, C.H. and Lee, K.H. (1995) Buckling and vibration of multilayer orthotropic composite shells with a simple higher-order layer wise theory, *Int. J. Solids Struct.* **32**, 3479-3497.

Vibration Analysis of a Rotating Vessel Composed of Circular Plates and a Circular Cylindrical Shell, 1st Stage: In-Plane Vibrations of a Rotating Circular Plate

by

Katsuyoshi Suzuki, Tomoaki Hijiki and Kenichi Suzuki

Department of Mechanical Systems Engineering
Faculty of Engineering, Yamagata University
4-3-16 Jyonan, Yonezawa, 992-8510, Japan

1. INTRODUCTION

There are a number of investigations, including the well-known paper by Southwell, which deal with the vibrations of a rotating circular plate^{(1)~(6)}. But almost all of them consider the bending vibrations of the plate under the effect of in-plane tensions due to the steady rotation. Moreover, the equations of motion for the steady rotation are based on the Timoshenko type equation⁽⁷⁾(hereafter is called the classical equation).

The authors have studied the in-plane vibrations of a rotating circular plate in order to analyze the free vibrations of a rotating vessel. Based on the theoretical analysis, we found that the classical equation is inaccurate because of the in-plane deformation of the plate being neglected when considering the centrifugal force. The in-plane vibrations of the rotating circular plate have been not so much interested in as the bending vibrations, and in the best of authors' knowledge, there is no paper that examines, in detail the in-plane vibrations of the rotating circular plate.

In this paper, a refined solution procedure is presented for the in-plane free vibrations of a circular plate, which vibrates infinitesimally under the initial tensions due to the steady rotations. The basic equations for both the steady rotation and the in-plane vibration are derived from the stationary conditions of the Lagrangians. The equations of motion are solved exactly by power series expansions. In the numerical calculations, in-plane stress distributions of the circular plate in the steady rotation and frequencies and mode shapes in the vibration are presented. The characteristics are discussed comparing the results by the present theory and those by the classical theory.

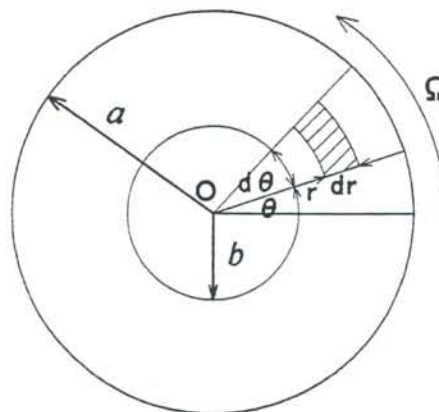


Fig.1 Geometry and co-ordinates of a rotating circular plate.

2. BASIC EQUATIONS

2. 1 For steady rotation

Let us consider the equation of motion of a uniform thin circular plate rotating at the angular velocity Ω .

Figure 1 shows the geometry and the co-ordinates of the circular plate. The origin is taken to be at the center O on the middle surface and the circular plate rotates about the vertical axis passing through the origin. The thickness, outer radius and inner radius are denoted by h , a and b , respectively. Let the displacement in the radial direction due to the steady rotation be u^* .

The classical equation of motion is given from Timoshenko⁽⁷⁾ as

$$d^2 U^* / dz^2 + (1/z) dU^* / dz - U^* / z^2 = -\alpha^2 z \quad (1)$$

where

$$z = r/a, \quad U^* = u^*/a, \quad \alpha^2 = (1 - \nu^2) \rho \Omega^2 a^2 / E \quad (2)$$

and E, ν, ρ are Young's modulus, Poisson's ratio, and the mass density, respectively. We propose the equation of motion as follows;

$$d^2U^*/dz^2 + (1/z)dU^*/dz - (\alpha^2 + 1/z^2)U^* = -\alpha^2 z \quad (3)$$

The boundary conditions at $z=1$ and $z=\eta$ ($=b/a$) are

$$(\partial U^*/\partial z + \nu U^*/z)\delta U^* = 0 \quad (4)$$

2. 2 For in-plane vibration

Next we consider the basic equations of the circular plate which vibrates infinitesimally under the initial tensions due to the steady rotation. Let the displacements in the radial and circumferential directions are u and v , respectively. Each displacement component is assumed as follows:

$$u = u^* + \tilde{u}, \quad v = \tilde{v} \quad (5)$$

where \tilde{u} and \tilde{v} are the displacements due to the vibration. The kinetic energy is

$$T = 1/2 \int_0^\eta \int_r \rho h [(\partial u/\partial t - \Omega u)^2 + (\partial v/\partial t + \Omega(r+u))^2] r dr d\theta \quad (6)$$

where t denotes the time. The strain energy is

$$V = Eh/2(1-\nu^2) \int_0^\eta \int_r [\varepsilon_r^2 + \varepsilon_\theta^2 + 2\nu\varepsilon_r\varepsilon_\theta + \{ (1-\nu)/2 \} \gamma_{r\theta}^2] r dr d\theta \quad (7)$$

where ε_r and ε_θ are the normal strain expressions and $\gamma_{r\theta}$ is the shearing strain expression and

$$\begin{aligned} \varepsilon_r &= \partial u/\partial r + 1/2\{(\partial u/\partial r)^2 + (\partial v/\partial r)^2\} \\ \varepsilon_\theta &= u/r + (1/r)\partial v/\partial \theta + 1/(2r^2)\{(\partial u/\partial \theta)^2 \\ &\quad + (\partial v/\partial \theta)^2\} \\ \gamma_{r\theta} &= (1/r)\partial u/\partial \theta + \partial v/\partial r - \nu/r \\ &\quad + 1/r(\partial u/\partial r \cdot \partial u/\partial \theta + \partial v/\partial r \cdot \partial v/\partial \theta) \end{aligned} \quad (8)$$

Now define the Lagrangian at any instant of time as

$$L = T - V \quad (9)$$

Substitute Eqs. (5) ~ (8) into Eq. (9) and neglect the higher order terms. Applying Hamilton's principle to the Lagrangian of the vibration, $\delta \int_0^t L dt = 0$, and subtracting the equation

of motion (3) and the boundary conditions (4), one can obtain the equations of motion and the boundary conditions for the in-plane vibrations. The equations of motion are

$$\begin{aligned} E_1 &= \lambda z \{ \Omega^2 \tilde{U} + 2\Omega \partial \tilde{V}/\partial t - \partial^2 \tilde{U}/\partial t^2 \} + z \partial^2 \tilde{U}/\partial z^2 \\ &\quad + \partial \tilde{U}/\partial z - \tilde{U}/z + (1-\nu)/(2z) \cdot \partial^2 \tilde{U}/\partial \theta^2 \\ &\quad + (1+\nu)/2 \cdot \partial^2 \tilde{V}/\partial z \partial \theta - (3-\nu)/2z \cdot \partial \tilde{V}/\partial \theta \\ &\quad + \partial/\partial z \{ z(h\sigma_z^*/D) \cdot \partial \tilde{U}/\partial z \} \\ &\quad + \partial/\partial \theta \{ (h\sigma_\theta^*/Dz) \cdot \partial \tilde{U}/\partial \theta \} - \nu \partial U^*/\partial z \cdot \partial \tilde{U}/\partial z \\ &\quad + \partial/\partial z \{ \partial U^*/\partial z [2z \partial \tilde{U}/\partial z + \nu(\tilde{U} + \partial \tilde{V}/\partial \theta)] \} \\ &\quad + (1-\nu)/2 \cdot \partial U^*/\partial z \{ (2/z) \partial^2 \tilde{U}/\partial \theta^2 \\ &\quad - (1/z) \partial \tilde{V}/\partial \theta + \partial^2 \tilde{V}/\partial z \partial \theta \} = 0 \\ E_2 &= \lambda z \{ \Omega^2 \tilde{V} - 2\Omega \partial \tilde{U}/\partial t - \partial^2 \tilde{V}/\partial t^2 \} \\ &\quad + (1-\nu)/2 \cdot z \partial^2 \tilde{V}/\partial z^2 + 1/z \cdot \partial^2 \tilde{V}/\partial \theta^2 \\ &\quad + (1-\nu)/2 \cdot (\partial \tilde{V}/\partial z - \tilde{V}/z) + (3-\nu)/2z \cdot \partial \tilde{U}/\partial \theta \\ &\quad + (1+\nu)/2 \cdot \partial^2 \tilde{U}/\partial z \partial \theta + \nu \partial U^*/\partial z \cdot \partial^2 \tilde{U}/\partial z \partial \theta \\ &\quad + \partial/\partial z \{ z(h\sigma_z^*/D) \cdot \partial \tilde{V}/\partial z \} \\ &\quad + \partial/\partial \theta \{ (h\sigma_\theta^*/Dz) \cdot \partial \tilde{V}/\partial \theta \} \\ &\quad + (1-\nu)/2 \cdot \{ \partial U^*/\partial z (1/z \cdot \partial \tilde{U}/\partial \theta + \partial^2 \tilde{U}/\partial z \partial \theta) \\ &\quad + \partial^2 U^*/\partial z^2 \cdot \partial \tilde{U}/\partial \theta \} = 0 \end{aligned} \quad (10)$$

where

$$\begin{aligned} z &= r/a, \quad \tilde{U} = \tilde{u}/a, \quad \tilde{V} = \tilde{v}/a, \quad \eta = b/a \\ D &= Eh/(1-\nu^2), \quad \lambda = \rho(1-\nu^2)a^2/E \\ \sigma_z^* &= E/(1-\nu^2) \cdot (dU^*/dz + \nu U^*/z) \\ \sigma_\theta^* &= E/(1-\nu^2) \cdot (U^*/z + \nu dU^*/dz) \end{aligned} \quad (11)$$

and $\sigma_z^*, \sigma_\theta^*$ are the initial stresses due to the steady rotation.

3. SOLUTIONS OF EQUATIONS OF MOTION

The solution of Eq. (1) is given as

$$U^* = K_1 z + K_2/z - (\alpha^2/8)z^3 \quad (12)$$

where K_1 and K_2 are arbitrary constants. The solution of Eq. (3) can be obtained as

$$U^* = K_1 J_1(\alpha z) + K_2 Y_1(\alpha z) + U_S \quad (13)$$

Here, K_1 and K_2 are arbitrary constants which can be determined by the boundary conditions. The functions $J_1(\alpha z)$ and $Y_1(\alpha z)$ are Bessel

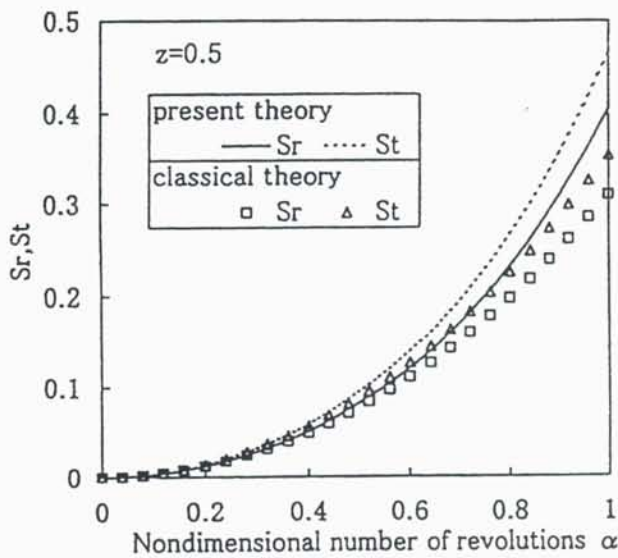


Fig.2 Relation between stress and nondimensional number of revolutions of a disk without a hole (edge free , $\eta = 0$)

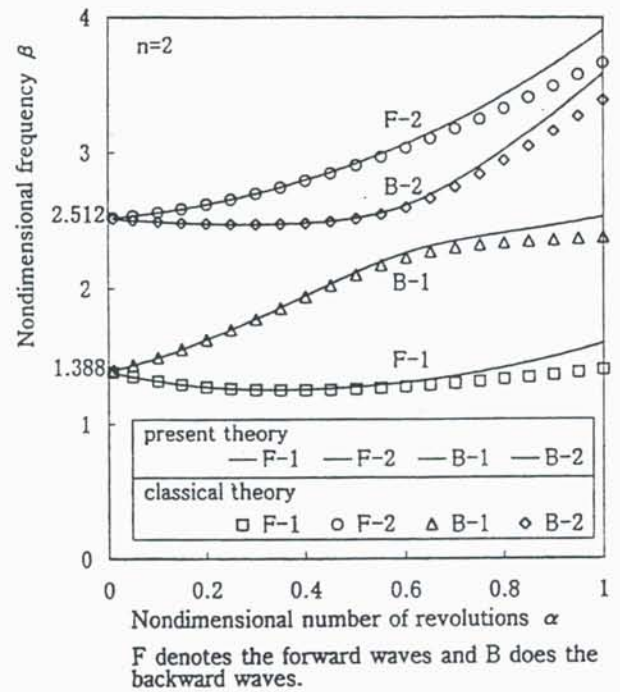


Fig.3 Relation between frequency and number of revolutions (edge free, $\eta = 0$)

functions of the first and the second kinds of order one and U_s is a particular solution which is expressed by a power series of z .

The solution of Eqs.(10) may be obtained as

$$\begin{aligned} \tilde{U} &= U(z) \sin(n\theta - pt), \quad \tilde{V} = V(z) \cos(n\theta - pt) \\ U(z) &= \sum_{m=0}^{\infty} Q_m Z^{2m+N}, \quad V(z) = \sum_{m=0}^{\infty} R_m Z^{2m+N} \end{aligned} \quad (14)$$

where n and p are the number of nodal diameter and the circular frequency, and Q_m, R_m are undetermined coefficients which are determined in turn by substituting Eqs.(14) into Eqs.(10) and N is a root of the characteristic equation.

4. NUMERICAL EXAMPLES

In the numerical calculations, Poisson's ratio is taken as $\nu = 0.3$.

Figure 2 shows the relation between the nondimensional number of revolution parameter α and nondimensional stress parameters S_r, S_t and Figure 3 does the relation between the nondimensional frequency parameter β and α , in which

$$\beta = \sqrt{\lambda} p, \quad (S_r, S_t) = E/(1 - \nu^2) (\sigma_z^*, \sigma_{\theta}^*) \quad (15)$$

REFERENCES

- (1) Southwell R.V., On the free transverse vibration of a uniform circular disk clamped at its center; and on the effects of rotation, Proc. of the Royal Society of London, 101 (1922), 133-153.
- (2) Eversman W. and Dodson R.O., Free vibration of a centrally clamped spinning circular disk, AIAA J., 7-10 (1969), 2010-2012.
- (3) Ramaiah G.K., Natural frequencies of spinning annular plates, J. Sound Vib., 74 (2) (1981), 303-310.
- (4) Lee H.P. and Ng T.Y., Vibration and critical speeds of a spinning annular disk of varying thickness, J. Sound Vib., 187 (1) (1995), 39-50.
- (5) Tomioka T., Kobayashi Y. and Yamada G., Analysis of free vibration of rotating disk-blade coupled systems by using artificial springs and orthogonal polynomials, J. Sound Vib., 191 (1) (1996), 53-73.
- (6) Mignolet M.P., Free vibration of flexible rotating disks, J. Sound Vib., 196 (5) (1996), 537-577.
- (7) Timoshenko S. and Goodier J.N., Theory of elasticity (1951), 2nd Edition, McGraw-Hill Book Company, Inc. 69-73.

USEFUL ANALOGIES WITH FINDING NATURAL FREQUENCIES OF STRUCTURES FROM DYNAMIC STIFFNESS MATRIX FORMULATIONS

F. W. Williams

Department of Building and Construction, City University of Hong Kong, Kowloon, Hong Kong

W. X. Zhong

Research Institute of Engineering Mechanics, Dalian University of Technology, Dalian 116024, P.R. China

W. P. Howson and A. Watson

Cardiff School of Engineering, Cardiff University, Cardiff CF24 0YF, UK

1. INTRODUCTION

The first author co-invented^{1,2} the Wittrick-Williams (W-W) algorithm, the only reliable method for solving transcendental eigenvalue problems arising when calculating the undamped natural frequencies of vibrating structures. Such problems arise when member differential equations include distributed member mass. Hence assembling the member stiffness matrices in the usual manner yields the transcendental eigenproblem

$$\mathbf{K}(\omega)\mathbf{D} = \mathbf{0} \quad (1)$$

where ω = circular frequency of vibration and \mathbf{D} = amplitude vector of the modal deflections $\mathbf{D} \sin \omega t$. The W-W algorithm gives J , the number of natural frequencies below ω_t , a trial value of ω , as

$$J = \sum J_m + s\{\mathbf{K}(\omega_t)\} \quad (2)$$

where: the summation is over all members; J_m is the number of natural frequencies of a member which would be exceeded by ω_t if its ends were to be clamped and; $s\{\mathbf{K}(\omega_t)\}$, the 'sign count' of $\mathbf{K}(\omega_t)$, can be calculated as the number of negative elements on the leading diagonal of $\mathbf{K}(\omega_t)^\Delta$, where the superscript Δ denotes the upper triangular matrix obtained numerically from $\mathbf{K}(\omega_t)$ by the usual form of Gauss elimination, in which appropriate multiples of the pivotal row are subtracted from all (unscaled) succeeding rows and rows become pivotal in sequence. Eqn.(2) enables the development of many logical procedures for converging on any required natural frequencies by choosing appropriate successive values of ω_t (of which bisection is simple but slow) because J is known for every ω_t used. Hence the W-W algorithm, i.e. Eqn.(2), requires $\mathbf{K}(\omega_t)$ to be assembled by solving the differential equations governing the components of the structure and also requires J_m to be found for each component member *from the same differential equations*.

2. INFORMATIVE PROOF OF THE W-W ALGORITHM

Of four early derivations of the W-W algorithm, the following³ is the most informative for the present purpose. It starts from the generalised linear eigenvalue problem

$$(\mathbf{K} - \lambda\mathbf{M})\mathbf{D} = \mathbf{0} \quad (3)$$

where \mathbf{K} = the ($N \times N$) static stiffness matrix; \mathbf{M} = the ($N \times N$) mass matrix, $\lambda = \omega^2$ and $\mathbf{D} \sin \omega t =$ the modal displacement vector of all freedoms retained in the mathematical model of the real structure.

The Sturm sequence property applies to Eqn.(3) when \mathbf{K} and \mathbf{M} are symmetric and \mathbf{K} is positive definite. In effect it states that the number of natural frequencies (i.e. J) below any trial value $\lambda_t (= \omega_t^2)$ of the eigenparameter equals $s\{\mathbf{K} - \lambda_t\mathbf{M}\}$, where $s\{\}$ has the meaning defined above.

The first step of the proof of the W-W algorithm is to start from the hypothetical 'infinite order Sturm sequence problem' obtained by letting $N \rightarrow \infty$ in Eqn.(3).

The second step is to apply the form of Gauss elimination described above to this matrix but to arrest it after $N_i = N - N_c$ rows have been pivotal, where $N_c =$ No. of freedoms at the joints (i.e. connection nodes) between members. Thus N_i is the infinite number of freedoms between their ends possessed by real numbers. Hence Eqn.(3) becomes Eqns.(4) and (5), from which the key result is Eqn.(6).

$$\begin{bmatrix} \mathbf{K}_{ii} - \lambda\mathbf{M}_{ii} & \mathbf{K}_{ic} - \lambda\mathbf{M}_{ic} \\ \mathbf{K}_{ic}^T - \lambda\mathbf{M}_{ic}^T & \mathbf{K}_{cc} - \lambda\mathbf{M}_{cc} \end{bmatrix} \begin{bmatrix} \mathbf{D}_i \\ \mathbf{D}_c \end{bmatrix} = \begin{bmatrix} \mathbf{0} \\ \mathbf{0} \end{bmatrix} \quad (4)$$

$$\begin{bmatrix} (\mathbf{K}_{ii} - \lambda\mathbf{M}_{ii})^\Delta & \mathbf{C} \\ \mathbf{0} & \mathbf{K}(\lambda) \end{bmatrix} \begin{bmatrix} \mathbf{D}_i \\ \mathbf{D}_c \end{bmatrix} = \begin{bmatrix} \mathbf{0} \\ \mathbf{0} \end{bmatrix} \quad (5)$$

$$\mathbf{K}(\lambda)\mathbf{D}_c = \mathbf{0} \quad (6)$$

Note that \mathbf{C} is of no further use and that with the exception that N is then finite, the process of obtaining Eqn.(6) from Eqn.(4) is that used to reduce by exact means the order of a finite element problem, e.g. by sub-structuring, although the matrix $\mathbf{K}(\lambda)$ is then often expressed as

$$\mathbf{K}(\lambda) = (\mathbf{K}_{cc} - \lambda\mathbf{M}_{cc}) - (\mathbf{K}_{ic}^T - \lambda\mathbf{M}_{ic}^T)(\mathbf{K}_{ii} - \lambda\mathbf{M}_{ii})^{-1}(\mathbf{K}_{ic} - \lambda\mathbf{M}_{ic}) \quad (7)$$

The third step is to recognise that *exactly* the same $\mathbf{K}(\lambda)$ as that of Eqn.(6) can be derived directly, by solving the differential equations for vibration of the component members of the structure to allow *exactly* for their distributed mass, instead of accepting the discretisation errors of traditional finite element methods. Because this obviates the necessity to use Eqns.(4) – (7) it also avoids the impossibility of assembling the infinite order eigenvalue problem of Eqn.(3) with $N \rightarrow \infty$, which is why it was referred to as *hypothetical* earlier.

The fourth step is to complete the arrested Gauss elimination that gave Eqn.(5). Hence

$$J = s\{\mathbf{K} - \lambda_t\mathbf{M}\} = s\{\mathbf{K}_{ii} - \lambda_t\mathbf{M}_{ii}\} + s\{\mathbf{K}(\lambda_t)\} \quad (8)$$

The fifth and final step is that $s\{\mathbf{K}_{ii} - \lambda_i \mathbf{M}_{ii}\}$ can be found via its physical interpretation as the sum of J_m for all members of the structure and hence Eqn.(8) becomes the W-W algorithm, i.e. Eqn.(2).

3. ANALOGOUS PROBLEMS IN OTHER DISCIPLINES

Analogies between problems in different disciplines can be advantageous to one or both of the problems. Apart from the obvious critical buckling problem, the W-W algorithm for vibration of continuous structures has been beneficially applied to: vibration of spinning structures⁴; heat diffusion in composite layers⁵; fluid vibration in pipe systems⁶; modes of flexible structures⁷; wave propagation along periodically supported prismatic structures⁸; H_∞ filtering in control theory⁹ and surface wave propagation in stratified material¹⁰. However there are almost certainly many other analogous problems and these are now being systematically sought by searching EDINA, The Web of Science and other databases, covering all disciplines. The key words used are designed to seek all problems solvable as a linear eigenproblem with a Sturm sequence property and then arguing, from the derivation of Section 2, that if the underlying physical problem is continuous and its differential equations are soluble (analytically or numerically) then 'technology transfer' with structural free vibration problems is potentially mutually beneficial. This includes transfer of the W-W algorithm, which is the subject of the authors' EPSRC grant GR/R05437/01.

REFERENCES

1. F.W.Williams and W.H.Wittrick, An automatic computational procedure for calculating natural frequencies of skeletal structures, *Int. J. Mech. Sci.*, **12:9**, 1970, 781–791.
2. W.H.Wittrick and F.W.Williams, A general algorithm for computing natural frequencies of elastic structures, *Q. J. Mech. Appl. Math.*, **24:3**, 1971, 263–284.
3. W.H.Wittrick and F.W.Williams, New procedures for structural eigenvalue calculations, *4th Australasian Conf. on the Mechs. of Structs. and Materials*, U. of Queensland, Brisbane, Australia, Aug., 1973, 299–308.
4. W.H.Wittrick and F.W.Williams, On the free vibration analysis of spinning structures by using discrete or distributed mass models, *J. Sound Vib.*, **82:1**, 1982, 1–15.
5. M.D.Mikhailov, M.N.Ozisik and N.L. Vulchanov, Diffusion in composite layers with automatic solution of the eigenvalue problem, *Int. J. Heat Mass Tran.*, **26:8**, 1983, 1131–1141.
6. A. Frid, Fluid vibration in piping systems: a structural mechanics approach I. Theory, *J. Sound Vib.*, **133:3**, 1989, 423–438.
7. A.V.Balakrishnan, On the Wittrick-Williams algorithm for modes of flexible structures, *Optimisation Meth. and Software*, **2:2**, 1993, 177–187.
8. F.W.Williams, H.J.Ouyang, D.Kennedy and C.B.York, Wave propagation along longitudinally periodically supported or stiffened prismatic plate assemblies, *J. Sound Vib.*, **186:2**, 1995, 197–205.
9. W.X.Zhong and F.W.Williams, H_∞ filtering with secure eigenvalue calculation and precise integration, *Int. J. Num. Meth. Engng.*, **146:7**, 1999, 1017–1030.
10. Wanxie Zhong, W.P.Howson and F.W.Williams, Precise solutions for surface wave propagation in stratified materials, *J. of Vib. and Acoustics*, ASME (in press).